Development of polycarbonate multifunctional foams with graphene nanoplatelets

A dissertation submitted to the Department of
Materials Science and Metallurgy
Universitat Politècnica de Catalunya
BarcelonaTech
By

Gabriel Eduardo Gedler Chacón

In partial fulfillment of the requirements for the degree of
Doctor of Philosophy
In
Materials Science and Engineering

Prof. José Ignacio Velasco Perero, Advisor
Dr. Marcelo de Sousa Pais Antunes, co-Advisor

July, 2016

UNIVERSITAT POLITÈCNICA DE CATALUNYA
BARCELONATECH
Escola de Doctorat

Assessment results for the doctoral thesis

Academic year:

Full name

Doctoral programme

Structural unit in charge of the programme

Decision of the committee

In a meeting with the examination committee convened for this purpose, the doctoral candidate presented the topic of his/her doctoral thesis entitled

_____

_____.

Once the candidate had defended the thesis and answered the questions put to him/her, the examiners decided to award a mark of:

☐ UNSATISFACTORY ☐ SATISFACTORY ☐ GOOD ☐ VERY GOOD

(Full name and signature) Chairperson	(Full name and signature) Secretary

(Full name and signature) Member	(Full name and signature) Member	(Full name and signature) Member

_____, _____

The votes of the members of the examination committee were counted by the Doctoral School at the behest of the Doctoral Studies Committee of the UPC, and the result is to award the CUM LAUDE DISTINCTION:

☐ YES ☐ NO

(Full name and signature) Chair of the Standing Committee of the Doctoral School	(Full name and signature) Secretary of the Standing Committee of the Doctoral School

Barcelona, _____

International doctoral degree statement

As the secretary of the examination committee, I hereby state that the thesis was partly (at least the abstract and the conclusions) defended in a language commonly used in scientific communication in the field that is not an official language of Spain. This does not apply if the stay, report or expert is from a Spanish-speaking country.

(Nom, cognoms i signatura) Secretary of the Examination Commitee

Acknowledgements

I am truly grateful for the many people that have helped me in one way or another through this entire process. First, I want to thanks Professor Jose Ignacio Velasco (Nacho) for giving me the opportunity to work with him and for sharing his knowledge and advice throughout many years. I am very appreciative for his guidance and all the support during my studies.

I want to acknowledge my co-Advisor Dr. Marcelo Antunes for his guidance, patience and time he dedicated not only to being an excellent reviewer for our papers but also for transmitting the knowhow to carry on the preparation and characterization of lightweight materials.

I am very grateful to Prof. Rahmi Ozisik for all his support carrying out the last stage of my research at Rensselaer Polytechnic Institute (RPI) in New York.

I am thankful for the Professors in the Centre Català del Plàstic (CCP) for all their support and all the theoretical and practical information shared during my studies. Professors Maria Lluisa Maspoch, Antonio Martinez Benasat, Miguel Sánchez, Orlando Santana, David Arencón, Silvia Illescas, Edgar Franco and last but not least Vera Realinho for not only be part of the research team but also for her support during the characterization of my samples.

A special acknowledgment goes to the CCP staff Anna Carreras and Alba Giménez for all your support and patience during my stay at the CCP.

Thanks to those who helped me in several ways with my experiments in Barcelona: Prof. Laia Haurie, Josep (ETSEIAT), Tariq (UB), Xavi and Maria (UB), Gerard (UB). In New York: Deniz Rende (MRC-RPI), Ray Dove (MRC-RPI), Prof. Hella (ECSE-RPI), Prof. Borrego (ECSE-RPI) and Kefei Wu (ECSE-RPI), Joel Morgan (CBIS-RPI) and the undergraduate students in Ozisik's research group.

It was a great pleasure for me share this time with all my fellow students at the CCP, most of them doctors by now Julio, Tobias, Jonathan, Jaime, Liang, Hakim, Hooman, Oona, Jonas, Noel, David.

I would like to thanks Prof. Crisanto Villalobos and Prof. José Maria Cabreras for allowing me to enter into the Phd program at the BarcelonaTech.

Thank you to Nasser, Julio, Emilio and Moises for all your support.

This thesis would not be possible without the financial support from the Centre Català del Plàstic (CCP) and its industrial partnership, along with the financial support of the Spanish Ministry of Economy and Competitiveness through the projects MAT2010-15565, MAT2011-26410 and MAT2014-56213.

I want to acknowledge Annika Havnaer, soon to be MD, for the patience and time dedicated to proofreading my chapters and some of my papers.

A special thanks to Adriana Schilperoort-Havnaer and Doug Havnaer (now my in-laws) for all your support and encouragement throughout this process. Thank you for having me every Christmas in NY when I was in Barcelona, and when I was in NY for having me over almost every single weekend. I have no words to express my gratitude.

I am indebted to the two women that I love and that in different ways supported me to finish this stage and that are a very important part of my life.

First my mother, your very positive influence on me made me the person that I am today. All your support and love all the way from Caracas, your patience, all the paperwork that we had to do, all worked out fine. It is impossible to express in words how much I am thankful to you. Thank you so much. I love you.

Last but certainly not least my beautiful wife Helen Marie Havnaer for all your love, patience, support, and great moments that we have lived throughout this period. Thank you for sharing your life with me. Thank you for being on my side all this time. I am looking forward to what is coming next, I love you.

Abstract

The goal of this research was to determine the relations between processing, structure and properties of polycarbonate-graphene nanoplatelets (PC-GnP) foams. Using two different foaming processes (in one and two steps) using supercritical carbon dioxide ($scCO_2$) as a physical foaming agent, a series of foams were prepared and investigated. The effects of processing variables (P, T and time) and the materials composition (% GnP) on the cellular morphology, microstructure and properties of the foams were investigated. The addition of GnP promoted cell nucleation in PC, allowing the preparation of foams with a broad range of relative densities, varying from 0.07 to 0.80, with average cell sizes ranging from a few to hundreds of micrometers. Changes in PC microstructure during processing in the presence of CO_2 and GnP were investigated as well as the variation of the thermal stability of the foams. At the microstructural level, the foams prepared in two steps (typical foaming temperature of 165 ºC) the foams remained amorphous, while the foams prepared in one step with typical foaming temperatures above 200 ºC, developed a degree of crystallinity. The thermal stability of the foams was observed to be higher when compared with the thermal stability of the unfoamed material, attributed to the thermal insulator effect of the cellular structure. In addition, the presence of GnP delayed the diffusion of gaseous products due to the barrier effect. These enhancements suggest the use of these foams in higher temperatures when compared with PC. The influence of density, morphology and microstructure on the mechanical and transport properties of the foams was analyzed. Regarding the viscoelastic properties of foams, it was observed different linear relations in terms of their storage modulus with density, depending on the density, composition and cellular morphology. The crystallinity in the foams prepared in one step allow to explain the stiffer nature when compared with the foams prepared in two steps, regardless of their comparatively smaller cell densities and larger cells. Regarding the electrical conductivity, in addition to the content of conductive nanoparticles, the effect of the cellular structure on the electrical conductivity of the foams was evident. The enhancement of conductivity while reducing the relative density of foams, suggesting the formation of a more effective conductive network, resulting from a better dispersion and/or distribution of nanoparticles when increasing the expansion ratio. This effect was also observed in the electromagnetic interference (EMI) shielding properties. In the case of the thermal conductivity, it was mainly controlled by foam densities, while the cellular morphology of foams had a smaller impact. It was observed a reduction of 90 % in density of pure PC promoted a reduction in thermal conductivity of 80 % approximately. The addition of a small fraction (0.5 wt%) of GnP promoted up to 95% enhancement of the thermal conductivity as compared to pure PC foams with similar relative

densities. This was attributed to a better thermal conductivity through the solid fraction with GnP. The addition of higher GnP contents (5 wt%) led to foams with thermal conductivities similar to that of the unfoamed composite (5 wt%). These results suggest the use of PC-GnP foams could be considered for applications where dissipation of heat is needed while using lightweight materials.

Resumen

Este trabajo fue llevado a cabo con el objetivo de determinar las relaciones entre procesado, estructura y propiedades de los nanocompuestos espumados de policarbonato con nanoparticulas de grafeno (PC-GnP). Se prepararon e investigaron series de espumas producidas según dos procesos diferentes de espumación (proceso en una etapa y en dos etapas) usando dióxido de carbono supercrítico ($scCO_2$) como agente físico de espumación. Se analizaron los efectos de las variables del proceso (presión, temperatura y tiempo) y de la composición del material (% GnP) sobre la morfología, estructura y propiedades de las espumas. La incorporación de GnP favoreció la nucleación celular en el polímero, permitiendo preparar espumas con un amplio rango de densidades relativas, entre 0.07 y 0.80, con tamaños celulares promedio de entre unos pocos micrómetros hasta varios cientos. Se investigaron, asimismo, los cambios microestructurales desarrollados por el PC durante el procesado en presencia de $scCO_2$ y GnP, así como la variación de la estabilidad térmica de las espumas. A nivel estructural, en el caso de espumación llevada a cabo en dos etapas (Temperatura típica de espumación 165 ºC) las espumas no desarrollaban cristalinidad, mientras que las espumas producidas directamente en una etapa, con temperatura típica de espumación superior a 200 ºC, presentaban un grado de cristalinidad. La estabilidad térmica de las espumas resultaba superior a la del material no celular, debido al efecto aislante de la estructura celular. Asimismo, las nanopartículas GnP limitaban la difusión de los productos gaseosos por efecto barrera. Ello sugiere, para estas espumas, eventuales aplicaciones de mayor temperatura que las del propio PC. Por otra parte, con respecto a las propiedades termomecánicas de las espumas, se encontraron diferentes relaciones entre los valores del módulo de almacenamiento con la densidad, dependiendo de la densidad, composición y morfología celular. Asimismo, la cristalinidad desarrollada en las espumas producidas en el proceso de una etapa, permitió explicar su mayor rigidez frente a las producidas en dos etapas, a pesar de tener menores densidades celulares y superiores tamaños de celda. Por lo que respecta a la conductividad eléctrica, además de la concentración de partículas conductoras GnP, se evidenció la influencia de la estructura celular de la espuma como una característica relevante sobre dicha propiedad. Así, se puso de manifiesto el aumento de la conductividad al disminuir la densidad relativa de las espumas, sugiriendo una red de conducción eléctrica más efectiva, que resultaría de una mayor dispersión y/o mejor distribución de las partículas al aumentar el grado de espumación. Este efecto se pudo observar sobre las propiedades de protección frente a la interferencia electromagnética (EMI-SE). En el caso de la conductividad térmica, esta fue determinada principalmente por la densidad relativa de las espumas y, en menor medida, por su morfología celular. Así, una disminución del 90 % en la

densidad del material conllevó una reducción de la conductividad térmica de un 80% aproximadamente. De igual modo, una fracción másica tan pequeña como un 0.5 % de GnP promovió hasta un 95% de incremento de conductividad térmica en espumas de similar densidad. El efecto se atribuye a una mejor conducción de la fase sólida que contiene las partículas GnP. En este sentido, las espumas con contenidos de GnP del 5 % en peso, manifestaron conductividades térmicas del mismo orden que las del compuesto no celular sin espumar. Estos resultados sugieren eventuales aplicaciones para las espumas de PC-GnP donde se requiera disipación de calor con materiales ligeros.

Index

Abbreviations and symbols

A – Area

AC – Alternating Current

AR – Aspect ratio

AFM – Atomic force microscopy

CO_2 – Carbon Dioxide

CNF – Carbon nanofibers

CNT – Carbon nanotubes

CVD – Chemical vapor deposition

d_{002} – Interplanar distance of the (002) plane

DC – Direct Current

D_d – Diffusion coefficient

DMTA – Dynamic mechanical thermal analysis

DSC – Differential scanning calorimetry

E – Elastic modulus

E' – Storage modulus

E'' – Loss modulus

EC – Empirical correlation

EMI SE – Electromagnetic interference shielding effectiveness

FWHM – Full width half maximum

GnP – Graphene nanoparticles/nanoplatelets

GO – Graphene oxide

I – Intensity

I_D, I_G – Intensity of D, G bands

K – Thermal conductivity

l – Thickness

L' – Lamellar thickness/graphene nanoplatelets thickness

l_a – Amorphous layer thickness

L_B – Long period/Long spacing

l_c – Crystal thickness

MEGO – Microwave-exfoliated graphite oxide

MFI – Melt flow index

M_0 – Maximum/initial concentration of carbon dioxide

M_t – Concentration of carbon dioxide at certain time

MVI – Melt volumetric index

MWCNT – Multiwalled carbon nanotubes

n – Number of cells per area/number of graphene layers in stacks of graphene

N_2 – Nitrogen

N_f – Cell density

PP – Polypropilene

PC – Polycarbonate

PMMA – Poly(methyl methacrylate)

PP – Polypropilene

Q – Invariant

q_{max} – Scattering vector

r – Direction of measurement of electron density

R_i – Interface thermal resistance

R_l – Heat loss resistance

RPUF – Rigid polyurethane foam

R_s – Sample thermal resistance

R_T – Overall/total conduction resistance

S_{11} – Scattering parameter (forward reflection coefficient)

S_{21} – Scattering parameter (forward transmission coefficient)

sc – Super critical

SAXS – Small angle X-rays scattering

SEM – Scanning electron microscopy

SLG – Single layer graphene

SWCNT – Single-walled carbon nanotubes

t – Time

$tan\ \delta$ – Loss factor

TEM – Transmission electron microscopy

T_g – Glass transition temperature

TGA – Thermogravimetic analysis

T_m – Melting temperature

T^0_m – Equilibrium melting temperature

V_{gas} – Gas volume fraction

VD – Vertical direction

VNA – Vector network analyzer

w_p – Weight fraction of polymer

WAXS – Wide angle X-rays scattering

WD – Width/horizontal direction

WR – Waveguide rectangular

Symbols

ε – Deformation

δ – Phase difference between the induced deformation and the tension

X_c – Crystallinity

ΔH_m – Melting enthalpy

ΔH^0_m – Theoretical 100% crystalline PC melting enthalpy

σ_e – Fold surface free energy

ρ – Density

ρ_v – Electrical resistivity

Å – Armstrong

$\Gamma(r)$ – One-dimensional correlation function

λ – Wavelength

ϕ – Average cell diameter

ϕ_{VD} – Average cell diameter in the vertical direction

ϕ_{WD} – Average cell diameter in the horizontal or lateral (width) direction

Ω – Ohm

σ – Electrical conductivity

2θ – Scattering angle

Units

A – Ampere

a.u. – Arbitrary units

bar – Bar

cm – Centimeter

dB – Decibel

eV – Electronvolt

g – Gram

GHz – Gigahertz

Hz – Hertz

K – Kelvin degree

KJ – Kilojoule

Kg – Kilogram

KV – Kilovolt

L – Litre

m – Meter

mm – Millimeter

nm – Nanometer

μm – Micrometer

min – Minute

MHz – Megahertz

ml – Milliliter

MPa – Megapascal

N – Newton

P – Pressure

Pa – Pascal

pA – Picoampere

S – Siemen

Tn – Ton

V – Volt

W – Watt

^{o}C – Celsius degree

^{o}F – Fahrenheit degree

Chapter 1

Introduction

1.1 Introduction.

This thesis is written in partial fulfillment of the requirements for the degree of Doctor of Philosophy in the Department of Ciència dels Materials I Enginyeria Metal.lúrgica (CMEM) of the Universitat Politècnica de Catalunya - BarcelonaTech (UPC). Most of the research activities were carried out in the facilities of the Centre Català del Plàstic (CCP) in Terrasa, Barcelona, Spain. In addition, as a partial fulfillment for the "International Doctorate certification" part of the research was carried out under the collaboration agreement of doctoral student mobility in the Department of Materials Science at Rensselaer Polytechnic Institute (RPI) in New York, USA.

This work is a continuation of the research conducted at the CCP, specifically by the research group developing new lightweight polymeric composites led by Prof. José Ignacio Velasco. Currently one of the focuses of the research group is to develop multifunctional polymer foams. As the trend moves for lighter weight materials in the aerospace, electronic and transportation industries, the importance of research in this area is growing exponentially. The goal of this thesis is to contribute with novel research to the scientific community's knowledge in this field. The general objective of this thesis is to contribute to the development of novel cellular composites by combining polymeric foam characteristics with nanosized materials such as graphene nanoplatelets (GnP) to achieve improved polycarbonate (PC) matrix properties in conjunction with weight reduction. The relationship between the processing conditions, cellular morphology and final properties will be discussed. The following section will display in more detail the objectives of this work.

The structure of this thesis is based on a compilation of published articles from the research carried out during the past 6 years. The articles have been published in international journals in the field of research related to this thesis (i.e. peer-reviewed), in addition to proceedings of international conferences attended, as indicated later in section 1.2. The publications included in the body of this thesis have been grouped in chapters covering fundamental topics such as the morphology of the cellular structures, microstructure, thermal and mechanical behaviors characterization of the different foams prepared, as well as characterization of multifunctional properties such as transport (electrical and thermal conductivities) and electromagnetic interference protection. Each chapter is preceded by an opening introductory section explaining the objective of the articles, the hypothesis

established, the theories used and the main conclusions as it will be detailed in the following section.

1.2 Overview and objectives.

This thesis addresses the preparation and characterization of different morphologies and final properties of Polycarbonate foams and Polycarbonate/graphene nanoplatelets nanocomposite foams. The idea comes from the opportunities that industries such as aerospace, automotive, electronics and construction currently offer when looking for lighter materials with different characteristics and functionalities that can substitute materials currently in used. With this in mind, the main hypothesis of choosing an engineering polymer such as Polycarbonate with a broad use in today's industry, which could be able to be foamed under high temperatures and pressures with minimum degradation and still have a decent mechanical behavior, was chosen to be the candidate. The second hypothesis was that the addition of carbon-based fillers such as graphene nanoplatelets could be used as a driver in order to aim the enhancing of mechanical behavior of foams while adding possible new functionalities to the developed materials, taking into consideration the characteristics of these fillers (i.e. transport, aspect ratio, stiffness that will be discussed in the following sections). In general, it would be expected that developing new polycarbonate systems will provide PC with a broad range of new characteristics and multi-functionalities that will enable it to have better chances when competing for a position in the race of lightweight materials in today's industry.

Particularly, the main and principal objective of this work is to **analyze, correlate and understand the effects of processing on the cellular morphology, microstructure and final properties of polycarbonate and polycarbonate-graphene nanoplatelets foams**. The study has been divided in two focused-objectives in order to display targeted goals. The focused-objectives take into account firstly, **the analysis of foaming processing and its effect on cellular morphology, microstructure and final properties of foams**. Secondly, the **analysis of the presence of graphene nanoplaletes effect on the characteristics of composite foams**. This has been displayed in such a way, taking into consideration that the understanding of the neat system (pure PC foams) needs to be addressed in order to later be able to understand the more complex system when graphene nanoparticles are part of it (polymer-gas-filler). The addition of this type of carbon filler has been focused in the one hand on the possible effect that the filler will have on the

cellular morphology and microstructure of the foams, and in the other hand, the effects that it will have on the final properties property of the foams, while at the same time targeting new multifunctional characteristics, which will promote a broader range of new applications for these lightweight systems.

These two focused-objectives are at the same time divided into more specific goals, allowing the display of results, analyses and correlations to take place in a clear, coherent and explicit manner. The following listing shows the different analyses and correlations carried out aiming to target very specific objectives. This enables a concise display of results, promoting the correlation and understanding of the different variables linked to different characteristics and properties of the prepared foams:

1. Correlate foaming process parameters with the final cellular morphology, microstructure and final properties of the developed foams taking into consideration:
   1.1 The use of industrial-scalable processes to prepared foams.
   1.2 Variations of process parameters to develop different cellular morphologies.
   1.3 Varying process parameters to control the microstructure of foams.
   1.4 Process and morphology's influence on the final properties of foams:
      1.4.1 On the viscoelastic behavior.
      1.4.2 On the thermal stability.
      1.4.3 On the thermal conductivity

2. Analyze the effect of the presence of graphene nanoparticles on the morphology, microstructure and final properties of the nanocomposite foams taking into consideration:
   2.1 The use of industrial-scalable processes to achieve a good dispersion of graphene nanoplatelets in Polycarbonate.
   2.2 The effect of the incorporation of different contents of graphene nanoplatelets on the CO_2 diffusion.
   2.3 The effect of the incorporation of different contents of graphene nanoplatelets on cellular morphologies.
   2.4 Influence of the process parameters and incorporation of graphene nanoplatelets on the final properties of nanocomposite foams:
      2.4.1 On the viscoelastic behavior.

2.4.2 On the thermal stability.

2.4.3 On the electrical conductivity.

2.4.4 On the thermal conductivity.

2.4.5 On the electromagnetic interference shielding effectiveness.

In this Chapter (Chapter 1) in addition to the introduction and objectives, the overview of the thesis is displayed; briefly introducing the contents of each chapter and presenting the structure of the thesis. Subsequently the chapter closes with the state of the art of the thesis.

Chapter 2 describes the materials used in this work, including the processes used for sample preparation and the characterization techniques utilized. Sample preparation includes the manufacturing of the foam precursors by means of melt mixing and compression-molding. For the preparation of foams with a broad range of densities, two different foaming processes were used; they are explained in detail in this chapter. Subsequently the description of the different characterization techniques used is displayed.

In Chapter 3, the study of the cellular morphology of PC and composite foams are presented along with their respective carbon dioxide desorption behavior. This chapter displays the characterization of the cellular structures by means of SEM analysis. In addition, the effects of the different processing parameters on the cellular morphology displayed are analyzed. This chapter is presented in the form of published papers in international journals and conferences proceedings, preceded by a preliminary introduction as mentioned before. In chapter 3 a total of four papers are presented, two papers regarding the preparation of PC-based foams using a one-step foaming process (one for pure PC foams and the other for PC/GnP foams) and the other two regarding the foams prepared by the two-step foaming process.

Chapter 4 focuses on the analysis of the effect of carbon dioxide and the combination of carbon dioxide - graphene nanoplatelets on the microstructure of PC during processing. In this section, techniques such as Raman spectroscopy, atomic force microscopy (AFM), wide angle and small angle X-Ray scattering (WAXS and SAXS) were employed to perform qualitative and quantitative analyses of polymer microstructure changes during processing in the presence of carbon dioxide and graphene nanoplatelets. In another section, this chapter compares the thermal stabilities of the PC foams and nanocomposites foams where the effect of the presence of graphene

nanoplatelets was analyzed. Similarly, the composite foams are studied and their different thermal stabilities are discussed and related to the dispersion of graphene nanoplatelets resulted from the different foaming parameters and processes used (i.e. 1- and 2-step foaming processes). For this aim thermogravimetric analyses in both nitrogen and air atmospheres are carried out including scanning electron microscopy imaging for graphene particles observation. Finally the effects of different cellular structures, process parameters, and the presence of graphene nanoparticles on the viscoelastic properties of PC and PC-GnP composite foams are discussed. The different mechanical behaviors of the foams prepared by one and two-step foaming processes were examined by means of dynamic mechanical thermal analysis.

In Chapter 5, the electrical conductivity of the nanocomposite foams is revised by means of DC electrical resistance measurements. The different graphene nanoplatelets dispersion degrees were demonstrated when the electrical conductivity was enhanced for some of the nanocomposite foams. Also the AC electrical conductivity was measured along with the electromagnetic shielding effectiveness of the nanocomposite foams. Graphene nanoplatelets observation was supported by transmission electron microscopy imaging analysis. Additionally this chapter focuses on the thermal conductivity characterization of PC foams and PC/graphene composite foams prepared by means of one and two-step foaming processes. Thermal conductivities were measured implementing a steady state one-dimensional heat conduction method, while transmission electron microscopy revealed the graphene nanoplatelets dispersion/exfoliation within the material.

Lastly, Chapter 6 displays a general discussion and summarizes the conclusions of the polycarbonate/graphene nanocomposite foams study. In addition, this chapter provides future research activities suggestions.

The information of the publications presented in this thesis is displayed in table 1.1. The different sections of the thesis where the articles are included are also indicated. Table 1.2 shows the list of conferences where the research carried out during this thesis was presented both as oral presentations and posters. In addition, it is shown whether the presentation was subsequently published in the conference proceedings or special issues of journals, indicating if the publication is part of the thesis or complementary/collaboration work. The publications not included in this thesis are presented in table 1.3, some of which were carried out not as a fundamental part of the thesis but related to the preparation and characterization of polymeric composites and composite foams.

Table 1.1. Publications included in this thesis.

International publications	Chapter
Authors: G. Gedler, M. Antunes, V. Realinho, J.I. Velasco. **Title:** Characterization of polycarbonate foam structure prepared by one-step sc-CO_2 dissolution process. **Journal:** Proceedings of the 10th International Conference on Foam Materials & Technology-SPE-FOAMS 2012.	3
Authors: G. Gedler, M. Antunes, V. Realinho, J.I. Velasco. **Title:** Novel polycarbonate-graphene nanocomposite foams prepared by CO_2 dissolution. **Journal:** IOP Conf. Series: Materials Science and Engineering 31 (2012) 012008.	3
Authors: G. Gedler, M. Antunes, J.I. Velasco. **Title:** Polycarbonate foams with tailor-made cellular structures by controlling the dissolution temperature in a two-step supercritical carbon dioxide foaming process **Journal:** The Journal of Supercritical Fluids. 2014;88(0):66-73.	3
Authors: G. Gedler, M. Antunes, J.I. Velasco. **Title:** Effects of graphene nanoplatelets on the morphology of polycarbonate–graphene composite foams prepared by supercritical carbon dioxide two-step foaming **Journal:** The Journal of Supercritical Fluids. 2015;100:167-74.	3
Authors: G. Gedler, M. Antunes, J.I. Velasco. **Title:** Graphene-induced crystallinity of bisphenol A polycarbonate in the presence of supercritical carbon dioxide **Journal:** Polymer. 2013;54(23):6389-98.	4
Authors: G. Gedler, M. Antunes, V. Realinho, J.I. Velasco. **Title:** Thermal stability of polycarbonate-graphene nanocomposite foams. **Journal:** Polymer Degradation and Stability. 2012;97(8):1297-304.	4
Authors: G. Gedler, M. Antunes, J.I. Velasco. **Title:** Low density polycarbonate-graphene nanocomposite foams produced by supercritical carbon dioxide two-step foaming. Thermal stability. **Journal:** Composites Part B: Engineering. 2016; 92:299-306.	4
Authors: G. Gedler, M. Antunes, J.I. Velasco. **Title:** Viscoelastic properties of polycarbonate-graphene nanoplatelets nanocomposite foams. **Journal:** Composites Part B: Engineering. 2016;93:143-52.	4
Authors: G. Gedler, M. Antunes, J.I. Velasco. **Title:** Enhanced electrical conductivity in graphene-filled polycarbonate nanocomposites by microcellular foaming with sc-CO_2. **Journal:** J. of Adhesion Science and Technology. 2016;30(9):1017-29.	5
Authors: G. Gedler, M. Antunes, T. Borca-Tasciuc, J.I. Velasco, R. Ozisik **Title:** Effects of graphene nanoplatelets and cellular morphology on the thermal conductivity of polycarbonate/graphene lightweight composites. **Journal:** European Polymer Journal. 2016; 75:190-9.	5
Authors: G. Gedler, M. Antunes, J.I. Velasco, R. Ozisik. **Title:** Enhanced electromagnetic interference shielding effectiveness of polycarbonate/graphene composites foamed using supercritical carbon dioxide by a 1-step process. **Journal:** Materials and Design. 2016; 90:906-14.	5

Authors: G. Gedler, M. Antunes, J.I. Velasco, R. Ozisik. **Title:** Electromagnetic shielding effectiveness of polycarbonate/graphene nanocomposite foams processed in 2-steps with supercritical carbon dioxide. **Journal:** Materials Letters. 2015; 160:41-4.	5

The research group developing multifunctional foams at the CCP is continuously working on different projects simultaneously; therefore the research productivity is highly efficient. Table 1.2 list the works presented at different conferences in the form of posters and oral presentations throughout the almost 6 years of this thesis. As mentioned before, some of these research works were published in conference proceedings or special issues of journals afterwards. It needs to be pointed out that two of the publications in conference proceedings were included in this thesis as a basis of subsequent research. These publications show the morphological characterization of the cellular structure for the different foams prepared as can be seen in the previous table.

Some of the articles from the research in this thesis and others in collaboration with different projects within the research on multifunctional foams were published; however they were not included in this thesis. These are listed on table 1.3.

Table 1.2. List of presentations at conferences

Communications at conferences.	**Section**
Authors: G. Gedler, M. Antunes, V. Realinho, J.I. Velasco. **Title:** Novel polycarbonate-graphene nanocomposite foams prepared by CO_2 dissolution. **Conference:** 6th EEIGM International Conference on Advanced Materials Research. Nancy, France, 2011. **Presented as:** Poster	*
Authors: G. Gedler, M. Antunes, V. Realinho, J.I. Velasco. **Title:** Characterization of polycarbonate foam structure prepared by one-step sc-CO_2 dissolution process. **Conference:** 10th International Conference on Foam Processing and Technology - FOAMS 2012. Barcelona, Spain, 2012) **Presented as:** Poster	*
Authors: M. Antunes, G. Gedler, V. Realinho, J.I. Velasco. **Title:** The influence of nanoparticles on the thermal-mechanical properties of polymeric foams. **Conference:** XXIX Encuentro del Grupo Español de Fractura. Bilbao, Spain, 2012. **Presented as:** Poster	**
Authors: M. Antunes, G. Gedler, M. Mudarra, J.I. Velasco. **Title:** Multifunctional nanocomposite foams based on polypropylene with carbon nanofillers. **Conference:** 14th International Conference on Blowing Agents and Foaming	**

Processes. Berlin, Germany, 2012. **Presented as:** Oral Presentation.	
Authors: G. Gedler, M. Antunes, V. Realinho, J.I. Velasco. **Title:** Influence of graphene nanoparticles on the thermal stability of polycarbonate nanocomposite foams. **Conference:** 7th MoDeSt Conference. Prague, Czech Republic, 2012. **Presented as:** Oral Presentation.	**
Authors: G. Gedler, M. Antunes, V. Realinho, A.B. Martínez, J.I. Velasco. **Title:** Combined effects of sc-CO_2 and graphene nanoparticles on the crystallinity of bisphenol A polycarbonate. **Conference:** Third International Symposium Frontiers in Polymer Science. Sitges, Spain, 2013. **Presented as:** Poster.	
Authors: M. Antunes, V. Realinho, G. Gedler, D. Arencón, J.I. Velasco. **Title:** Diffusion of CO_2 in polymer nanocomposites containing different types of carbon nanoparticles and nanoclays for solid-state microcellular foaming applications. **Conference:** 9th International Conference on Diffusion in Solids and Liquids–DSL-2013. Madrid, Spain, 2013. **Presented as:** Oral Presentation.	**
Authors: G. Gedler, M. Antunes, M. Sánchez-Soto, M.Ll. Maspoch, J.I. Velasco. **Title:** Two-step supercritical carbon dioxide dissolution foaming of bisphenol A polycarbonate: Effects of the heating stage parameters on foam characteristics. **Conference:** 9th International Conference on Diffusion in Solids and Liquids–DSL-2013. Madrid, Spain, 2013. **Presented as:** Poster.	
Authors: M. Antunes, V. Realinho, G. Gedler, D. Arencón, J.I. Velasco. **Title:** Graphene in multifunctional polymeric materials. **Conference:** II Jornada Internacional de Innovaciones Técnicas en Plásticos. Barcelona, Spain, 2013. **Presented as:** Oral presentation.	
Authors: G. Gedler, M. Antunes, V. Realinho, J.I. Velasco. **Title:** Comportamiento mecánico dinámico de espumas de policarbonato. **Conference:** XXXI Encuentro del Grupo Español de Fractura. San Lorenzo del Escorial, Spain, 2014. **Presented as:** Oral Presentation.	**
Authors: G. Gedler, M. Antunes, J.I. Velasco. **Title:** Graphene nanoplatelets as multifunctional fillers for polymer foams. **Conference:** International conference on Diamond and Carbon Materials. Madrid, Spain, 2014. **Presented as:** Oral Presentation.	
Authors: G. Gedler, M. Antunes, D. Rende, L.S. Schadler, J.I. Velasco, R. Ozisik. **Title:** Microstructural characteristics of polycarbonate/graphene nanocomposite foams. **Conference:** 12th International Conference on Foam Materials and Technology – FOAMS 2014. New Jersey, USA, 2014. **Presented as:** Oral Presentation.	**

* Published in conference proceedings and included in this thesis (Table 1.1).

**Published in the conference proceedings/special issue not included in this thesis (Table 1.3).

Table 1.3. Other publications not included in this thesis.

Other publications
Authors: M. Antunes, G. Gedler, J.I. Velasco. **Title:** Multifunctional nanocomposites foams based on polypropylene with carbon nanofillers. **Journal:** Journal of Cellular Plastics. 49 (3): 259-79, 2013.
Authors: M. Antunes, V. Realinho, G. Gedler, D. Arencón, J.I. Velasco. **Title:** Diffusion of CO_2 in polymer nanocomposites containing different types of carbon nanoparticles for solid-state microcellular foaming applications. **Journal:** Journal of Nano Research. 26: 63-74, 2014.
Authors: Marcelo Antunes, Gabriel Gedler, Hooman Abbasi, José Ignacio Velasco. **Title:** Graphene Nanoplatelets as a Multifunctional Filler for Polymer Foams. **Journal:** Materials Today: Proceedings, Volume 3, Supplement 2, 2016, Pag S233-9.

1.3 State of the art.

Polycarbonate as an engineering thermoplastic.

Polycarbonate (PC) is one of the most versatile engineering polymers due to its attractive combination of mechanical properties, low moisture absorbency, transparency, toughness and good dimensional and thermal stability [1]. Its amorphous nature makes polycarbonate attractive for optical applications [2]. Aromatic polycarbonates derived from Bisphenol A are particularly interesting because of their useful aforementioned properties; attributable to Bisphenol A's rigid molecular structure [3-6]. Polycarbonates also offer excellent moldability and extrudability, good fire resistance and high dimensional stability, and are useful in a wide range of industrial applications [7-8]. Other properties such as modulus, dielectric strength and tensile strength are comparable to other amorphous thermoplastics at similar temperatures below their respective glass transition temperatures (Tgs). However, while most amorphous polymers are stiff and brittle below their Tg values, polycarbonate retains its ductility and impact resistance below its Tg values (~150^{o}C) [7]. Although Polycarbonate is well known as an amorphous polymer, it has been shown that it can crystallize under certain conditions. In 1966 Bonart [9] published a study which characterized the crystalline structure of Polycarbonates. More recently, Sohn et al. [10] studied PC's multiple melting behavior, and found the presence of primary and secondary crystals. Zhai et al. [11] also showed the crystallinity of PC, in this case in the presence of supercritical Carbon Dioxide ($scCO_2$) that acted as a plasticizer displaying the double melting behavior previously observed by Sohn. Other solvents have been used to induce crystallization in PC. Fan et al. [12]

used acetone in PC and observed the double melting behavior of PC crystals. Therefore, the processing of PC has to be taken into account in order to control its microstructure.

Graphene as multifunctional material.

In the past few years, graphene (the basic building block of all graphitic forms of carbon [13] consisting of an isolated single atomic layer of graphite, an ideal realization of such a two-dimensional system [14]) has attracted a great deal of attention due to its incorporation into polymer matrices for development of graphene-based composites [15]. Because graphene displays high mechanical properties (Young modulus of 1 TPa and breaking strength of 40 N/m [16]), the addition of a filler with such impressive mechanical properties would be expected to lead to significant improvements in the mechanical properties of the host polymer matrix [17]. In addition, graphene's excellent transport properties makes it suitable for developing conductive nanocomposites, which could be useful for electronic applications [18]. Graphene synthesis has been widely reported, however it is still not easy to prepare graphene monolayer in large quantities. Graphene monolayers are often prepared by different methods such as micromechanical cleavage (repeated peeling/exfoliation) of small mesas of highly oriented pyrolytic graphite [19], by chemical vapor deposition (CVD) [20], by chemical oxida- tion-reduction methods , by epitaxial growth on SiC [21], by plasma deposition techniques [22], chemical conversion [23], unzipping carbon nanotubes [24] among others. The use of a few layers of graphene or graphene nanoplatelets (GnP) and graphene oxide is commonly used in polymeric composites for multifunctional properties purposes. Zhu et al. [25] prepared graphene oxide by exfoliation and dispersion in propylene carbonate by bath sonication. Qi et al. [26] prepared graphene platelets by a one-step thermal exfoliation and reduction of graphite oxide, subsequently they prepared PS/Graphene composites by solution mixing and compressing-molding. They reported the formation of a conduction network thus promoting an enhanced electrical conductivity for the PS/graphene composites. Rafiee et al. [27] prepared few-layered graphene sheets by firstly oxidizing graphite in a solution of sulfuric acid, nitric acid, and potassium chlorate obtaining graphite oxide, then thermal exfoliation of graphite oxide took place by rapid heating (>2000 ^{o}C min^{-1}). The graphene was solution mixed with PMC (1-octadecanol (stearyl alcohol)) composite exhibiting an enhanced thermal conductivity [28]. They also prepared epoxy/graphene by unzipping MWCNT. The composites with 0.3% weight fraction of nanofillers exhibited 30% increase of Young's modulus as compared to its MWCNT composite counterpart. Ramanathan et al. [29] prepared PMMA/graphene composites by

solution mixing. The resulting composites demonstrated that reduced particle size, high surface area, and increased surface roughness can significantly alter the graphene/polymer interface and enhance the mechanical, thermal, and electrical properties of the polymer matrix.

Polycarbonate composites.

Polycarbonate has been widely used for composites applications. Fillers such as nanoclays, carbon nanofibers (CNF), carbon nanotubes (CNT) including single-walled carbon nanotubes (SWCNT) and multi-walled carbon nanotubes (MWCNT) are the most common fillers used in Polycarbonate composites. Yoon et al. [30] prepared PC/organoclay composites by extrusion. The composites exhibited tactoids structures containing intercalated polymer. Increments in modulus were attributed to partially exfoliated platelets within PC. Lee et al. [31] prepared PC/natural montmorillonite by extrusion. Increment in dynamic moduli was attributed to an increase in the surface area of dispersed and partially exfoliated layered silicates as the concentration of fillers was increased. Hsieh et al. [32] investigated the effect of clay loading on the mechanical behavior and melt state linear viscoelastic properties of intercalated PC nanocomposites. They reported that at low frequency the linear dynamic oscillatory moduli data revealed diminished frequency dependence with increasing nanoclay loading. The nanocomposites also exhibited a significant decrease in the extent of tensile elongation and ductility with respect to the nanoclay incorporation. Nayak et al. [33] prepared PC/layered silicate nanocomposites by melt blending technique followed by injection molding. Morphological observation revealed that the organoclay platelets were exfoliated thus the mechanical and thermal behavior of PC matrix was enhanced for 3 wt.% of fillers content. In the case of PC/CNF composites there is a wide range of publications [34]. Higgins et al. [35] prepared PC/CNF composites by in situ polymerization and subsequently compression-molded. The composites exhibit an electrical conductivity percolation threshold of 6.3 wt% and an increase in thermal stability of 40 ^{o}C as the CNF loading increases from 0 to 9 wt%. Kumar el al. [36] prepared PC composites adding carbon nanofibers (CNF) by solution mixing. The composites exhibit a 282% increment of the storage modulus at 165 ^{o}C as compared to pure PC. In addition an enhanced DC electrical conductivity (up to 10^{-2} S/m for 3 wt.% of CNFs) was attributed to the well dispersed fillers. CNTs are one of the most common fillers used in PC composites [37-44]. Potschke et al [45] prepared PC composites with different amounts of multiwalled carbon nanotubes (MWNT) by melt mixing, they reported an excellent dispersion observed by TEM and an electrical percolation of MWNT between 1and 1.5 wt%. Pande et al. [38] prepared PC/MWCNT

using solvent casting and a combination of solvent casting and compression molding techniques for electrostatic discharge (ESD) and electromagnetic interference (EMI) shielding applications. Composite films at 20 wt% loading reached 43 dB in the X-band (8.2–12.4 GHz). The primary mechanism of shielding was absorption, suggesting possible use as an EMI absorbing material. By using low pressure in compression molding the EMI shielding properties of bulk composites (2 mm thickness) improved by about 14 dB at 10 wt% MWCNT loading. More recently, Bautista-Quijano et al. [46] prepared PC/MWCNT composites by melt mixing and subsequently prepared monofilament fibers by melt spinning with conductive properties, finding that piezoresistivity effects could be characterized only for fibers with MWCNT amounts of 3 wt% or higher. Koratkar et al. [47] prepared PC/SWCNT composites by a solution mixing. The loss modulus increased with the addition of 2% weight fraction of oxidized single-walled nanotube fillers. They showed that the increase in damping was derived from frictional sliding at the nanotube-polymer interfaces. The nanosize of CNTs resulted in large interfacial contact area, generating high damping efficiency.

The addition of nanosized ceramics to PC also has been used allowing tailoring of its properties such as thermomechanical and optical. The incorporation of ceramic fillers such as alumina and silica (silicon dioxide) has been reported. Hanemann et al. [48] reported the impact of nanosized alumina to PC. The composites were prepared by extrusion. The refractive indices of the polycarbonate-alumina-composites increased with increasing filler content attributed to nanoparticles agglomeration. Although the Young's modulus remained almost constant, the impact strength as well as the glass transition temperature were reduced with increasing nanofiller content attributed to polymer degradation. However the agglomeration of fillers could have been one of the causes of the deterioration of those properties. Hakimelahi et al. [49] reported the preparation of transparent nanocomposite films fabricated by blending a concentrated nanocomposite formed by in-situ polymerization of polycarbonate in the presence of alumina nanowhisker with PC. Functionalization of alumina nanowhisker enhanced tensile properties (Young's modulus and tensile strength) relative to the pure polycarbonate and blends produced with raw alumina nanowhisker, attributed to the interaction between polymer matrix and fillers during polymerization. The use of other ceramic fillers has been attempted. Motaung et al. [50] prepared PC/silica nanocomposites with different silica quantities by melt mixing. The addition of 1 wt.% silica content showed a decrease in the storage and loss moduli below the glass transition temperature, attributed to plasticization effect. However, an increase in the amount of silica increased the moduli. The presence of silica in PC slightly increased the thermal stability, except for

high (5 wt.%) silica content which showed a decrease. Yang et al. [51] prepared PC/silica by single-screw extrusion. The composites exhibited improved mechanical performance, thermal stabilities (up to 30 ^{o}C) and flammability behavior according to vertical burning tests, attributed to strong interfacial interactions and good particle dispersion.

Polycarbonate/graphene composites.

Polycarbonate as a thermoplastic material, which has been the subject of extensive research due to its potential use in applications such as a matrix for advanced composite material seems to be one of the ideal candidates for the development of graphene-based polymer composites. Recently, Polycarbonate composites containing graphene have been recommended for applications that require the combination of good transport and mechanical properties. Because of the aforementioned properties of graphene, this is considered a good candidate to give multifunctional properties to polymeric matrices such as PC. However, there is still a lack of studies regarding PC/graphene composites. Kim et al. [52] prepared PC/graphene composites by means of conventional melt-compounding and injection molding, and reported enhanced electrical conductivity compared to the pure PC, reaching values of 10^{-9} S/m for composites containing approximately 2 wt.% of graphene. Composite properties were influenced by both dispersion and orientation of graphene particles. King et al. [53] prepared polycarbonate/graphene composites by extrusion followed by injection molding from a commercial masterbatch. They reported electrical resistivity values of $2.8x10^{4}$ ohm-cm, a thermal conductivity of 0.48 W/m.K and a tensile modulus of 5.9 GPa at 15 wt% of graphene, finding enhanced properties when compared to pure PC, which was attributed to the presence of conductive and stiffer fillers. Yoonessi et al. [54] prepared PC/graphene composites with 0.14 vol.% of graphene by the emulsion method. They also prepared composites by solution mixing followed by compression molding (0.38 Vol.% graphene), and reported electrical conductivities of 10^{-7} S/m. This was attributed to the improved dispersion of the graphene particles, promoted by the emulsion preparation method. Potts et al. [55] stated to present the first report of polymer composites using microwave-exfoliated graphite oxide (MEGO). They produced PC/MEGO composites at various loadings and evaluated their morphology and properties. The composites showed significant increases in electrical conductivity, with an onset of electrical percolation around 1.3wt% of MEGO. They reported the improvements in stiffness while rheological measurements suggested an onset of connectivity percolation (2.1 wt.%). Jun et al. [56] prepared nanocomposites of PC/graphene (0.5 wt.%) by solution mixing and reported that the

rheology of PC can be modified by the addition of small graphene content. They stated that graphene can be utilized as a flow modifier for PC in various applications such as polymer composites and a coating process.

Polycarbonate foams.

Polymeric materials and Polycarbonate in particular are widely used in many important applications, including appliances, electronics, packaging and vehicles components, to name a few. By reducing the weight of polymeric materials via inducing the formation of a cellular structure, the range of potential applications broadens. Polymeric foams, characterized by their exceptional lightness, have become increasingly prominent in industrial applications in which weight is a key factor [57]. Both the volume of material used and weight of foams is extremely low, and may be of immense benefit to industries such as transportation and aerospace, in which costs are driven by power and fuel usage. A significant weight reduction in materials could lead to remarkable reductions in energy and cost.

The preparation of thermoplastic polymeric foams is mainly carried out by chemical and physical foaming [58-59]. In this thesis the foaming process considered is physical foaming. In which different gases can be used as physical blowing agents. Nitrogen (N_2) and Carbon Dioxide (CO_2) are two of the most common gases used as blowing agents [60-62]. In this research, carbon dioxide is selected as the blowing agent due to its combination of chemical inertness, non-flammability and mild supercritical conditions (Tc = 31 ºC, Pc = 7,38 MPa) [63], and its well known plasticizing effect in a remarkable number of thermoplastics including Polycarbonate [63-65], which facilitates ease of the foaming process. Another advantage of using CO_2 as a physical blowing agent is that the cell structure may be controlled through the processing temperature and pressure, enabling optimization of the foam properties [66]. Because it is known that foaming reduces the mechanical properties of the solid base materials, an evenly distributed micrometric-sized closed cell structure is desirable in order to counteract the effect of foaming on decrementing the mechanical behavior of the base polymer [67].

Since microcellular foams were developed in the early 1980s [68], different preparation techniques have emerged. For instance, the batch foaming process [69-70] (which is the technique used in this work), the extrusion foaming [61, 71] and injection molding foaming (Mucell®) [72-75]

are the most common. These techniques induce the thermodynamic instability needed for nucleation and growth of cells to take place [76], the so called foaming. In the batch process [69], gases (blowing agents) are dissolved into the polymer commonly under high pressure and temperature. The thermodynamic instability is then caused when the pressure is dropped, causing foaming to occur. In the extrusion process [61], the gas is introduced to the polymer melt. Subsequently when the material leaves the extruder, a rapid pressure drop causes foaming. Similarly, in the injection molding foaming process [73-74], the gas is added to the melt polymer while traveling through the screw. When the mix gas/polymer enters the mold, the pressure drop induces foaming. As a variation of the batch foaming process, the so-called solid-state foaming process [77] uses low temperatures and low pressures (below T_g) to dissolve the gases into the polymers, using a batch process in which the sample does not leave the solid/rigid phase during the blowing agent dissolution. Then a thermodynamic instability is caused when the sample is heated generally in a hot bath inducing the thermal instability needed for foaming.

Polycarbonate foams have been prepared using the aforementioned foaming processes [78-81]. For Instance, PC foams with cell sizes ranging from 1 to 10 μm were prepared by extrusion and the solid-state method, producing foams with high cell densities but lacking both small cells and low foam density [77, 79]. Lee et al. [82] reported the development of high cell density PC foams with low densities by extrusion, however the presence of open cells content was detected, which could be detrimental for the final mechanical properties of the PC foams. On the other hand, Mascia et al. [78] reported the preparation of closed-cells PC foams using a batch foaming process, which produced foams with cell sizes ranging from 20 to 40 μm. Although, the densities of foams were not reported, the development of crystalline structures in PC foams measured by Wide angle X-ray scattering (WAXS) and differential scanning calorimetry (DSC) was reported, revealing the effect of the foaming process on the PC microstructure. This process could be advantageous in terms of mechanical properties.

Polycarbonate composite foams.

Current trends focus on improving the specific mechanical response of PC microcellular foams while adding functional properties and taking into consideration both the material's composition and cellular structure control [83]. Producing cellular structures with smaller and uniform cell sizes is necessary to improve the specific mechanical properties. A common solution to this problem is

the use of fillers that act as nucleation sites, helping all cells nucleate simultaneously after rapid depressurization. These fillers could be considered heterogeneous nucleating agents [84] and depending on their characteristics, may also act as nanoreinforcements and add multifunctional characteristics to the composite foam [85].

Fillers such as clay particles have been incorporated into PC foams looking for mechanical and gas barrier properties enhancements. Mitsunaga et al.[86] prepared PC/clay nanocomposites, reporting that intercalation of clay particles had a nucleation effect, displaying smaller cell sizes as compared to the pure PC foams. This remarkably enhanced the mechanical properties of the composites when compared to PC without clay. Ito et al. [87] investigated the influence of clay loading to the morphology of PC/clay foams, they reported that the dispersion of clay particles hinder CO_2 diffusion under a low saturation CO_2 pressure (10 MPa) by creating a more tortuous path. While at higher saturation pressures a large population of cell nuclei formed upon depressurization, changing the cellular morphology from microcellular (20 μm) to nanocellular (600 nm). They stated that the incorporation of nanoclay induced heterogeneous nucleation because of a lower activation energy barrier compared with homogeneous nucleation. Polycarbonate foams with other types of fillers such as fiber glass, silica and wood fibers have been study and patented [88-89].

Carbon fillers such as carbon nanofibres (CNF) and carbon nanotubes (CNT) have been used in polymeric composites foams to enhance not only the mechanical properties of the foams but also the transport properties [70, 83, 90]. In the case of Polycarbonate, Monnereau et al. [91] prepared PC/MWCNT composite foams by means of melt mixing and compression-molding followed by solid state foaming (saturating with CO_2 and then heated to induce foaming). They produced foams with densities down to 0.65 g/cm^3, cell sizes of 2 to 30 μm and cell densities of 10^{11} cells/cm^3 for 2 wt.% MWCNT content. In addition 20% crystallinity induced after the process was reported.

Polymer/graphene composite foams.

More recently graphene nanoplatelets have attracted a great deal of interest due to their high theoretical properties and particularly flat morphology [13, 17]. The fact that graphene not only displays high mechanical properties [16], but also excellent transport properties [18] suggests that

graphene nanoplatelets may be a good candidate for adding multifunctional properties to lightweight composite foams. Currently, the application of graphene in the field of nanocomposites is increasing rapidly [17, 92-93]. Thus, the combination of its favorable properties with its good thermal stability could lead to the development of polymer nanocomposites foams with specific tailored properties.

It has been shown that Polycarbonate has an excellent affinity for carbon dioxide, enabling relatively high solubility and rates of diffusion compared to other gas-polymer systems. Microcellular Polycarbonate presents a very uniform, homogeneous cellular structure with many desirable properties [94]. This affinity might induce changes in the Polycarbonate microstructure particularly in the presence of an inorganic phase such as graphene nanoplatelets. Microstructural changes could lead to effects on cellular morphology, as well as thermal, mechanical and transport properties of the final foams. It has also been found that in all foams, foam density is the primary structural variable that governs mechanical behavior [95]. Therefore, a detailed understanding of how foam density, cell sizes and microstructure of polymers are affected by different processing conditions is necessary before a full evaluation of the mechanical, thermal and transport properties of a given microcellular system can be completed.

A full understanding of polymeric foams filled with graphene nanoplatelets remains evasive, mainly due to their multiphase nature, a direct result of the combination of a complex developed cellular structure and polymer microstructure [96]. The influence of the foaming conditions has been considered in order to decrease cell size while incorporating inorganic functional fillers [97].

Despite increasing interest in the preparation and characterization of polymer nanocomposite foams, investigation into the dynamic mechanical thermal behavior of these materials remains scarce. For instance, the effective mechanical reinforcement effect of graphene nanoplatelets in PP foams prepared by CO_2 dissolution foaming was reported [85], which was related to a homogeneous cellular structure with high cell densities.

Generally, the addition of graphene nanoplatelets to polymer foams has proven beneficial not only with regard to mechanical properties but also for multifunctional properties. Antunes et al. [83] recently showed that physical foaming using supercritical carbon dioxide may further enhance the electrical conductivity of composites containing conductive carbon-based nanofillers while

lowering their density. This was attributed to an improved dispersion of the nanofillers and preferential orientation within cell walls during foaming, promoting an efficient interconnected conductive network throughout the material [83, 98-99]. The enhanced electrical conductivity of polymer/graphene nanocomposite foams has been reviewed for polymers such as PMMA [99] and PVDF [100]. Ultimately, these systems exhibit enhanced electromagnetic interference shielding properties [101]. In addition, Ling et al. [102] reported the electrical conductivity of PEI/graphene nanocomposite foams, which was 10^{-5} S/cm for 10 wt.% of graphene content. This was advantageous for electromagnetic interference shielding effectiveness (EMI SE) that took place throughout absorption (10dB) of the electromagnetic waves in the X-band (~8-12 GHz). This electromagnetic interference consists of many unwanted radiated signals which can cause unacceptable degradation of system or equipment performance, a consequence of the increasing complexity of electronic devices/systems in the form of higher packing density for quick response [103]. The EMI shielding effectiveness of a material measures the ability to attenuate electromagnetic waves [104]. Electromagnetic interference protection is required for applications in electronics, aerospace and any industry that requires protection for electronics. The development of polymeric nanocomposite foams with EMI shielding properties provides an opportunity to replace conventional metals that exhibit disadvantageous characteristics such as high densities, easy corrosion and costly processing.

Regarding thermal conductivity of polymeric foams, only few studies have used the addition of carbon fillers into cellular composite materials for thermal conductivity characterization. Antunes et al. [105] studied the thermal conductivity behavior of PP-CNF composite foams. The fillers were not efficient in increasing the thermal conductivity of composites, and the resulting value was independent of CNF's volume fraction. Because graphene displays a thermal conductivity at room temperature of 3000 W/mK [106], is suitable for the preparation of thermally conductive cellular composites. Verdejo et al. [107] reported the enhancement of 6% of thermal conductivity of silicone foams with 0.25 wt. % of graphene nanoplatelets. Yan et al. [108] prepared rigid polyurethane foam (RPUF) nanocomposites based on graphene. They reported that changes in the thermal conductivity of the nanocomposites were negligible. Due to the lack of studies regarding thermal conductivity behavior of thermoplastic/graphene composite foams, this topic is studied in this thesis.

Polycarbonate/graphene composite foams.

More recently, Ma et al. [109] prepared PC/graphene oxide (GO) and PC/graphene nanocomposites by solution mixing, then foaming by saturating with CO_2 and immersion in a preheated hot oil bath to induce cell nucleation and growth. They reported cell sizes of the order of a few micrometers (up to 5 μm) and cell densities of the order of 10^{11} cell/cm^3. Enhanced electrical conductivity of the composite foams was observed, nanocomposite foams exhibited similar or even higher electrical conductivity in comparison to their solid counterparts for PC/GO foams. Additionally, for PC/graphene, a slight decrease in electrical conductivity after foaming was observed, perhaps due to the high interaction between particles enabling a better dispersion within the matrix.

The ability to produce a family of Polycarbonate/graphene foams provides an opportunity to explore the effect of process parameters on the morphology and microstructure of nanocomposite foams, as well as the multifuctional properties of these cellular materials.

1.4 References

[1] Jang BN, Wilkie CA. A TGA/FTIR and mass spectral study on the thermal degradation of bisphenol A polycarbonate. Polymer Degradation and Stability. 2004;86(3):419-30.

[2] Janković B. A kinetic study of the isothermal degradation process of Lexan® using the conventional and Weibull kinetic analysis. J Polym Res. 2009;16(3):213-30.

[3] Park J, Hyun J, Kim W, Kim S, Ryu S. Extensional and complex viscosities of linear and branched polycarbonate blends. Macromol Res. 2002;10(3):135-9.

[4] Liu ZQ, Cunha AM, Yi XS, Bernardo AC. Key properties to understand the performance of polycarbonate reprocessed by injection molding. Journal of Applied Polymer Science. 2000;77(6):1393-400.

[5] Lee J-Y, Song C-H, Kim J-I, Kim J-H. Preparation of Aromatic Polycarbonate Nanoparticles using Supercritical Carbon Dioxide. Journal of Nanoparticle Research. 2002;4(1-2):53-9.

[6] Kricheldorf HR, Luebbers D. Polymers of carbonic acid. 3. Thermotropic polycarbonates derived from 4,4'-dihydroxybiphenyl and various diphenols. Macromolecules. 1990;23(10):2656-62.

[7] Mark H. Polycarbonates. In Encyclopedia of Polymer Science and Technology. New York, NY: John Wiley & Sons, Inc; 2004.

[8] Ballistreri A, Montaudo G, Scamporrino E, Puglisi C, Vitalini D, Cucinella S. Intumescent flame retardants for polymers. IV. The polycarbonate–aromatic sulfonates system. Journal of Polymer Science Part A: Polymer Chemistry. 1988;26(8):2113-27.

[9] Bonart VR. Zur kristallstruktur der polycarbonate aus 4,4′-dihydroxydiphenyl-2,2-propan, 4,4′-dihydroxydiphenylsulfid und 4,4′-dihydroxydiphenylmethan. Die Makromolekulare Chemie. 1966;92(1):149-69.

[10] Sohn S, Alizadeh A, Marand H. On the multiple melting behavior of bisphenol-A polycarbonate. Polymer. 2000;41(25):8879-86.

[11] Zhai W, Yu J, Ma W, He J. Influence of Long-Chain Branching on the Crystallization and Melting Behavior of Polycarbonates in Supercritical CO2. Macromolecules. 2006;40(1):73-80.

[12] Fan Z, Shu C, Yu Y, Zaporojtchenko V, Faupel F. Vapor-induced crystallization behavior of bisphenol-A polycarbonate. Polymer Engineering & Science. 2006;46(6):729-34.

[13] Geim AK, Novoselov KS. The rise of graphene. Nat Mater. 2007;6(3):183-91.

[14] Zhang Y, Tan Y-W, Stormer HL, Kim P. Experimental observation of the quantum Hall effect and Berry's phase in graphene. Nature. 2005;438(7065):201-4.

[15] Galpaya D, Wang M, Meinan. L, Motta N, Waclawik E, Yan C. Recent Advances in Fabrication and Characterization of Graphene-Polymer Nanocomposites. Graphene. 2012;1(2):30-49.

[16] Lee C, Wei X, Kysar JW, Hone J. Measurement of the Elastic Properties and Intrinsic Strength of Monolayer Graphene. Science. 2008;321(5887):385-8.

[17] Young RJ, Kinloch IA, Gong L, Novoselov KS. The mechanics of graphene nanocomposites: A review. Composites Science and Technology. 2012;72(12):1459-76.

[18] Kuilla T, Bhadra S, Yao D, Kim NH, Bose S, Lee JH. Recent advances in graphene based polymer composites. Progress in Polymer Science (Oxford). 2010;35(11):1350-75.

[19] Novoselov KS, Geim AK, Morozov SV, Jiang D, Zhang Y, Dubonos SV, et al. Electric Field Effect in Atomically Thin Carbon Films. Science. 2004;306(5696):666-9.

[20] Kim KS, Zhao Y, Jang H, Lee SY, Kim JM, Kim KS, et al. Large-scale pattern growth of graphene films for stretchable transparent electrodes. Nature. 2009;457(7230):706-10.

[21] Seyller T, Bostwick A, Emtsev KV, Horn K, Ley L, McChesney JL, et al. Epitaxial graphene: a new material. physica status solidi (b). 2008;245(7):1436-46.

[22] Zhang H, Feng PX. Fabrication and characterization of few-layer graphene. Carbon. 2010;48(2):359-64.

[23] Zhi L, Mullen K. A bottom-up approach from molecular nanographenes to unconventional carbon materials. Journal of Materials Chemistry. 2008;18(13):1472-84.

[24] Jiao L, Zhang L, Wang X, Diankov G, Dai H. Narrow graphene nanoribbons from carbon nanotubes. Nature. 2009;458(7240):877-80.

[25] Zhu Y, Stoller MD, Cai W, Velamakanni A, Piner RD, Chen D, et al. Exfoliation of Graphite Oxide in Propylene Carbonate and Thermal Reduction of the Resulting Graphene Oxide Platelets. ACS Nano. 2010;4(2):1227-33.

[26] Qi X-Y, Yan D, Jiang Z, Cao Y-K, Yu Z-Z, Yavari F, et al. Enhanced Electrical Conductivity in Polystyrene Nanocomposites at Ultra-Low Graphene Content. ACS Applied Materials & Interfaces. 2011;3(8):3130-3.

[27] Rafiee J, Rafiee MA, Yu Z-Z, Koratkar N. Superhydrophobic to Superhydrophilic Wetting Control in Graphene Films. Advanced Materials. 2010;22(19):2151-4.

[28] Yavari F, Fard HR, Pashayi K, Rafiee MA, Zamiri A, Yu Z, et al. Enhanced Thermal Conductivity in a Nanostructured Phase Change Composite due to Low Concentration Graphene Additives. The Journal of Physical Chemistry C. 2011;115(17):8753-8.

[29] Ramanathan T, Stankovich S, Dikin DA, Liu H, Shen H, Nguyen ST, et al. Graphitic nanofillers in PMMA nanocomposites—An investigation of particle size and dispersion and their influence on nanocomposite properties. Journal of Polymer Science Part B: Polymer Physics. 2007;45(15):2097-112.

[30] Yoon PJ, Hunter DL, Paul DR. Polycarbonate nanocomposites. Part 1. Effect of organoclay structure on morphology and properties. Polymer. 2003;44(18):5323-39.

[31] Lee KM, Han CD. Effect of hydrogen bonding on the rheology of polycarbonate/organoclay nanocomposites. Polymer. 2003;44(16):4573-88.

[32] Hsieh AJ, Moy P, Beyer FL, Madison P, Napadensky E, Ren J, et al. Mechanical response and rheological properties of polycarbonate layered-silicate nanocomposites. Polymer Engineering & Science. 2004;44(5):825-37.

[33] Nayak SK, Mohanty S, Samal SK. Retracted: Mechanical and thermal properties enhancement of polycarbonate nanocomposites prepared by melt compounding. Journal of Applied Polymer Science. 2010;117(4):2101-12.

[34] Choi YK, Sugimoto KI, Song SM, Endo M. Mechanical and thermal properties of vapor-grown carbon nanofiber and polycarbonate composite sheets. Materials Letters. 2005;59(27):3514-20.

[35] Higgins BA, Brittain WJ. Polycarbonate carbon nanofiber composites. European Polymer Journal. 2005;41(5):889-93.

[36] Kumar S, Lively B, Sun LL, Li B, Zhong WH. Highly dispersed and electrically conductive polycarbonate/oxidized carbon nanofiber composites for electrostatic dissipation applications. Carbon. 2010;48(13):3846-57.

[37] Loutfy R, Withers JC, Abdelkader M, Sennett M. Carbon Nanotube-Polycarbonate Composites. In: Ōsawa E, ed. Perspectives of Fullerene Nanotechnology: Springer Netherlands 2002, p. 317-25.

[38] Pande S, Chaudhary A, Patel D, Singh BP, Mathur RB. Mechanical and electrical properties of multiwall carbon nanotube/polycarbonate composites for electrostatic discharge and electromagnetic interference shielding applications. RSC Advances. 2014;4(27):13839-49.

[39] Zhang W, Suhr J, Koratkar N. Carbon Nanotube/Polycarbonate Composites as Multifunctional Strain Sensors. Journal of Nanoscience and Nanotechnology. 2006;6(4):960-4.

[40] Scardaci V, Sun Z, Wang F, Rozhin AG, Hasan T, Hennrich F, et al. Carbon Nanotube Polycarbonate Composites for Ultrafast Lasers. Advanced Materials. 2008;20(21):4040-3.

[41] Chen L, Pang X-J, Yu Z-L. Study on polycarbonate/multi-walled carbon nanotubes composite produced by melt processing. Materials Science and Engineering: A. 2007;457(1–2):287-91.

[42] Pegel S, Pötschke P, Petzold G, Alig I, Dudkin SM, Lellinger D. Dispersion, agglomeration, and network formation of multiwalled carbon nanotubes in polycarbonate melts. Polymer. 2008;49(4):974-84.

[43] Ding W, Eitan A, Fisher FT, Chen X, Dikin DA, Andrews R, et al. Direct Observation of Polymer Sheathing in Carbon Nanotube−Polycarbonate Composites. Nano Letters. 2003;3(11):1593-7.

[44] Handge UA, Pötschke P. Deformation and orientation during shear and elongation of a polycarbonate/carbon nanotubes composite in the melt. Rheol Acta. 2007;46(6):889-98.

[45] Pötschke P, Bhattacharyya AR, Janke A. Carbon nanotube-filled polycarbonate composites produced by melt mixing and their use in blends with polyethylene. Carbon. 2004;42(5–6):965-9.

[46] Bautista-Quijano JR, Pötschke P, Brünig H, Heinrich G. Strain sensing, electrical and mechanical properties of polycarbonate/multiwall carbon nanotube monofilament fibers fabricated by melt spinning. Polymer. 2016;82:181-9.

[47] Koratkar NA, Suhr J, Joshi A, Kane RS, Schadler LS, Ajayan PM, et al. Characterizing energy dissipation in single-walled carbon nanotube polycarbonate composites. Applied Physics Letters. 2005;87(6):-.

[48] Hanemann T, Haußelt J, Ritzhaupt-Kleissl E. Compounding, micro injection moulding and characterisation of polycarbonate-nanosized alumina-composites for application in microoptics. Microsyst Technol. 2009;15(3):421-7.

[49] Hakimelahi HR, Hu L, Rupp BB, Coleman MR. Synthesis and characterization of transparent alumina reinforced polycarbonate nanocomposite. Polymer. 2010;51(12):2494-502.

[50] Motaung TE, Saladino ML, Luyt AS, Chillura Martino DF. The effect of silica nanoparticles on the morphology, mechanical properties and thermal degradation kinetics of polycarbonate. Composites Science and Technology. 2012;73(0):34-9.

[51] Yang F, Nelson GL. Polymer/silica nanocomposites prepared via extrusion. Polymers for Advanced Technologies. 2006;17(4):320-6.

[52] Kim H, Macosko CW. Processing-property relationships of polycarbonate/graphene composites. Polymer. 2009;50(15):3797-809.

[53] King JA, Via MD, Morrison FA, Wiese KR, Beach EA, Cieslinski MJ, et al. Characterization of exfoliated graphite nanoplatelets/polycarbonate composites: electrical and thermal conductivity, and tensile, flexural, and rheological properties. Journal of Composite Materials. 2012;46(9):1029-39.

[54] Yoonessi M, Gaier JR. Highly Conductive Multifunctional Graphene Polycarbonate Nanocomposites. ACS Nano. 2010;4(12):7211-20.

[55] Potts JR, Murali S, Zhu Y, Zhao X, Ruoff RS. Microwave-Exfoliated Graphite Oxide/Polycarbonate Composites. Macromolecules. 2011;44(16):6488-95.

[56] Il Jun S, Sang Lee H. Negative normal stress differences in graphene/polycarbonate composites. Applied Physics Letters. 2012;100(16):-.

[57] Landrock A. Handbook of Plastic Foams. New Jersey: Noyes; 1995.

[58] Antunes M, Velasco JI, Realinho V, Martínez AB, Rodríguez-Pérez M-Á, de Saja JA. Heat Transfer in Polypropylene-Based Foams Produced Using Different Foaming Processes. Advanced Engineering Materials. 2009;11(10):811-7.

[59] Antunes M, Realinho V, Velasco JI. Study of the Influence of the Pressure Drop Rate on the Foaming Behavior and Dynamic-Mechanical Properties of CO2 Dissolution Microcellular Polypropylene Foams. Journal of Cellular Plastics. 2010;46(6):551-71.

[60] Di Maio E, Mensitieri G, Iannace S, Nicolais L, Li W, Flumerfelt RW. Structure optimization of polycaprolactone foams by using mixtures of CO2 and N2 as blowing agents. Polymer Engineering & Science. 2005;45(3):432-41.

[61] Park CB, Baldwin DF, Suh NP. Effect of the pressure drop rate on cell nucleation in continuous processing of microcellular polymers. Polymer Engineering & Science. 1995;35(5):432-40.

[62] Gómez-gómez JF, Arencón D, Sánchez-soto MA, Martínez AB. Influence of the Injection-Molding Parameters on the Cellular Structure and Thermo-Mechanical Properties of Ethylene-Propylene Block Copolymer Foams. Advances in Polymer Technology. 2013;32(S1):E692-E704.

[63] Cooper AI. Polymer synthesis and processing using supercritical carbon dioxide. Journal of Materials Chemistry. 2000;10(2):207-34.

[64] Lan Q, Yu J, Zhang J, He J. Enhanced Crystallization of Bisphenol A Polycarbonate in Thin and Ultrathin Films by Supercritical Carbon Dioxide. Macromolecules. 2011;44(14):5743-9.

[65] Hu X, Lesser AJ. Enhanced crystallization of bisphenol-A polycarbonate by nano-scale clays in the presence of supercritical carbon dioxide. Polymer. 2004;45(7):2333-40.

[66] Yun MS, Lee WI. Analysis of bubble nucleation and growth in the pultrusion process of phenolic foam composites. Composites Science and Technology. 2008;68(1):202-8.

[67] Lee LJ, Zeng C, Cao X, Han X, Shen J, Xu G. Polymer nanocomposite foams. Composites Science and Technology. 2005;65(15–16):2344-63.

[68] Matini J, Waldman FA, Suh NP. The production and analysis of microcellular thermoplastic foams. SPE ANTEC Technol; p. 674.

[69] Urbanczyk L, Calberg C, Detrembleur C, Jérôme C, Alexandre M. Batch foaming of SAN/clay nanocomposites with scCO2: A very tunable way of controlling the cellular morphology. Polymer. 2010;51(15):3520-31.

[70] Zhai W, Wang J, Chen N, Naguib HE, Park CB. The orientation of carbon nanotubes in poly(ethylene-co-octene) microcellular foaming and its suppression effect on cell coalescence. Polymer Engineering & Science. 2012;52(10):2078-89.

[71] Lee YH, Wang KH, Park CB, Sain M. Effects of clay dispersion on the foam morphology of LDPE/clay nanocomposites. Journal of Applied Polymer Science. 2007;103(4):2129-34.

[72] Spörrer ANJ, Altstädt V. Controlling Morphology of Injection Molded Structural Foams by Mold Design and Processing Parameters. Journal of Cellular Plastics. 2007;43(4-5):313-30.

[73] Tomasko DL, Burley A, Feng L, Yeh S-K, Miyazono K, Nirmal-Kumar S, et al. Development of CO2 for polymer foam applications. The Journal of Supercritical Fluids. 2009;47(3):493-9.

[74] Gómez-Gómez FJ, Arencón D, Sánchez-Soto MÁ, Martínez AB. Influence of the injection moulding parameters on the microstructure and thermal properties of microcellular polyethylene terephthalate glycol foams. Journal of Cellular Plastics. 2013;49(1):47-63.

[75] Xi Z, Sha X, Liu T, Zhao L. Microcellular injection molding of polypropylene and glass fiber composites with supercritical nitrogen. Journal of Cellular Plastics. 2014;50(5):489-505.

[76] Baldwin DF, Park CB, Suh NP. A microcellular processing study of poly(ethylene terephthalate) in the amorphous and semicrystalline states. Part I: Microcell nucleation. Polymer Engineering & Science. 1996;36(11):1437-45.

[77] Kumar V, Weller J. Production of Microcellular Polycarbonate Using Carbon Dioxide for Bubble Nucleation. Journal of Engineering for Industry. 1994;116(4):413-20.

[78] Mascia L, Re GD, Ponti PP, Bologna S, Giacomo GD, Haworth B. Crystallization effects on autoclave foaming of polycarbonate using supercritical carbon dioxide. Advances in Polymer Technology. 2006;25(4):225-35.

[79] Gendron R, Daigneault LE. Continuous extrusion of microcellular polycarbonate. Polymer Engineering & Science. 2003;43(7):1361-77.

[80] Bledzki AK, Kirschling H, Rohleder M, Chate A. Correlation between injection moulding processing parameters and mechanical properties of microcellular polycarbonate. Journal of Cellular Plastics. 2012;48(4):301-40.

[81] Weller JE, Kumar V. Solid-state microcellular polycarbonate foams. I. The steady-state process space using subcritical carbon dioxide. Polymer Engineering & Science. 2010;50(11):2160-9.

[82] Lee JWS, Wang K, Park CB. Challenge to Extrusion of Low-Density Microcellular Polycarbonate Foams Using Supercritical Carbon Dioxide. Industrial & Engineering Chemistry Research. 2004;44(1):92-9.

[83] Antunes M, Mudarra M, Velasco JI. Broad-band electrical conductivity of carbon nanofibre-reinforced polypropylene foams. Carbon. 2011;49(2):708-17.

[84] Wool R. Composites and Foams from Plant Oil-Based Resins. London: Elsevier Science; 2005.

[85] Antunes M, Velasco JI. Multifunctional polymer foams with carbon nanoparticles. Progress in Polymer Science. 2014;39(3):486-509.

[86] Mitsunaga M, Ito Y, Ray SS, Okamoto M, Hironaka K. Intercalated Polycarbonate/Clay Nanocomposites: Nanostructure Control and Foam Processing. Macromolecular Materials and Engineering. 2003;288(7):543-8.

[87] Ito Y, Yamashita M, Okamoto M. Foam Processing and Cellular Structure of Polycarbonate-Based Nanocomposites. Macromolecular Materials and Engineering. 2006;291(7):773-83.

[88] Allen RB, Avakian RW. Foamable polycarbonate compositions, articles and methods. Google Patents 1985.

[89] Finley MD. Foamed thermoplastic polymer and wood fiber profile and member. Google Patents 2000.

[90] Ameli A, Jung PU, Park CB. Through-plane electrical conductivity of injection-molded polypropylene/carbon-fiber composite foams. Composites Science and Technology. 2013;76(0):37-44.

[91] Monnereau L, Urbanczyk L, Thomassin J-M, Alexandre M, Jérôme C, Huynen I, et al. Supercritical CO2 and polycarbonate based nanocomposites: A critical issue for foaming. Polymer. 2014;55(10):2422-31.

[92] Singh V, Joung D, Zhai L, Das S, Khondaker SI, Seal S. Graphene based materials: Past, present and future. Progress in Materials Science. 2011;56(8):1178-271.

[93] Young RJ, Kinloch IA, Nicolais L. Graphene Composites. Wiley Encyclopedia of Composites: John Wiley & Sons, Inc. 2011.

[94] Kumar V, Weller J, Hoffer H. Processing of polymers and polymeric composites. ASME Winter Annual Meeting. Dallas: TX, USA; p. 197.

[95] Gibson L.J A, M.F. Cellular Solids, Structure and Properties. 2nd ed. ed. Oxford: Pergamon Press; 1999.

[96] Beechem T, Lafdi K. Novel high strength graphitic foams. Carbon. 2006;44(8):1548-59.

[97] Antunes M, Realinho V, Velasco JI. Foaming Behaviour, Structure, and Properties of Polypropylene Nanocomposites Foams. Journal of Nanomaterials. 2010.

[98] Ameli A, Jung PU, Park CB. Electrical properties and electromagnetic interference shielding effectiveness of polypropylene/carbon fiber composite foams. Carbon. 2013;60(0):379-91.

[99] Zhang H-B, Yan Q, Zheng W-G, He Z, Yu Z-Z. Tough Graphene−Polymer Microcellular Foams for Electromagnetic Interference Shielding. ACS Applied Materials & Interfaces. 2011;3(3):918-24.

[100] Eswaraiah V, Sankaranarayanan V, Ramaprabhu S. Functionalized Graphene–PVDF Foam Composites for EMI Shielding. Macromolecular Materials and Engineering. 2011;296(10):894-8.

[101] Shen B, Zhai W, Lu D, Zheng W, Yan Q. Fabrication of microcellular polymer/graphene nanocomposite foams. Polymer International. 2012;61(12):1693-702.

[102] Ling J, Zhai W, Feng W, Shen B, Zhang J, Zheng Wg. Facile Preparation of Lightweight Microcellular Polyetherimide/Graphene Composite Foams for Electromagnetic Interference Shielding. ACS Applied Materials & Interfaces. 2013;5(7):2677-84.

[103] Geetha S, Satheesh Kumar KK, Rao CRK, Vijayan M, Trivedi DC. EMI shielding: Methods and materials—A review. Journal of Applied Polymer Science. 2009;112(4):2073-86.

[104] Gupta A, Chen G, Joshi P, Tadigadapa S, Eklund. Raman Scattering from High-Frequency Phonons in Supported n-Graphene Layer Films. Nano Letters. 2006;6(12):2667-73.

[105] Antunes M, Realinho V, Solórzano E, Rodríguez-Pérez MA, de Saja JA, Velasco JI. Thermal Conductivity of Carbon Nanofibre-Polypropylene Composite Foams. Defect and Diffusion Forum. 2010;297-301:996-1001.

[106] Teweldebrhan D, Balandin AA. Modification of graphene properties due to electron-beam irradiation. Applied Physics Letters. 2009;94(1):013101.

[107] Verdejo R, Barroso-Bujans F, Rodriguez-Perez MA, Antonio de Saja J, Lopez-Manchado MA. Functionalized graphene sheet filled silicone foam nanocomposites. Journal of Materials Chemistry. 2008;18(19):2221-6.

[108] Yan D, Xu L, Chen C, Tang J, Ji X, Li Z. Enhanced mechanical and thermal properties of rigid polyurethane foam composites containing graphene nanosheets and carbon nanotubes. Polymer International. 2012;61(7):1107-14.

[109] Ma H-L, Zhang H-B, Li X, Zhi X, Liao Y-F, Yu Z-Z. The Effect of Surface Chemistry of Graphene on Cellular Structures and Electrical Properties of Polycarbonate Nanocomposite Foams. Industrial & Engineering Chemistry Research. 2014;53(12):4697-703.

Chapter 2

Materials and experimental procedure

2.1 Materials

Nowadays polymers composites are widely used in many important applications such as appliances, electronics, packaging and in components for automotive and aerospace industries. It is very important to know the main characteristics of the materials used for the composite preparation and understand the processes carried out for such preparation.

This chapter focuses on presenting the main characteristics of primary materials used in this thesis, the processing and the experimental techniques used for the characterization of these materials.

2.1.1. Polycarbonate Bisphenol A (PC)

Polycarbonate (PC) is a thermoplastic polyester with excellent mechanical and thermal properties, due to its high tenacity today it is considered one of the toughest polymers at room temperature and exhibits a fairly high glass transition temperature (Tg) [1]. This engineering thermoplastic is commonly found in a fully amorphous state, presenting transparency and heat resistance as characteristic properties [2].

Polycarbonate used to be obtained from the reaction of a di-hydroxyl compound such as Bisphenol A and phosgene. Figure 2.1 shows the molecular structure of PC. An alternative method to obtain PC is through the ester exchange between a di-hydroxyl compound and a carbonic acid diester.

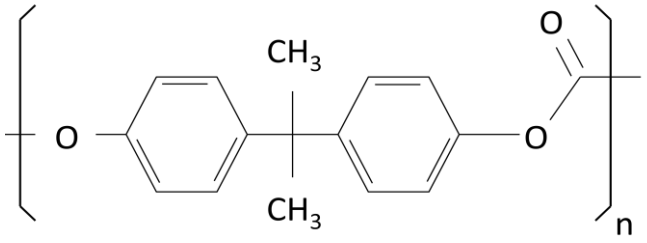

Figure 2.1. Structure of Polycarbonate Bisphenol A.

The most widely used polycarbonates are Bisphenol-A based polycarbonate (i.e.,aromatic polycarbonates), however aliphatic polycarbonates do exist as previously mentioned. In the present

study, only Bisphenol-A polycarbonate has been used so sample nomenclature from now on will be PC for Bisphenol-A polycarbonate.

Commercial PC Lexán 123R from Sabic was used in this work; its main characteristics are presented in table 2-1.

Tabla 2.1. Main characteristics of PC Lexan 123 R de Sabic

Company	*Sabic.*		
General characteristics	High stiffness and fairly tenacy over 140ºC		
Material	PC Bisphenol A		
Typical properties			
Physical properties	**Method**	**Value**	**Unit**
MFI (300ºC,1.2 Kg)	ASTM D 1238	17.5	g/10 min
Density @ 73 ºF	ASTMD792	1.2	g/cm^3
Water absorption 24hr	ASTMD570	0.15	%
Electricla properties	**Method**	**Value**	**Unit**
Volumetric resistivity	ASTM D 257	$>10^{15}$	Ohm*cm
Mechanical properties	**Method**	**Value**	**Unit**
Yield stress	ASTM D 638	61.4	MPa
Ultimate tensile strength	ASTM D 638	64.8	MPa
Yield strength	ASTM D 638	7	%
Breaking strain	ASTM D 638	110	%
Young modulus	ASTM D 790	2337.3	MPa
Impact Izod (notch-depth 1/8 in)	ASTM D 256	0.722	KJ/m

2.1.2 Graphene nanoplatelets (GNP)

Graphene is considered a novel material with excellent multi-functional reinforcement characteristics, for making versatile new nanocomposites for nanotech applications. Due to its excellent mechanical and electronic properties graphene is called to be the candidate both for scientific and technological perspectives [3-4]. Graphene is the basic building block of all graphitic forms of carbon, as for example graphite (Fig. 2.2a). Graphene consists of a single atomic layer of sp^2 hybridized carbon atoms arranged in a honeycomb structure as shown in Figure 2.2b. Graphene as just one atom thick, thus considered a 2D crystal, presents outstanding mechanical properties with a Young modulus of 1 TPa and breaking strength of 40 N/m [5], as well as good thermal properties with a thermal conductivity at room temperature of 3000 W/mK [6]. Besides these interesting and exciting physical properties such as high levels of stiffness, strength, and thermal conductivity, graphene also presents impermeability to gases having the well known barrier effect [7]. As a consequence graphene opens up to a large number of applications, electronic circuits [8], sensors [9], photovoltaic conversion due to its excellent charge carrier mobility and large specific surface area [10] among others. In addition it has been said that one obvious application of graphene is in the field of nanocomposites [3, 11-12].

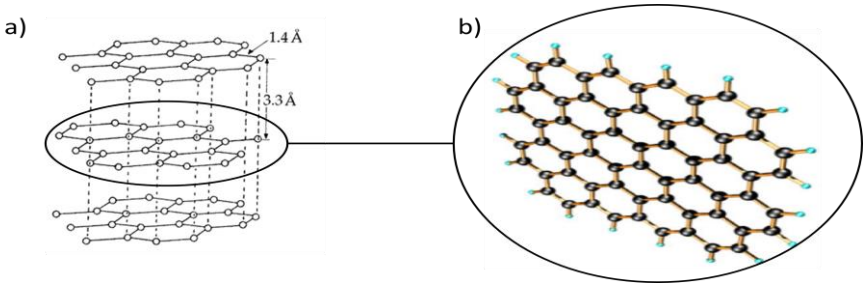

Figure 2.2. a) Graphite structure, b) Graphene structure.

Graphene as a single layer (SLG) is currently considered a filler with enormous potential for a variety of applications, including use in composite materials. However, taking into consideration that the production of graphene as a single layer (SLG) is currently quite expensive and still not produced on a large scale, we have decided to use an intermediate filler between graphite (as more than 100 layers of stacked graphene) and graphene (SLG). These rigid layered nanofillers not only

reinforced the matrix but also enabled us to study the changes that the processes in the presence of the fillers induced, during the preparation of lightweight composites.

The fillers used in this study were commercial stacks of graphene nanoparticles (GnP) (from now on graphene nanoplatelets) supplied by XG Sciences, Inc. These xGnP-Grade-M nanoplatelets are 6 to 8 nm thick with a 15 μm average diameter, a typical surface area of 120-150 m^2/g and a density of 2.2 g/cm^3, as reported by the manufacturer.

A continuous characterization of these graphene nanoplatelets was carried out after each process that the materials went though. Starting from its original state (as supplied), continuing with the characterization of the unfoamed composites (PC-GnP) after having melt-mixed, compression-molded and finishing after being foamed with the foamed composites (PC-GnP-f) under different processing conditions.

2.1.3 Carbon dioxide (CO_2)

Since the use of many foaming agents has been banned due to environmental reasons, the use of carbon dioxide as a foaming agent has increased taking into consideration that it has an easily attainable critical point (T_c=31.1ºC, P_c=73.8 bar) [13], meaning that these parameters represent the highest pressure and temperature at which gaseous and liquid CO_2 can coexist in equilibrium, above the critical point CO_2 remains in a single phase. In addition, properties such as density, viscosity and diffusion coefficients can be tuned by changing its pressure and temperature, which provides it with plasticizing characteristics during polymer processing. It also has been shown that its low toxicity, variable density, low viscosity, low surface tension, high levels of solubility/easy removal in typical polymer systems make carbon dioxide an ideal candidate as a foaming agent for the preparation of microcellular foams [14-17].

2.2 Sample preparation

2.2.1 Melt compounding

The content of absorbed water in the PC pellets was minimized by drying them in an oven at 110 °C at least for 3 hours before melt processing. Right after, the PC + 0.5, 2 and 5 wt% graphene,

so-called for now on PC-05GnP, PC-2GnP and PC-5GnP respectively, were physically mixed and melt blended, using a Brabender Plasti-Corder counter-rotating twin screw melt mixer.

The mix was prepared by placing the material in the internal mixer for 2 min at a temperature of 180 ºC and rotating screw speed of 30 rpm. The rotating speed was then increased to 60 rpm and 120 rpm for 1 and 3 min, respectively.

Table 2.2. Melt mixer main characteristics

Brabender Plastic-Corder W 50 EHT

Characteristic	**Value**
Capacity	55 cm^3
Torque Max	200 N.m
Maximum working temperature	500 ºC

2.2.2 Compression molding

For the neat polycarbonate samples preparation, PC pellets were first dried in an oven at 110 °C for at least 3 hours before being directly compress-molded into PC discs. For the composites, Polycarbonate and graphene nanoplatelets were melt mixed, pelletized and immediately compression-molded. Neat PC and pelletized composite material were compression-molded at 220 ºC and 45 bar in a hot-plate press (IQAP LAP PL-15) to discs with a thickness of 3.5 mm and diameter of 74 mm in 3 steps. In the first step the upper hot plate was used to melt the mixed material by slowly lowering the upper plate at a temperature of 220 ºC. The second step consisted in allowing air to escape the material by pulsating the upper plate in an up and down motion using a pressure of 45 bar and a temperature of 220 ºC during 1.5 min. For the third step the material was pressed continuously for 1 min at 220 ºC and 45 bar. Lastly, the mold with the sample still inside was left to cool for 15 min in the cooling station of the press applying a constant pressure of 45 bar. The samples used in the CO_2 desorption kinetics study were obtained from these solid discs by reducing the disc diameter to a typical value of 40 mm.

Table 2.3. Hot-plate press main characteristics

IQAP-LAP PL-15

Characteristic	Value
Force*	15 Tn.
Motor maximum power	1.5 kW
Heating power	2.4 kW
Electrical resistance heaters (P-104 230×75 380 V/600W)	4 units
Temperature sensor (FE/KO nº2 × 2 m, wire M12×100)	2 units
Digital temperature indicators	2 digits
Between columns	400 mm
Between plates	230 mm
Piston diameter	100 mm
Piston stroke	100 mm
Dimensiones máximas de los moldes	230 × 300 mm
Refrigeración por circuito de agua	1.4 ´´ G
Height	1030 mm
Working height	1050 mm
Length	1280 mm
Width	400 mm
Weight	340 kg

*Maximum force: 200 kg/cm^2

2.2.3. Foaming

2.2.3.1. One step foaming process

A supercritical carbon dioxide (sc-CO_2) dissolution one-step batch foaming process was used to prepare the cellular materials studied. Foaming was carried out using a *Büchi Glasuster,* high pressure vessel with a capacity of 2.1 L (table 2.4). The process consisted of saturating the solid discs with CO_2 inside the high pressure vessel at pressures varying from 120 to 160 bar. The

supercritical conditions were reached at T_c= 31.1ºC, P_c= 73.8 bar [18] by injecting CO_2 using a pump-compressor system while heating the vessel.

Table 2.4. High pressure vessel Büchi Glasuster Stirrer vessel type 3

Characteristic	Value
Capacity	2.1 L
Maximum pressure	350 bar
Maximum temperature	350 ºC
Electrical heating system	Electrical resistance jacket
Cooling system	Water cooling system
Heating system precision	0.01 ºC
Cooling system precision	0.1 ºC

The final values of the saturation/foaming temperature were reached by adjusting the process conditions (pressure/temperature) in order to attain the desired parameters. The saturation/foaming pressure ranged between 200 and 213 ºC, and times at saturation conditions varied from 0 to 120 min in order to achieve a homogeneous mixture [19]. The saturation time is defined as the period of time that the sample stayed at the saturation conditions once those said conditions were reached and until depressurization/cooling started. It is important to take into account that once the samples were placed and the CO_2 was introduced into the vessel, the heating time from 30 to 200 ºC was 38min.

Foaming was done in one-step by applying a sudden pressure drop, inducing an thermodynamic instability within the system producing an immiscibility in the polymer-gas system [20]. Therefore, the system induced a phase separation that promoted cell nucleation. Once the cell was nucleated, cell growth took place due to the diffusion of the gas molecules from the solution to the gas phase nucleated. The phenomena governing the expansion of the cells are related to the transport properties of the gas in the polymeric melt and to the rheological and surface properties of the matter around the cell. The rate at which the cells grow is limited by the diffusion rate and the stiffness of the viscoelastic of the polymer-gas solution [21]. For instance cooling and the presence of crystals or fillers could restrict cell growth until the blowing agent has been consumed. Generally

speaking, the cell growth process is controlled primarily by the time allowed for the cells to grow, the temperature of the system, the state of supersaturation, the hydrostatic pressure or stress applied to the polymer matrix and the viscoelastic properties of the polymer-gas solution [21].

The pressure drop rate was controlled by regulating a release valve, which was closed in order to leave a residual pressure depending on the case of study (Figure 2.3 illustrates the process). The pressures used for one-step foaming ranged between 100 and 220 bar with residual pressures ranging from 0 to 20 bar and the temperatures varied from 200 to 213 ºC as will be further detailed in Chapter 3.

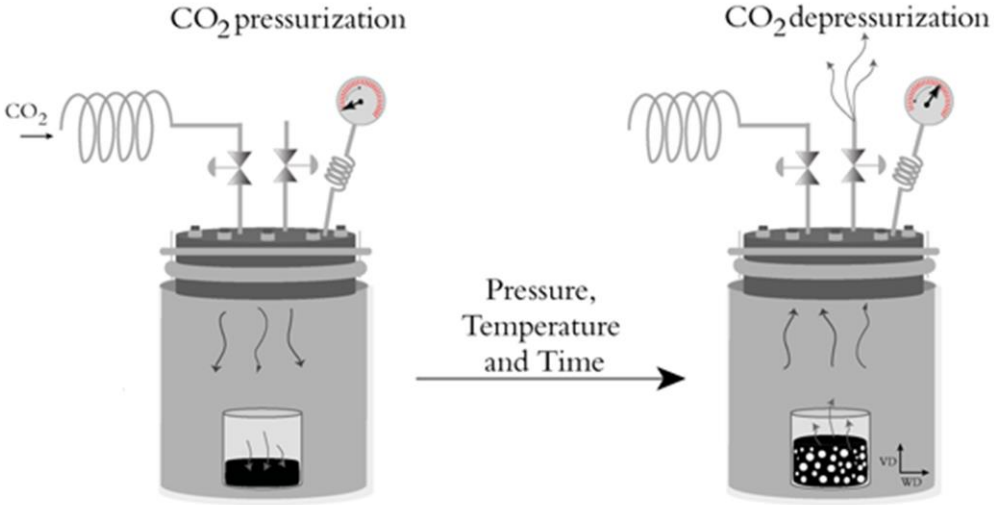

Figure 2.3. Illustration of one-step batch foaming process. Figure displays both the CO_2 dissolution and depressurization stages used in the one-step foaming process.

2.2.3.2. Two-step foaming process.

Stage I - Supercritical carbon dioxide dissolution

Once obtained by compression-molding, the PC/composite foam precursors were foamed by placing them inside a high pressure vessel and initially dissolving supercritical carbon dioxide (sc-CO_2). Two sc-CO_2 dissolution temperatures were used: 80 and 100 ºC, in both cases applying a total dissolution time of 210 min. The sc-CO_2 was introduced in the vessel at room temperature at a pressure of 70 bar, reaching a final dissolution pressure of 140 and 170 bar, for a dissolution temperature of 80 and 100 ºC respectively. Once carbon dioxide was dissolved into the foam precursors, they were cooled down to room temperature by re-circulating water through the vessel's

cooling jacket while keeping the vessel pressurized. After slow depressurization of the sc-CO_2 at room temperature, the PC foam precursors containing CO_2 were taken out of the vessel and left to stabilize at room temperature and atmospheric pressure for 120 min.

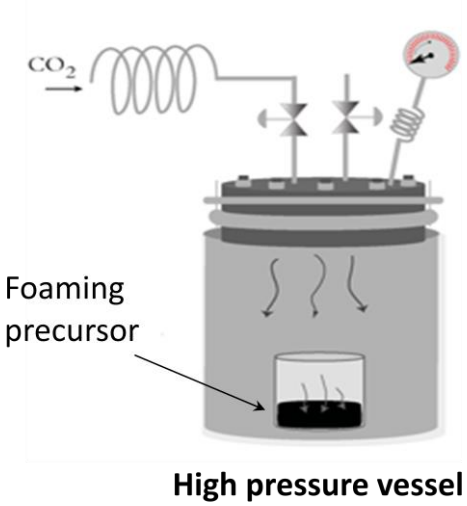

Figure 2.4. Illustration of the CO_2 pressurization/dissolution step used in the two-step foaming process.

Stage II - Double contact restricted foaming

The PC/composite foam precursors containing CO_2 obtained at the end of Stage I were once again placed in the circular-cavity mold and foamed in the hot-plate press by compression-molding at a constant temperature of 165 ºC and constant pressure of 60 bar. The compression-molding double contact used in this stage guaranteed the homogeneous heating of the precursors and at the same time restricted their initial expansion. After applying a heating time that varied between 40 and 120 seconds, the applied pressure was quickly released, allowing the PC foam precursors containing CO_2 to expand in both vertical and width directions. After the expansion, the obtained foams were quickly removed from the plates and left to cool at room temperature with direct contact to air.

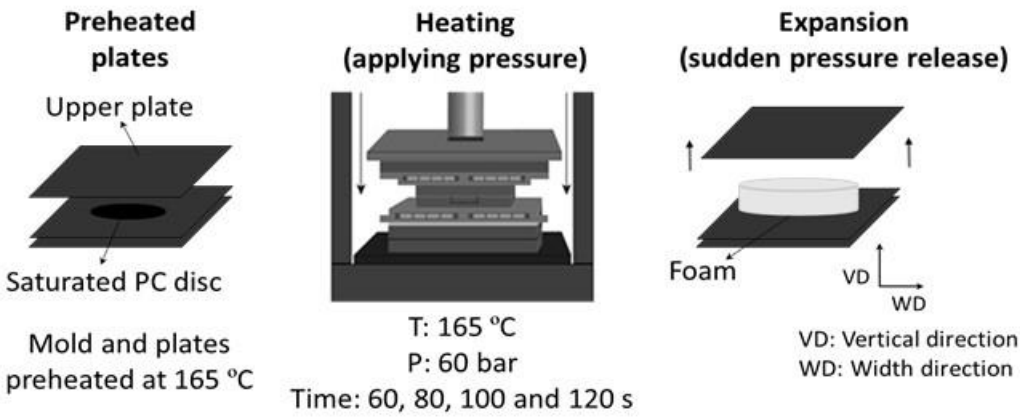

Figure 2.5. Illustration of the double contact restricted foaming step used in the two-step foaming process.

2.3 Experimental procedure

2.3.1 Density measurements

Density is one of the main fundamental parameters in the macroscopic characterization of foams. Density measurements were carried out using the geometric method following UNE-EN ISO 1183-1 [22]. The values obtained from the solids were compared to the values obtained using the Archimedes principle, allowing the density of the foam precursors to be determined [13] using the weight of a known solid sample and a known liquid (density). The liquid used was distilled water due to its lower density when compared to the solid polycarbonate.

The density (ρ) was determined using the following equation:

$$\rho = \frac{P_1}{P_2}\,\rho_a \tag{2.1}$$

Being P_1 the weight of the dry sample, P_2 the weight of the sample submerged in the liquid and ρ_a is the density of the distilled water at the temperature during the measurement.

The elements of the system used were:

1 – Electronic scale

2 – Base-holder

3 – Metallic hook
4 – Vessel 250 ml (with distilled water)
5 – Submerged sample.

It needs to be pointed out that this method was used for the foam precursors due to the higher density presented by the unfoamed material when compared to the density of the distilled water. Even though the foams presented a closed-cells characteristic, the density was lower than the density of distilled water. Therefore the density of foams was measured geometrically by direct measurement of volume, by means of the ration between the weight and the volume.

2.3.2 Melt flow index measurements

It has been reported that melt flow index (MFI) can be associated to the melt viscosity of polymeric materials and it has been reported that changes on the MFI can affect the final morphologies of polymer foams [23]. The addition of content of fillers can also affect the melt viscosity of composites [24], expecting to increase the melt viscosity of the composites when adding higher contents of fillers. Low viscosity is generally accompanied by low melt strength, which facilitates the occurrence of cell coalescence [24]. Therefore, the addition of high amount of fillers is expected to increase the melt viscosity and it could be observed as the decrease of MFI values. With this in mind, the melt flow index of the composites prepared were measured using a flow test apparatus 4106B Zwick Materialprüfung.

2.3.2 Carbon dioxide diffusion experiments

Desorption experiments were carried out in order to measure the CO_2 diffusion coefficient in PC for the two different dissolution temperatures. As previously mentioned, the samples used in these experiments were directly obtained from the PC foam precursors by reducing their diameter to 40 mm. After applying the conditions already indicated in Stage I of the foaming process, i.e., a sc-CO_2 dissolution temperature of 80 or 100 ºC and pressure of 140 or 170 bar for a total dissolution time of 210 min, samples were cooled down to room temperature, removed from the vessel and quickly transferred to a scale in order to record the evolution of CO_2 mass loss with the desorption time.

The maximum concentration of CO_2 in the samples after decompression (M_0) was calculated by extrapolating to zero desorption time following the initial slope method [14]. Assuming one-dimensional diffusion in a plane sheet, the CO_2 diffusion coefficient (D_d) was determined by plotting M_t/M_0 as a function of t/l^2, where M_t is the CO_2 concentration at time t and l is the thickness of the sample, according to the following equation [1]:

$$\frac{M_t}{M_o} = 1 - \frac{8}{\pi^2} exp\left(\frac{-Dt}{l^2}\right) \tag{2.2}$$

The CO_2 diffusion coefficient was determined from the slope of the M_t/M_0 vs. t/l^2 curve taking into account the last data range and the calculated value of M_0.

2.3.3 Cellular morphology characterization.

2.3.3.1 *Scanning electron microscopy (SEM)*

The cellular structure of the foams was analyzed from scanning electron microscopy images obtained using a JEOL JSM-5610 microscope applying a voltage of 15 kV and a working distance of 30 mm. Samples were previously prepared by fracturing at room temperature and depositing a thin layer of gold onto their surface in argon atmosphere using a BAL-TEC SCD005 Sputter Coater.

The average cell sizes (ϕ) in the vertical (ϕ_{VD}) and width (ϕ_{WD}) foaming directions were measured using the intercept counting method [25]. The cell aspect ratio (AR) was determined by dividing the value of the average cell size in the vertical direction by the value measured in the horizontal direction ($AR = \phi_{VD}/\phi_{WD}$). The cell density (N_f) was calculated using the following equation [26]:

$$N_f = \left(\frac{n}{A}\right)^{\frac{3}{2}} \left(\frac{\rho_s}{\rho_f}\right) \tag{2.3}$$

Where n is the number of cells per area, A (cm^2), and ρ_s and ρ_f are respectively the solid and foam densities.

2.3.4 Microstructure characterization

2.3.4.1 *Wide angle X-rays scattering (WAXS)*

WAXS was carried out using a Panalytical diffractometer with Cu Kα radiation (λ= 1.54 Å), operating at 40 kV and 40 mA at room temperature, scanning from 2 to 60º using a step of 0.02º. By using the Bragg's law the interplanar distance was determined.

$$n\,.\lambda = 2d_{002}\sin\theta \tag{2.4}$$

where n is an whole number y λ the wave length of the beam used during the measurement. The Debye-Scherrer relationship was used to estimate the lamellar thickness (L') in this case the graphene nanoplatelets thickness (L'). Where K is a shape constant of the crystal or the filler and the full width half maximum (FWHM).

$$FWHM = \frac{K.\lambda}{L'\cos\theta} \tag{2.5}$$

Once the interplanar distance (d_{002}) and the FWHM were achieved by using the WAXS data, the K constant for flat morphologies used was 0.89 [27] and the thickness of graphene stacks (L') was calculated by the Debye-Scherrer relationship, the number of layers (n) in the stacks of graphene was achieved using the following equation.

$$n = \frac{L'}{d_{002}} \tag{2.6}$$

The crystallinity percentage (X_c) was determined using the following equation:

$$X_c\,(\%) = \frac{A_c}{A_c + A_a} \times 100 \tag{2.7}$$

Where Ac corresponds to the sum of the crystalline peak areas and A_a to the amorphous halo area.

2.3.4.2 *Small angle x-ray scattering (SAXS)*

Small angle x-ray scattering was used to determine any density fluctuation in the materials and estimate the lamellar thickness of the bulk crystalline unfoamed and foamed polycarbonate and composites. Experiments were performed at room temperature using an Anton Paar SAXSess mc^2 Nanostructure Analyzer. The X-ray source consisted on a sealed-tube (line collimation) operating at 40 kV and 50 mA, using a CuKα radiation (λ =1.54 Å). The incident X-ray beam was collimated by a block collimator, slits and a focusing graded multilayer mirror. The sample to detector distance was 261.2 mm. A semi-transparent beam stop was used. The total exposure time of each of the samples was 1 h. The scatter intensity was detected by an X-ray detector image-plate type for two dimensional data acquisition. The measurable scattering vector ranged from 0.08 to 28 nm^{-1}. The scattering intensity I(q) and the scattering vector q data was acquired using a SAXSquant 2D software and plotted as scattering curves. The curves that displayed a signal at low vector q values were corrected using a Lorentz approach and the scattering vector corresponding to the maximum scattering intensity was used to calculate the long spacing. The long spacing, also known as long period (L_B), is the sum of the distance corresponding to the crystalline (crystal thickness, l_c) and amorphous (amorphous layer thickness, l_a) phases considering an ideal two-phase structure [28]. The long period was calculated from the maximum of the peak of the Lorentz-corrected SAXS profiles (q_{max}) using Bragg's equation [29]:

$$L_b = \frac{2\pi}{q_{max}} \tag{2.8}$$

In order to determine the average thickness of both crystalline and amorphous phases the one-dimensional correlation function approach was used. The correlation function is the Fourier transform of the scattering curve and may be analyzed in terms of an deal lamellar morphology [28]. The one-dimensional correlation function ($\Gamma(r)$) is related to the electron density fluctuation within the system. CORFUNC software was used in order to perform the correlation function from the obtained one-dimensional SAXS data [30]. Since the experimental q data is finite, extrapolation of intensity to both low and high values of q was necessary. Data was back-extrapolated to $q = 0$ by fitting the Vonk model to the first few genuine data points after beam stop (q = 0.08 nm^{-1}), while tail-fitting data was extrapolated using Porod's function [31]:

$$I(q) = B + \frac{K}{q^4} \tag{2.9}$$

where B is the Bonart thermal background and K is the so-called Porod's constant. Once the extrapolation process was completed (back and tail fitting), we confirmed that the extrapolated data superimposed well to the original values.

Once the extrapolation was successfully completed, the transformation process was carried out, which consisted initially on determining the one-dimensional correlation function ($\Gamma(r)$) [31]:

$$\Gamma(r) = \frac{1}{Q}\int_0^\infty I(q)q^2 \cos(qr)\, dq \tag{2.10}$$

where $I(q)$ is the scattering intensity obtained from the SAXS measurements, r is the direction of measurement of electron density, Q is the invariant of $I(q)$, given by:

$$Q = \int_0^\infty I(q)q^2\, dq \tag{2.11}$$

and q is the scattering vector:

$$q = \frac{4\pi}{\lambda}\sin\theta \tag{2.12}$$

where λ is the wavelength and the scattering angle is 2θ. Once the one-dimensional correlation function was obtained, it was re-transformed back into a scattering curve and compared with the original data in order to make sure that the function tended to zero as q tended to infinity. Assuming a two-phase model, the one-dimensional correlation function was used in order to estimate the long period (L_B) and lamellar thickness of both crystalline and amorphous phases (l_c and l_a, respectively).

Measurements of small angle X-ray scattering were also carried out at room temperature on a Bruker Nanostar-U instrument. In this case the X-ray source consisted of a rotating anode with a copper target and 0.1×1.0 mm spot focus filament operated at 50 kV and 24 mA. The SAXS detector was a multi–wire proportional counter (Bruker Hi-Star) with 1024 × 1024 pixels and a beryllium front window 11.5 cm across. The detector was placed approximately 105 cm from the sample allowing measurement of scattering angles (2θ) from 0.2 to 2.8º. Assuming a wavelength

that is a weighted average of Cu-Kα, this corresponds to q values in reciprocal Angstroms of approximately 0.01 to 0.20.

2.3.4.3 Raman spectroscopy

Raman spectroscopy was used because is a technique useful as an in situ, non-contact, non-destructive measurement tool that can be used at room operating conditions, and it can provide information on chemical states of the materials and it is characterized for being fast with a short time used for sample preparation [32]. This optical technique can reveal information about material quality, thicknesses, doping and stress in crystal lattices among others due to its sensitivity to changes in bond angles or strength. This technique is commonly used for characterization of polymers [33-35]

Raman spectroscopy is a vibrational technique based upon the Raman effect, which is a scattering phenomenon. Laser excitation on the sample takes place. The laser light is scattered by the molecules. Most of the scattered radiation will have the same energy that the original light possessed (light shifted from its originally frequency). This type of scattering is called Rayleigh scattering. The elastic scatter light is rejected using blocking filters. A very small part of the laser light undergoes a slight energy change, known as the Raman shift. The difference in energy between the incident laser excitation and the Raman scattered light is equal to a vibrational transition energy of the molecule. The inelastic scattering of light is usually associated with the emission (Stokes process) or absorption (anti-Stokes process) of phonons [32]. By knowing the energy shift of the scattered light relative to the incident light, which yields Raman spectra in cm^{-1}, the phonon frequency can be obtained, which is useful for identifying the origin of an unknown structure of a newly discovered molecule or of a new material in chemistry [36].

With this in mind a micro-Raman spectrometer Jobin-Yvon LabRam HR 800 was used at 532 nm with an incident power of 0.5 mW, 50x and 100X objectives were used with an incorporated optic microscope Olympus BXFM. The measurements were performed on the surface of the sample previously brittle fractured.

2.3.4.4 Atomic Force Microscopy (AFM)

This technique was used to carry out qualitative observations of the lamellar structures in the semi-crystalline samples and structures resulting from possible ordered of PC in the composites.

Also quantitative characterization was performed to study the morphology of the graphene nanoplatelets. For this an atomic force microscopy (Multimode 8 AFM head attached to a Nanoscope V electronics (Bruker)) was operated in tapping mode at room temperature using a silicon cantilever probe with a silicon oxide tip with a nominal spring constant of 0.35nN/nm and a vertical resolution (Z-axis) of 0,2 nm as brand new.
The images were collected in height mode. Thus, enabling to estimate the number of layers relating the measured thickness of the nanoplatelets (L') and the interplanar distance (d_{002}) as it has been previously reported in the literature [3, 27].

$$n = \frac{L'}{d_{002}} \tag{2.13}$$

2.3.4.5 Transmission electron microscopy (TEM)

For transmission electron microscopy (TEM) imaging, the samples were previously ultramicrotomed in the direction of foaming (cross section/through plane) to slices of approximately 60-80 nm thickness using a diamond knife, then placed onto copper TEM grids (Ted Pella 400 mesh). The microtome used was a PowerTome XL Ultramicrotome from Boeckeler Instruments, Inc. The TEM images were acquired on a JEOL JEM-2011 LaB_6 TEM at 200 kV, using an AMT-XR280 side mount camera.

2.3.5 Thermal characterization

2.3.5.1 Differential scanning calorimetry (DSC)

Differential Scanning Calorimetry (DSC) was used for monitoring the possible thermal transitions of the materials studied. With this aim a Perkin Elmer, Pyris 1 model with a glycol-based Perkin Elmer Intracooler IIP differential scanning calorimeter was used at a heating rate of 10 ºC/min, within a range of temperature of 30 - 300 ºC using samples weighing around 4.0 mg. This machine allows for the use of small quantities of sample due to the fair signal-noise ratio displaying fair results. The data is displayed in form of thermograms, plotting the variation of heat flow ($d\Delta Q/dt$) as a function of temperature. This is possible because there are two independent furnaces, therefore, two heat flows (dQ/dt) can be obtained as a function of temperature, one from the sample

and one from the "reference" (which is an empty sample holder). These are different because the sample and the reference are heated/cooled in each of the independent furnaces. Each furnace measures the temperature thus; any temperature difference can be detected, supplying then the heat flow necessary to the coldest furnace keeping the two furnaces at the same temperature. Therefore the endothermic or exothermic transition of the sample can be displayed as.

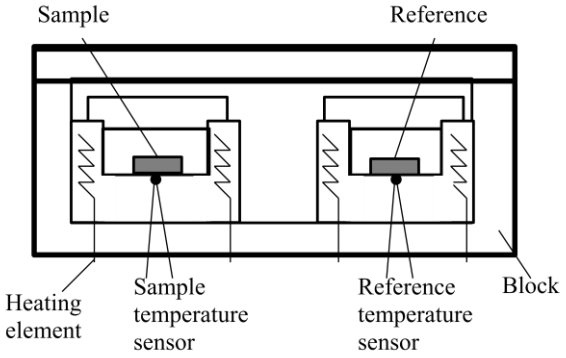

Figure 2.5. Independent furnaces in the DSC

The glass transition temperature (T_g) of samples was determined using the inflection point heat capacity method. The melting temperature (T_m) was determined as the maximum temperature of the melting peak appearing in the melting endotherm, while the heat of fusion (ΔH_m) was obtained by direct integration of this peak. The crystallinity percentage (X_c) was calculated according to:

$$\chi_c = \frac{\Delta H_m}{\Delta H_m^o w_p} \text{x} 100 \tag{2.14}$$

where w_p is the weight fraction of PC and ΔH^0_m is the theoretical 100% crystalline PC melting enthalpy (147.79 J/g [37]).

Also the thickness of the lamellar crystals (l) was estimated using the Gibbs-Thomson equation, which takes into account the experimental melting temperature (T_m) and the fold surface free energy (σ_e = 94 erg/cm^2) and equilibrium melting temperature of PC (T^0_m = 318 ºC [38]):

$$T_m = T_m^o\left(1 - \frac{2\sigma_e}{l \text{x} \Delta H_m^o}\right) \tag{2.15}$$

2.3.5.2 Dynamic-Mechanical-Thermal Analysis, (DMTA)

The study of the dynamic mechanical behavior of the materials allowed us to study the viscoelastic properties as a function of temperature of the materials. The method used for this machine consists on sinusoidal stimuli that induce sample deformation. The ratio between the dynamic tension and deformation represents the complex modulus. Therefore the storage modulus which is the capacity of the sample to absorb energy (elastic component) and the loss modulus which is related to the absorbed energy due to molecular mobility (viscous/inelastic component) can be express as follow.

$$E^* = \frac{\delta}{\varepsilon} = E' + E'' \tag{2.16}$$

Where ε is the deformation and δ is the phase difference between the induced deformation and the tension. This phase difference δ, is determined by the ratio of the two aforementioned modulus components $tan\ \delta = E''/\ E'$ and it is known as tan delta, displaying the changes of the mechanical behavior of the sample throughout the thermal transitions.

These measurements were carried out by using a dynamic mechanical thermal analysis test equipment (DMTA), DMA Q800 (TA Instruments) in a single cantilever configuration with a span of 17.5 mm under strain control (dynamic strain of 0.02%), constant frequency of 1 Hz and a temperature range from 30 to 180 ºC. A heating rate of 2 ºC/min was applied. The test equipment was previously calibrated according to the standard procedure. In each experiment the storage modulus (*E*') and the loss factor (*tan δ*) were registered as a function of temperature. For the analysis, specimens cut directly from the solid discs and foams, with a nominal length of 35 mm, width of 13 mm and thickness between 3.0 and 3.5 mm, were used.

2.3.5.3 Thermogravimetric analysis (TGA)

The thermogravimetric analysis was carried out in order to study the thermal stability of the materials. It was performed in a TGA/DSC 1 Mettler Toledo Star System analyzer by heating samples of around 10.0 mg from 30 to 1000 ºC at a heating rate of 10 ºC/min under both nitrogen (constant 30 ml/min N_2 flow) and air atmospheres (constant 60 ml/min air flow). The temperatures corresponding to mass losses of 1, 5 and 50%, as well as the mass of the final residue obtained at

1000 ºC, were reported for the unfoamed and foamed unfilled and graphene-reinforced polycarbonate composites.

2.3.5.4 Thermal conductivity measurements

The heat conductivity of the samples was measured using a steady state one-dimensional heat conduction method. The experimental setup consisted of an electrical heater, a heat sink and two thermocouples to measure the temperature gradient (Figure 2.6). To minimize the interface thermal resistance, fine diameter electrically insulated thermocouples were embedded into two soft indium layers to measure the temperature at both sides of the cylindrical samples (previously the samples were cut and sanded down from the original unfoamed and foamed samples to a typical diameter of 6 mm and thickness of 3 mm). Pressure was applied using a screw mechanism that is thermally insulated from the sample by a thick Teflon block (insulation block) that would not deform easily during applying pressure. The rest of the set up was thermally insulated by a very low thermal conductivity material (~ 0.02 $W.m^{-1}.K^{-1}$) in order to reduce any heat loss by convection or radiation. Once the sample was in place and the set up ready to start the measurement, a dome was place on top of the entire set up to reduce the influence of any current of air that could affect the measurement.

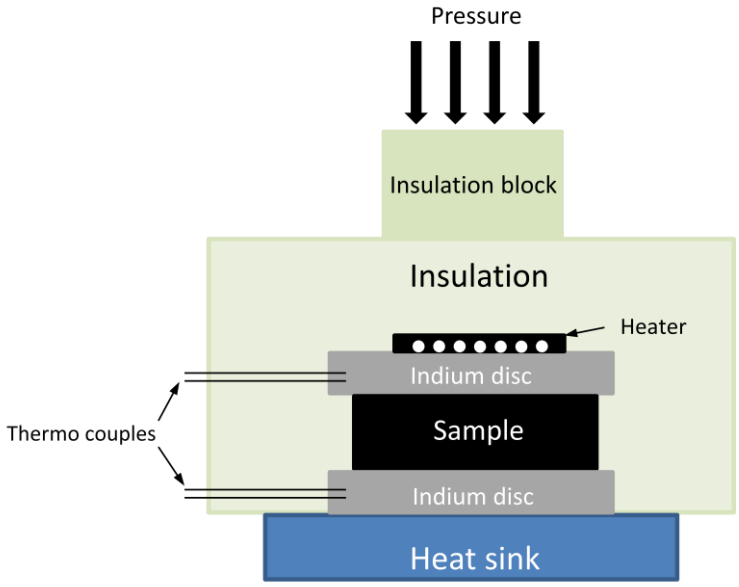

Figure 2.6. Scheme of the setup used for thermal resistance measurements.

The heat losses in the experimental setup were calibrated using glass samples of known conductivity. The thermal conductivity of neat polycarbonate was measured with this setup (K ~0.18 W/m.K) the result being very close to the value reported in the literature [39-40]. To measure K, the experimental thermal resistance was first obtained from the slope of the temperature difference across the sample as a function of heater power. Next, the calibrated heat loss (R_l) contribution was taken into account by using a parallel thermal resistance network arrangement. To find the intrinsic thermal conductivity (K), the interface thermal resistance (R_i) between the composite sample and the indium layer was subtracted from the overall conduction resistance (R_T). This interface thermal resistance was determined by testing samples with different thicknesses, then extrapolating the plot of (R_s + R_i) Vs thickness to zero thickness using linear regression. The thermal resistance and conductivity of the sample are calculated using the following equations:

$$R_s = \frac{R_T \times R_l}{R_l - R_T} - R_i \tag{2.17}$$

$$K = \frac{t}{R_s \times A} \tag{2.18}$$

where t and A are the thickness and cross sectional area of the sample, respectively. The value of K was obtained using the aforementioned method for all the samples.

2.3.6 Electrical characterization

2.3.6.1 DC Electrical conductivity measurements

The transverse dc conductivity, i.e., the through-plane electrical conductivity, of the composites was measured on samples having a nominal thickness of 1 mm. A pA meter/dc voltage source HP 4140B with a two-probe set was used. The connections were set up in the electrostatic light-shielded test box HP 16055A using electrolytic copper sheet electrodes. Samples were coated with silver paint in order to reduce the contact resistance.

The samples used for transverse dc resistance were cut to 20 mm × 20 mm squares and their thickness was reduced to approximately 1 mm by using sandpaper. After reducing the thickness, a thin silver conductive paint layer with a resistance per area ranging from 0.01 to 0.1 Ω/cm^2 was deposited on both top and bottom surfaces of the sample in order to guarantee a good electrical

contact. A programmable dc voltage feature with a range of 0 V - 0.05 V and a voltage step of 0.01 V, a hold time of 5 seconds and a step delay time of 5 seconds, was used. In order to obtain the value of the electrical resistance of the sample (*R*), a characteristic I-V curve was plotted for each sample, with *R* calculated as the slope of the I-V curve. The electrical resistivity (ρ_v) was determined by simply dividing the product of the resistance (R) and the surface area of each sample (*A*) by their respective thicknesses (*t*), as shown in equation 2.19. The electrical conductivity (σ) was then calculated as the reciprocal of the electrical resistivity.

$$\rho_v = \frac{\mathrm{R}\times\mathrm{A}}{\mathrm{t}} \tag{2.19}$$

2.3.6.2 AC Electrical conductivity

The ac electrical conductivity of the solid and respective foamed composites was measured between 10^{-3} and 10^{6} Hz using a Novocontrol high resolution dielectric, conductivity and impedance modular measurement system. A typical sample thickness of 1 mm and a diameter of 20 mm was used. The surfaces of the samples were coated with silver paint in order to reduce the interface electrical resistance due to contact. The samples were placed in the Novocontrol dielectric spectrometer between electrodes with a diameter of 20 mm. The measurements were carried out in the through-plane/cross section direction.

2.3.7 Electromagnetic interference shielding effectiveness measurements

The measurements for electromagnetic interference effectiveness (EMI SE) were carried out in the X-band frequency range (8.0-12.4 GHz) using a Anritsu 37397C vector network analyzer (VNA). The set up consisted of the mentioned VNA with two port test fixture connected to two WR-90 coaxial waveguides and a sample holder that was placed between the 2 waveguides. The port 1 side of the VNA was connected to the waveguide/transmission line. Then the transmission line was attached to the sample holder, subsequently the sample holder was fixed to a mirror-like arrangement to the port 2 of the VNA. The samples were cut to the opening dimension of the waveguide sample holder (22.9 mm x 10.2 mm) with thicknesses around 2 mm. A two-port VNA calibration was performed at the beginning of each measurement with no sample in the sample holder to be subtracted from the subsequent measurement. The energy generated in the VNA was

directed from the test port though the waveguide into the target test sample. The measured scattering parameters of S_{11} (forward reflection coefficient) and S_{21} (forward transmission coefficient), whose magnitudes are expressed in decibels (dB), were used for the analysis.

To understand how the electromagnetic shielding can take place in a material, a brief explanation of the mechanisms taking place is presented. It can be said that when microwave radiation is incident on a shielding material, transmission, reflection, and absorption can be observed. Wave absorption and reflection are the major electromagnetic attenuation mechanisms; however the multiple reflections also can be detected (see Figure 2.7). The reflection is related to the impedance mismatch between air and absorber; the absorption can be regarded as the energy dissipation of the electromagnetic microwave in the absorber; and the multiple reflections are considered as the scattering effect of the inhomogeneity or heterogeneity within the materials[41].

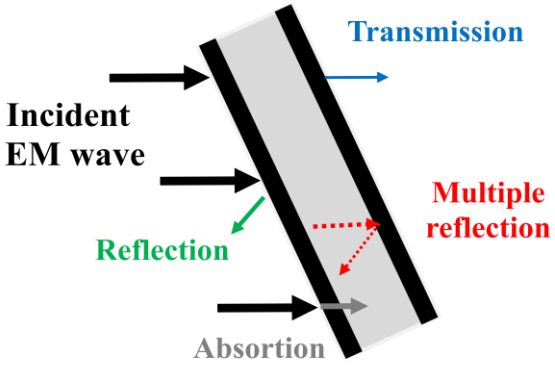

Figure 2.7. Schematic representation of the mechanisms involved in the EMI shielding process.

The EMI shielding effectiveness (SE) of a material is defined as the ratio between the incoming power (P_i) and outgoing/transmitted power (P_t) of an electromagnetic wave through a shielding material, which in other words is the addition of three contributions from absorption (SE_A), reflection (SE_R) and multiple reflections inside the material (SE_M) [42-43]. In order to better understand the effect of foaming and the presence of GnP in polycarbonate on the shielding mechanisms, the contribution of absorption, multiple reflections and reflection mechanisms to the total SE (SE_T) were quantified. The utilized EMI SE characterization setup enabled determining the measured scattering parameters (i.e., forward transmission S_{21} and forward reflection S_{11}), with these parameters it was possible to calculate the shielding effectiveness of transmitted power (SE_t) and the shielding effectiveness of reflected power (SE_R) using the following equations [43-45]:

$$SE_T = 20log(S_{21}) \quad (2.20)$$

$$SE_R = 20log(S_{11}) \quad (2.21)$$

With this in mind the contribution of absorption (SE_A) and multiple reflections (SE_M) could be expressed as:

$$SE_A + SE_M = SE_T - SE_R \quad (2.22)$$

The maximum EMI shielding effectiveness at 8.5 GHz was chosen to be reported for composite foams prepared. With this, the power attenuation factor of the EM radiation is calculated from:

$$SE = 10.Log\frac{P_i}{P_t} \quad (2.23)$$

$$P_i = 10^{\frac{SE}{10}}.P_t \quad (2.24)$$

$$Power\ attenuation\ factor = 10^{\frac{SE}{10}} \quad (2.25)$$

The percentage of transmission (P_t) is then obtained from:

$$P_t = \frac{P_i}{10^{\frac{SE}{10}}}.100 \quad (2.26)$$

2.4. References

[1] Cheung YW, Stein RS. Critical Analysis of the Phase Behavior of Poly(.epsilon.-caprolactone) (PCL)/Polycarbonate (PC) Blends. Macromolecules. 1994;27(9):2512-9.

[2] Pham HT, Weckle CL, Ceraso JM. Rheology Enhancement in PC/ABS Blends. Advanced Materials. 2000;12(23):1881-5.

[3] Young RJ, Kinloch IA, Gong L, Novoselov KS. The mechanics of graphene nanocomposites: A review. Composites Science and Technology. 2012;72(12):1459-76.

[4] Song P, Cao Z, Cai Y, Zhao L, Fang Z, Fu S. Fabrication of exfoliated graphene-based polypropylene nanocomposites with enhanced mechanical and thermal properties. Polymer. 2011;52(18):4001-10.

[5] Lee C, Wei X, Kysar JW, Hone J. Measurement of the Elastic Properties and Intrinsic Strength of Monolayer Graphene. Science. 2008;321(5887):385-8.

[6] Teweldebrhan D, Balandin AA. Modification of graphene properties due to electron-beam irradiation. Applied Physics Letters. 2009;94(1):013101.

[7] Antunes M, Realinho V, Ardanuy M, Maspoch ML, Velasco JI. Mechanical properties and morphology of multifunctional polypropylene foams. Cellular Polymers 2011;30 187-200.

[8] Kuilla T, Bhadra S, Yao D, Kim NH, Bose S, Lee JH. Recent advances in graphene based polymer composites. Progress in Polymer Science (Oxford). 2010;35(11):1350-75.

[9] Yavari F, Koratkar N. Graphene-Based Chemical Sensors. The Journal of Physical Chemistry Letters. 2012;3(13):1746-53.

[10] Wang H, Robinson JT, Diankov G, Dai H. Nanocrystal Growth on Graphene with Various Degrees of Oxidation. Journal of the American Chemical Society. 2010;132(10):3270-1.

[11] Singh V, Joung D, Zhai L, Das S, Khondaker SI, Seal S. Graphene based materials: Past, present and future. Progress in Materials Science. 2011;56(8):1178-271.

[12] Young RJ, Kinloch IA, Nicolais L. Graphene Composites. Wiley Encyclopedia of Composites: John Wiley & Sons, Inc. 2011.

[13] Urbanczyk L, Calberg C, Detrembleur C, Jérôme C, Alexandre M. Batch foaming of SAN/clay nanocomposites with scCO2: A very tunable way of controlling the cellular morphology. Polymer. 2010;51(15):3520-31.

[14] Tomasko DL, Burley A, Feng L, Yeh S-K, Miyazono K, Nirmal-Kumar S, et al. Development of CO2 for polymer foam applications. The Journal of Supercritical Fluids. 2009;47(3):493-9.

[15] Jacobs LJM, Kemmere MF, Keurentjes JTF. Sustainable polymer foaming using high pressure carbon dioxide: a review on fundamentals, processes and applications. Green Chemistry. 2008;10(7):731-8.

[16] Lee LJ, Zeng C, Cao X, Han X, Shen J, Xu G. Polymer nanocomposite foams. Composites Science and Technology. 2005;65(15–16):2344-63.

[17] Ibeh CC, Bubacz M. Current Trends in Nanocomposite Foams. Journal of Cellular Plastics. 2008;44(6):493-515.

[18] Cooper AI. Polymer synthesis and processing using supercritical carbon dioxide. Journal of Materials Chemistry. 2000;10(2):207-34.

[19] Baldwin DF, Park CB, Suh NP. A microcellular processing study of poly(ethylene terephthalate) in the amorphous and semicrystalline states. Part I: Microcell nucleation. Polymer Engineering & Science. 1996;36(11):1437-45.

[20] Di Maio E, Mensitieri G, Iannace S, Nicolais L, Li W, Flumerfelt RW. Structure optimization of polycaprolactone foams by using mixtures of CO2 and N2 as blowing agents. Polymer Engineering & Science. 2005;45(3):432-41.

[21] Park CB, Baldwin DF, Suh NP. Effect of the pressure drop rate on cell nucleation in continuous processing of microcellular polymers. Polymer Engineering & Science. 1995;35(5):432-40.

[22] ISO. Methods for determining the density of non-cellular plastics -- Part 1: Immersion method, liquid pyknometer method and titration method. UNE-EN ISO 1183-1 2004.

[23] Bledzki AK, Faruk O. Effects of the chemical foaming agents, injection parameters, and melt-flow index on the microstructure and mechanical properties of microcellular injection-molded wood-fiber/polypropylene composites. Journal of Applied Polymer Science. 2005;97(3):1090-6.

[24] Zhai W, Park CB, Kontopoulou M. Nanosilica Addition Dramatically Improves the Cell Morphology and Expansion Ratio of Polypropylene Heterophasic Copolymer Foams Blown in Continuous Extrusion. Industrial & Engineering Chemistry Research. 2011;50(12):7282-9.

[25] Sims GLA, C. K. Cell Polym. 1994;13:137.

[26] Sorrentino L, Di Maio E, Iannace S. Poly(ethylene terephthalate) foams: Correlation between the polymer properties and the foaming process. Journal of Applied Polymer Science. 2010;116(1):27-35.

[27] Sakintuna B, Yürüm Y, Çetinkaya S. Evolution of Carbon Microstructures during the Pyrolysis of Turkish Elbistan Lignite in the Temperature Range 700−1000 °C. Energy & Fuels. 2004;18(3):883-8.

[28] Glatter O, Kratky O. Small angle X-ray scattering. London: Academic Press Inc; 1982.

[29] Xu J-Z, Chen C, Wang Y, Tang H, Li Z-M, Hsiao BS. Graphene Nanosheets and Shear Flow Induced Crystallization in Isotactic Polypropylene Nanocomposites. Macromolecules. 2011;44(8):2808-18.

[30] King S, Flannery D. New Functionality in CORFUNC. Fibre Diffraction Review. 2005;13(13):19-22.

[31] Baltá-Calleja FJ, Vonk CG. X-ray scattering of synthetic polymers: Elsevier; 1989.

[32] Bower DI, Maddams WF. The vibrational spectroscopy of polymers. Cambridge: Cambridge University press; 1989.

[33] Stuart BH. The application of Raman spectroscopy to the tribology of polymers. Tribology International. 1998;31(11):687-93.

[34] Kuptsov AH. Handbook of fourier transform Raman and infrared spectra of polymers. New York: Elsevier; 1998.

[35] Lee SN, Stolarski V, Letton A, Laane J. Studies of bisphenol-A–polycarbonate aging by Raman difference spectroscopy. Journal of Molecular Structure. 2000;521(1–3):19-24.

[36] Haberer D, Vyalikh DV, Taioli S, Dora B, Farjam M, Fink J, et al. Tunable Band Gap in Hydrogenated Quasi-Free-Standing Graphene. Nano Letters. 2010;10(9):3360-6.

[37] Brandrup J IRH. Polymer Handbook. 2nd ed. New York: Wiley; 1975.

[38] Legras R, Mercier JP. Crystallization of bisphenol-A polycarbonate. III. Spherulitic growth rate of the plasticized polymer. Journal of Polymer Science: Polymer Physics Edition. 1979;17(7):1171-81.

[39] Han Z, Fina A. Thermal conductivity of carbon nanotubes and their polymer nanocomposites: A review. Progress in Polymer Science. 2011;36(7):914-44.

[40] T'Joen C, Park Y, Wang Q, Sommers A, Han X, Jacobi A. A review on polymer heat exchangers for HVAC&R applications. International Journal of Refrigeration. 2009;32(5):763-79.

[41] Zhang H-B, Yan Q, Zheng W-G, He Z, Yu Z-Z. Tough Graphene−Polymer Microcellular Foams for Electromagnetic Interference Shielding. ACS Applied Materials & Interfaces. 2011;3(3):918-24.

[42] Yang Y, Gupta MC, Dudley KL, Lawrence RW. Novel Carbon Nanotube−Polystyrene Foam Composites for Electromagnetic Interference Shielding. Nano Letters. 2005;5(11):2131-4.

[43] Joo J, Epstein AJ. Electromagnetic radiation shielding by intrinsically conducting polymers. Applied Physics Letters. 1994;65(18):2278-80.

[44] Joo J, Lee CY. High frequency electromagnetic interference shielding response of mixtures and multilayer films based on conducting polymers. Journal of Applied Physics. 2000;88(1):513-8.

[45] Kim HM, Kim K, Lee CY, Joo J, Cho SJ, Yoon HS, et al. Electrical conductivity and electromagnetic interference shielding of multiwalled carbon nanotube composites containing Fe catalyst. Applied Physics Letters. 2004;84(4):589-91.

Chapter 3

Morphology and cellular structure

3.1 Summary.

This chapter is focused on the effects that process variables have on the cellular morphology of foams. As a consequence, the final cellular morphology of these foams will play a key role in the behavior and functionalities of the final materials. With that in mind, this chapter displays the characterization and analysis of the cellular structure of Polycarbonate (PC) and Polycarbonate with graphene nanoparticles (PC-GnP) foams prepared by two different physical foaming processes using carbon dioxide in supercritical conditions (i.e., one-step and two-step as previously explained in chapter 2).

The idea is to be able to prepare foams with a broad range of densities and different morphological characteristics (i.e. cell size, expansion ratio, aspect ratio), taking into consideration that the variation of foaming processes and the selection of specific process parameters will enable the production of foams to satisfy a wide-range of applications [1]. In general, foams with different cellular structures and densities will have different final properties. For instance, the mechanical properties of polymeric foams will be expected to decrease due to the presence of the cellular structure (i.e. less solid fraction) [2]. In order to target the enhancing of foams' properties, the addition of stiff fillers such as graphene nanoplatelets with high mechanical properties (such as stiffness and strength [3]) and high aspect ratios, will have the particular potential to enhance the physical performance of the final cellular composite [4]. However, the presence of fillers will be expected to modify the resulting cellular structure of the foams, which will be discussed and presented in this chapter.

[1] Hansen R. Handbook of polymeric foams and foam technology, Daniel Klempner and Kurt C. Frisch, eds., Hanser Publishers, Munich, Germany, 1992, 442 pp. (Distributed in the U.S. and Canada by Oxford University Press, New York.). Journal of Polymer Science Part A: Polymer Chemistry. 1993;31(5):1344.
[2] Lee LJ, Zeng C, Cao X, Han X, Shen J, Xu G. Polymer nanocomposite foams. Composites Science and Technology. 2005;65(15–16):2344-63.
[3] Young RJ, Kinloch IA, Gong L, Novoselov KS. The mechanics of graphene nanocomposites: A review. Composites Science and Technology. 2012;72(12):1459-76.
[4] Verdejo R, Saiz-Arroyo C, Carretero-Gonzalez J, Barroso-Bujans F, Rodriguez-Perez MA, Lopez-Manchado MA. Physical properties of silicone foams filled with carbon nanotubes and functionalized graphene sheets. European Polymer Journal. 2008;44(9):2790-7.

The studies presented in this chapter were based on different hypotheses that were thought through in order to establish the different objectives of the study. A first hypothesis takes into consideration that the presence of GnP could significantly modify the diffusivity behavior of CO_2 within the polymer. As a second hypothesis, it was thought that different foaming processes and the variation of foaming parameters such as temperature/pressure of foaming and time of CO_2 dissolution could enable the production of foams with a wide range of densities and different cellular morphologies. At the same time, the cellular morphology of foams can significantly be affected by the content of graphene nanoplatelets, affecting the cell nucleation and cells' growth. Indeed, it was thought that foaming conditions applied could induce anisotropy in the cellular morphologies developed. While the combined effect of foaming conditions and the formation of anisotropic cellular morphologies could lead to orientation of GnP within the foams.

After having discussed through the hypotheses displayed above, the main objective of this chapter was established, being to determine the influence of processing parameters and the presence of GnP on the final cellular morphology of foams prepared via two different foaming processes with carbon dioxide. For this end, four specific objectives were established. Firstly it was necessary to analyze the kinetics of diffusion of CO_2 in Polycarbonate and PC-GnP composites. This was then linked to the final cellular structure of foams, after characterizing the cellular morphology of foams prepared via two foaming methods. Subsequently, the correlation of values such as temperature, time and pressure used during foaming with the final morphology characteristics of foams (i.e. relative densities, cell sizes, cell densities, aspect ratios, expansion ratios) was pursued [5,6]. This chapter was completed after investigating the influence of the presence of GnP contents on the final morphology of foams [7,8].

In order to satisfy the hypotheses and objectives established above, experiments and measurements of density, CO_2 desorption in PC and composites, as well as scanning electron

[5] Gedler G, Antunes M, Realinho V, Velasco JI. Characterization of polycarbonate foam structure prepared by one-step sc-CO2 dissolution process. Proceedings of the 10th International Conference on Foam Materials & Technology-SPE-FOAMS 2012.
[6] Gedler G, Antunes M, Velasco JI. Polycarbonate foams with tailor-made cellular structures by controlling the dissolution temperature in a two-step supercritical carbon dioxide foaming process. The Journal of Supercritical Fluids. 2014;88(0):66-73.
[7] Gedler G, Antunes M, Realinho V, Velasco JI. Novel polycarbonate-graphene nanocomposite foams prepared by CO2 dissolution. IOP Conference Series: Materials Science and Engineering. 2012;31(1):012008.
[8] Gedler G, Antunes M, Velasco JI. Effects of graphene nanoplatelets on the morphology of polycarbonate–graphene composite foams prepared by supercritical carbon dioxide two-step foaming. The Journal of Supercritical Fluids. 2015;100(0):167-74.

microscopy were carried out. The results have been analyzed and discussed in terms of the Fick's law of diffusion [9,10], that takes into account that the flux will go from regions of high concentration to regions of low concentration, with a magnitude that is proportional to the concentration gradient. The diffusion of CO_2 within the polymer was remarkably affected for contents of GnP of 5 wt.% when compared to contents of 0.5 and 2 wt.%., showing that large contents of GnP will restrict the diffusion of CO_2 in the composites, which is known as the barrier effect. The diffusion of CO_2 within the polymer under different conditions and content of GnP led to different quantities of gas dissolved in the material (i.e. varying from 3 to 7 wt.% CO_2), which had an effect on cell nucleation when the system was seeking for a state of lower free energy after creating the thermodynamic instability (in our case achieved by lowering the solubility of the solution decreasing the pressure), for this end, the kinetics of nucleation [11,12] was used for the analysis of cellular morphology. Especially when introducing the presence of GnP into the system that promoted a faster cell nucleation, reducing the cell sizes from 160 μm for neat PC foams to 30 μm for composites with 5 wt.% GnP in the case of foams prepared via the one-step foaming process, while for foams prepared via the two-step foaming process the cell sizes experienced a reduction from 700 μm for neat PC foams to 7 μm for composite foams with 5 wt.% GnP content.

The use of CO_2 as a foaming agent introduced the theory of the free volume [13] in this chapter, which was used to analyze the plasticizing effect of CO_2 in supercritical conditions in PC and PC-GnP composites. That effect lowered the glass transition temperature of the systems promoting a larger difference between the foaming temperature and the actual lowered-T_g of the systems, allowing the cell growth to larger extends until the molecular structure could freeze when the T_g of the system was reached. It needs to be pointed out that the systems experienced a fast temperature drop during depressurization in addition to the cooling applied to the foam environment. The temperature effect was evident in the composite foams prepared via the one-step foaming process, where the cell sizes increase from ~60 μm to 150 μm for foaming temperatures of 200 ^oC and 213 ^oC respectively. The used of these theories allowed us to observed changes in the diffusion coefficient, the nucleation speed/cell sizes, as well as the plasticization effect of the CO_2.

[9] Crank J. The mathematics of diffusion. London: Oxford University Press; 1956.
[10] Mills N. Polymer Foams Handbook: Engineering and Biomechanics Applications and Design Guide: Elsevier Science; 2007.
[11] Gibson LJ, Ashby MF. Cellular Solids, Structure and Properties. 2nd ed. ed. Oxford: Pergamon Press; 1999.
[12] Park CB, Baldwin DF, Suh NP. Effect of the pressure drop rate on cell nucleation in continuous processing of microcellular polymers. Polymer Engineering & Science. 1995;35(5):432-40.
[13] Godwin A. Plasticizers. In: Craver CDC, Charles E., Jr, ed. Applied Polymer Science: 21st Century. Oxford: Elsevier Science. 2000.

From this chapter the following conclusions can be extracted:

1) The one-step foaming process allowed the preparation of foams with relative densities ranging from 0.3-0.8 with cell sizes between 50 μm and 200 μm.

2) Low relative density foams (< 0.3) with large range of cell sizes (i.e. 7 μm and 700 μm) were successfully prepared via the two-step foaming process.

3) The foaming temperature was found to have a large effect on the final morphology of the foams prepared via the one-step foaming process, with foams increasing cell sizes from 50 μm to 200 μm, when the foaming temperature was increased from 200 ºC to 220 ºC).

Particularly, for the foams prepared via one-step, the resulted morphology was attributed to the combined effect of high temperatures which is related to the quantity of CO_2 dissolved in the material in the absence of cell coalescence.

4) In the case of the foams prepared via the two-step process, the morphology of the foams was found to be dependent on the quantity of CO_2 dissolved in the material previous expansion. It was observed that cell sizes increased from 7 μm to 700 μm while increasing the quantity of dissolved CO_2 from 4 wt.% to 7 wt.%. The development of larger cell sizes was attributed to cell coalescence.

5) The presence of graphene nanoplatelets promoted the increment of nucleation speed of cells thus increasing the cell density and reducing the cell sizes. For composite foams with 0.5 wt.% GnP (i.e. cell size 15 μm - 200 μm), while for the 5 wt.% GnP a reduction of cell sizes (i.e. 7 μm-20 μm) was observed as a consequence of the combined effect of the heterogeneous nucleation and the restriction to the flow of polymer during foaming due to the presence of larger contents of GnP.

3.2 Published articles.

This chapter displays the analyses and results throughout four publications. The first one entitled ***Characterization of polycarbonate foam structure prepared by one-step sc-CO_2***

dissolution process published in the proceedings of the **10th International Conference on Foam Materials & Technology-SPE-FOAMS 2012, Barcelona, Spain,** focuses on the analysis of the morphological structure of PC foams with medium relative densities (i.e.~0.3-0.5) prepared via one-step process and displays their morphological characterization.

The second publication entitled ***Novel polycarbonate-graphene nanocomposite foams prepared by CO_2 dissolution*** published in **IOP Conference Series: Materials Science and Engineering. 2012; 31(1):012008,** focuses on the morphological analysis in a similar fashion than the first publication but in this case the foams studied were PC-GnP foams with medium-high densities (i.e.~0.3-0.8), also prepared via the one-step process.

The third publication entitled ***Polycarbonate foams with tailor-made cellular structures by controlling the dissolution temperature in a two-step supercritical carbon dioxide foaming process,*** published in **The Journal of Supercritical Fluids. 2014; 88(0):66-73,** centered the analysis on the morphological analysis of neat PC foams in the low relative density range (< 0.3) prepared via the two-step process.

In a similar fashion, the fourth publication entitled ***Effects of graphene nanoplatelets on the morphology of polycarbonate–graphene composite foams prepared by supercritical carbon dioxide two-step foaming,*** published in **The Journal of Supercritical Fluids. 2015;100(0):167-174,** focuses on the morphological characterization of PC-GnP foams prepared via two-step foaming process ranging from low relative densities (i.e. < 0.3) to medium range relative densities (i.e. ~0.4-0.6). It is necessary to point out that complementary results regarding morphological characterization will be show in next chapters when necessary.

CHARACTERIZATION OF POLYCARBONATE FOAM STRUCTURE PREPARED BY ONE-STEP SC-CO_2 DISSOLUTION PROCESS

Gabriel Gedler, Marcelo Antunes, Vera Realinho and José I. Velasco.
Centre Català del Plàstic, Departament de Ciència dels Materials i Enginyeria Metal·lúrgica, Universitat Politècnica de Catalunya, BarcelonaTech. C/Colom 114.08222 Terrassa.Barcelona, Spain.

Abstract

In this communication, polycarbonate foams were prepared by a supercritical CO_2 dissolution one-step batch foaming process. Firstly, CO_2 diffusion behavior in polycarbonate was studied by means of desorption experiments. The cellular structure of foams prepared under different foaming conditions was characterized through scanning electron microscopy. Different foaming temperatures as well as CO_2 saturation pressures and times were applied. The foams displayed typical closed-cell structures with cell densities ranging from 3×10^5 to 6×10^6 cells/cm^3 and cell average sizes from around 70 to 150 μm. Analysis by X-ray diffraction and differential scanning calorimetry seemed to suggest that slight crystallization took place because of the plasticizing effect of CO_2 during saturation and foaming. Thermogravimetric analysis showed a higher thermal stability of the foams when compared to the compact polymer.

The preliminary results shown in this work suggest the possibility of developing lightweight polycarbonate components with improved specific thermal properties through carefully controlling the foaming parameters.

Introduction

Polycarbonate (PC) is one of the most used engineering plastics and polymeric foams are currently used in industrial applications where lightness is a key factor [1]. The final properties of these foams depend on their cellular structure, which includes parameters such as the average cell size and size distribution, cell volume fraction and cell arrangement within the matrix [2]. Nevertheless, the use of polymer foams is somewhat limited due to the inherent reduction of their mechanical properties with foaming when compared to the unfoamed base material. These foams are known for displaying better specific properties when cell sizes are reduced to a micrometer scale, hence having the potential to significantly alter the way plastics are employed in a wide variety of applications [3]. One of the most common microcellular foaming processes uses a physical blowing agent that creates an evenly distributed micrometric-sized closed cell structure, which significantly improves the mechanical properties compared to more heterogeneous or open cell structures [4]. Supercritical carbon dioxide (sc-CO_2) is one of the most favorable foaming agents due to its combination of chemical inertness, non-flammability and mild supercritical conditions (T_c = 31 ºC, P_c = 7.38 MPa) [5], also being environmentally benign [6]. One of the advantages of using physical blowing agents is that cell structure may be controlled through the processing temperature and pressure. Nevertheless, in order to optimize the foam properties, an overall understanding of the gas diffusion and the nucleation and growth mechanisms is required [2]. The influence of the foaming conditions has lately been considered, mainly focused in obtaining high performance foams by means of decreasing cell size [7].

It is known that some polymers, when processed with CO_2 undergo kinetically favorable configuration rearrangement of polymer chains, hence forming crystalline structures. For polycarbonate, the crystallization is very slow due to its inherent chain rigidity, which retards chain diffusion and ultimately inhibits crystallization at commonly used industrial processing conditions [8]. Thus, different strategies such as the addition of organic solvents [9], vapors [10], low melting point polymers [11], supercritical carbon dioxide [12], vapor-grown carbon fibres [13] or nano-sized fillers [14] have been used to induce the crystallization of polycarbonate. Therefore, foaming using sc-CO_2 could have a significant effect in the possible crystallization of PC.

The purpose of this study was to prepare polycarbonate foams through a physical sc-CO_2 one-step batch foaming process and to characterize them in terms of the developed cellular structure morphology and observe the effect of the foaming process on the crystallinity of polycarbonate.

Materials and foaming

Polycarbonate (Lexan-123R-PC, supplied by Sabic), with a density of 1.2 g/cm^3 and MFI of 17.5 dg/min, measured at 300 ºC and 1.2 kg, was melt-mixed using a Brabender Plasti-Corder internal mixer.

Firstly, the PC pellets were slowly introduced in the internal mixer at a temperature of 180 ºC using a rotating speed of 30 rpm during 2 min. Then the rotating speed was increased to 60 rpm and 120 rpm for 1 and 3 min,

respectively. The material was cooled at room temperature, grinded and compression-moulded at 220 ºC and 4.5 MPa (45 bar) in a hot-plate press (IQAP LAP PL-15) to discs with a thickness of 3.5 mm and diameter of 74 mm in 3 steps. In the first step the upper hot plate was used to soften the material at a temperature of 220 ºC. The second step consisted in allowing air to escape the material by pulsating the upper plate in an up and down motion. The pressure applied from the upper plate was 4.5 MPa (45 bar) at a temperature of 220 ºC during 1.5 min. For the third step the material was continuously compressed for 1 min at 220 ºC and 4.5 MPa. Lastly, the mould with the sample still inside was left to cool for 15 min in the cooling station of the press applying a constant pressure of 4.5 MPa. The discs used in the CO_2 desorption measurements were prepared by mechanically reducing the disc diameter to a typical value of 40 mm.

The resulting compression-molded discs were used to prepare the foams by sc-CO_2 dissolution using a one-step batch process that consisted in saturating the discs with CO_2 inside the high pressure vessel at pressures varying from 13 to 22 MPa during time periods between 0 and 40 min. The values of the saturation/foaming temperature varied between 200 and 213 ºC, and foaming was done in one-step by applying a sudden pressure drop, keeping residual pressure of 1 MPa (10 bar), as it was the optimal residual pressure to attain spherical-like cellular structures (AR = 1), found in one of our previous work [15].

Measurements and testing

In order to determine both the solubility and diffusion coefficient of CO_2 in the polycarbonate, CO_2 desorption measurements were carried out. Samples were introduced in the high pressure vessel and heated up to 210 ºC at a CO_2 pressure of 16 MPa. After reaching the saturation conditions, the samples were cooled to 40 ºC and the vessel was fully decompressed. Next, the saturated samples were removed from the vessel and quickly transferred to a digital balance (Mettler Toledo PB303 DeltaRange, with a sensitivity of 1 mg) at room temperature and atmospheric pressure, in order to record the CO_2 mass loss as a function of desorption time.

The maximum concentration of CO_2 in the samples after full decompression (M_o) was calculated by extrapolating to zero desorption time using the initial slope method [16]. Assuming one-dimensional diffusion in a plane sheet, the CO_2 desorption diffusion coefficient (D_d) was determined by plotting M_t/M_o vs. t/l^2, where M_t is the CO_2 concentration at time t and l is the thickness of the sample, according to the following equation [17]:

$$\frac{M_t}{M_t} = 1 - \frac{8}{\pi^2} exp\left(\frac{-D_d t}{l^2}\right) \quad (1)$$

The cellular structure of the foams was analyzed from scanning electron microscopy images obtained using a JEOL JSM-5610 microscope applying a voltage of 15 kV and a working distance of 30 mm. Samples were previously prepared by fracturing at room temperature and depositing a thin layer of gold onto their surface in argon atmosphere using a BAL-TEC SCD005 Sputter Coater.

The average cell sizes (ϕ) in the vertical (ϕ_{VD}) and width (ϕ_{WD}) foaming directions were measured using the intercept counting method [18]. The cell aspect ratio (AR) was determined by dividing the value of the average cell size in the vertical direction by that measured in the horizontal one ($AR = \phi_{VD}/\phi_{WD}$). The cell density (N_f) was calculated using the following equation [19]:

$$N_f = \left(\frac{n}{A}\right)^{3/2} \left(\frac{\rho_s}{\rho_f}\right) \quad (2)$$

WAXS was carried out using a Panalytical diffractometer using Cu Kα radiation with a λ= 1.54 Å operating at 40 KV and 40 mA at room temperature. Scans were taken from 2 to 60 deg (2θ) using a calibration with an accuracy of 0.02 deg. The crystallinity percentage (*X*c) was determined taking into consideration the WAXS patterns according to:

$$X_c(\%) = \frac{A_c}{A_c + A_a} 100 \quad (3)$$

where A_c corresponds to the crystalline peak area and A_a to the amorphous halo area.

DSC was carried out using a Perkin Elmer, Pyris 1 model with a glycol-based Perkin Elmer Intracooler IIP calorimeter at a heating rate of 10 ºC/min from 30 to 300 ^oC using samples weighting around 4.0 mg. The glass transition temperature (T_g) of the unfoamed and foamed polycarbonate was determined using the inflection point heat capacity method. The melting temperature (T_m) was determined as the maximum temperature of the melting peak appearing in the melting endotherm, while the heat of fusion (ΔH) was obtained by direct integration of the peak. The crystallinity percentage (X_c) was determined according to:

$$X_c = \frac{\Delta H_m}{\Delta H_m^0 w_p} 100 \quad (4)$$

where w_p is the weight fraction of PC, ΔH_m is the melting enthalpy of the sample obtained by DSC and ΔH_m^o is the theoretical 100 % crystalline PC melting enthalpy (147.79 J/g)[17]).

Thermogravimetric analysis was performed in a TGA/DSC 1 Mettler Toledo Star System analyzer by heating samples of around 10.0 mg from 30 to 1000 ºC at a heating rate of 10 ºC/min under both nitrogen (constant 30 ml/min N_2 flow) and air atmospheres (constant 60 ml/min air flow). The temperatures corresponding to mass losses of 1, 5 and 50%, as well as the mass of the final residue obtained at 1000 ºC, were reported for the unfoamed and foamed polycarbonate.

Results and discussion

CO_2 diffusion coefficient from desorption measurements

The maximum concentration of CO_2 dissolved into PC was calculated by extrapolating to zero desorption time from the desorption measurements show in figure 1, finding a value of 42.6 mg CO_2/g material. As a result, the calculated diffusion coefficient (D_d) was 4.45×10^{-12} m^2/s obtained from the slope of figure 1(see graph embedded in Figure 1).

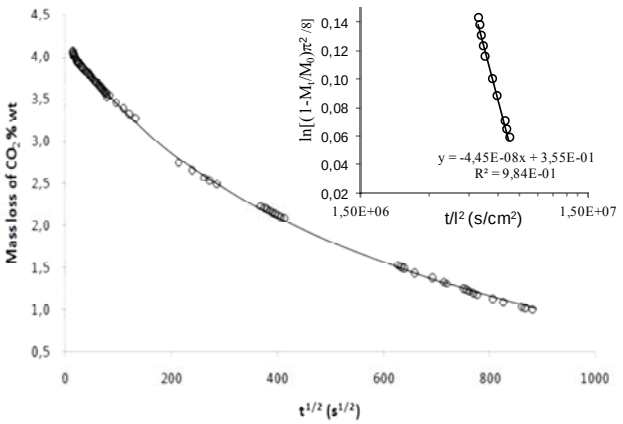

Figure 1. Results from the desorption study.

This value of the CO_2 diffusion coefficient in PC was found to be comparable to others presented in the literature, where D_d was found to be within 2.55×10^{-11} and 4.60×10^{-12} m^2/s [20] or between 1.55×10^{-12} and 6.93×10^{-12} m^2/s [21]. This result might suggest that the different in the values could be related to the degree of resistance that the CO_2 may have when desorbing the material, which could be related to the degree of crystallinity.

Cellular structure of PC foams

Polycarbonate foams (PC-f) were characterized by analyzing several scanning electron micrographs at different magnifications for each foam (typical SEM micrographs are displayed in Figure 2). The average cell size was determined for each foam obtained at a given saturation/foaming temperature, resulting in a variation in the cell density value from 1.04×10^6 to 2.70×10^6 cells/cm^3. The relative densities of the PC-f ranged from 0.33 to 0.46. As expected, a characteristic homogeneous microcellular structure was obtained due to the CO_2 saturation and sudden depressurization applied during foaming, with both the sudden pressure drop and time at saturation influencing the cell nucleation stage.

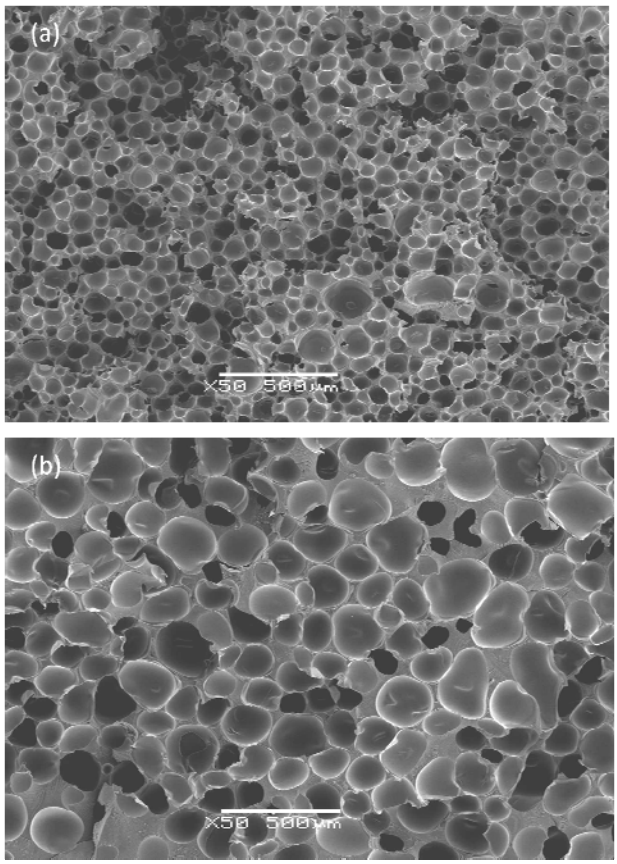

Figure 2. Typical SEM micrographs of the PC foams obtained at different saturation/foaming temperatures: (a) 200 ºC and (b) 205 ºC.

Figure 3 shows how cell size was clearly affected by the saturation/foaming temperature. Generally speaking, cell size increased from 70 to 160 μm with increasing the saturation/foaming temperature from 200 to 213 ºC, attributed to a higher concentration of CO_2 dissolved in the material. Decreasing the foaming temperature restricted cell growth and resulted in foams with higher relative densities. During the sudden depressurization stage, the temperature of the growing sample decreased quickly, mainly due to the adiabatic expansion of the gas, and in a minor way due to the water cooling system of the vessel. Hence, this behavior can be explained by a faster rigidization of the softened material foamed at a lower

temperature during the depressurization stage, reaching faster the glass transition temperature of the polymer than the samples foamed at higher temperatures.

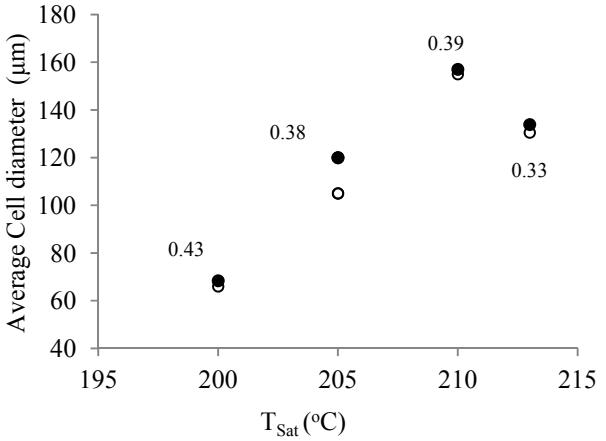

Figure 3. Influence of the saturation/foaming temperature on the average cell size of the PC foams. Hollow symbols: ϕ_{VD}; filled symbols: ϕ_{WD}. The relative density is indicated.

Crystalline structure of PC foams

WAXS measurements revealed the presence of a crystalline structure with diffractograms characterized by one strong peak at 2θ = 17.3º, corresponding to the monoclinic lattice reflections of (020),($\bar{2}$01) of crystalline PC [22]. Figure 4a shows a broad amorphous halo for the unfoamed PC and the presence of crystallization in the PC-f. The PC-f samples presented different degrees of crystallization depending on the process parameters used during the saturation/foaming stage. The increment of the temperature, pressure and time at CO_2 saturation conditions suggests the increment of crystallinity of the samples.

Table 1. Values of crystallinity calculated by WAXS and DSC.

Sample	Relative density	χ_c (%) by WAXS	χ_c (%) by DSC
PC	1	0	0
PC-s	1	0	0.2
1PC-f	0.43	0.95	0
2PC-f	0.46	0	0.57
3PC-f	0.38	0.51	0.97
4PC-f	0.39	1.04	0.45
5PC-f	0.33	0	0

It has been mentioned in the literature that crystalline PC may show other reflections as the (213) for a 2θ of 21.1º and the reflection of ($\bar{2}$22),(303),(223) around a 2θ of 25.3º [22, 23]. For the PC-f samples these aforementioned reflections were not very strong. However, very weak signals were noticed around 2θ = 20º and 2θ =25.3º, similar to the values found in the literature.

The differential scanning calorimetry analysis also showed that the PC-f samples obtained by sc-CO_2 dissolution presented melting peaks corresponding to PC crystallization (Figure 4(b)). The DSC study suggests that the saturation/foaming pressure might have an important effect on the crystallinity of the polycarbonate foams, showing a higher crystallinity for foams prepared with higher foaming pressures. Table 1 resumes the results of crystallinity calculated from WAXS and DSC measurements.

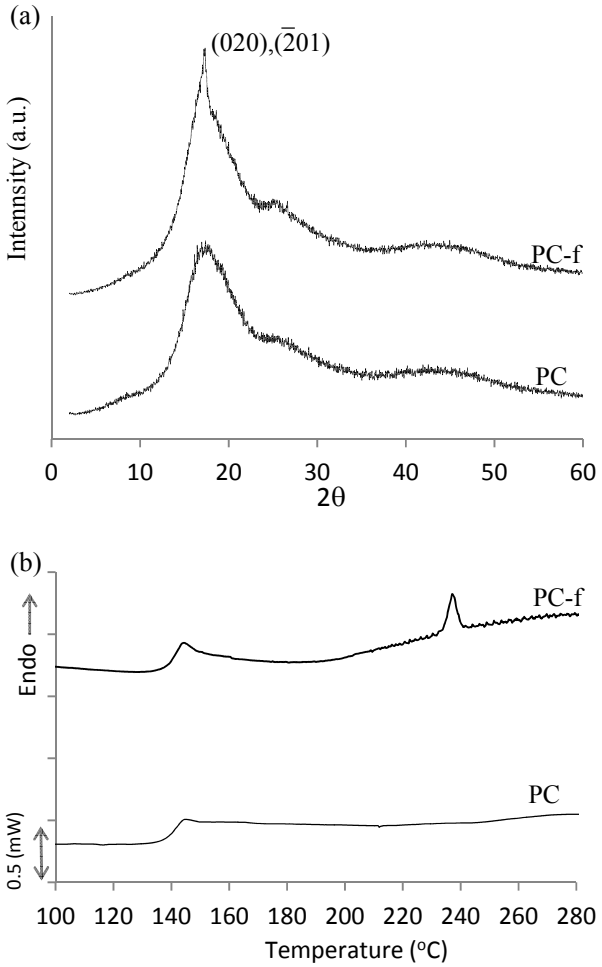

Figure 4. (a)WAXS spectra and (b) DSC heating curves of PC-f with a relative density of 0.38 and the unfoamed PC.

Enhanced thermal stability

The TGA and respective DTG thermograms of the unfoamed and foamed polycarbonate (PC and PC-f respectively) were obtained under both nitrogen and air atmospheres. For instance, PC showed a characteristic one-step decomposition process with an onset temperature

at 1 wt% loss of 388 ºC and a T_{max}, defined as the temperature at maximum mass loss rate in the DTG curve, of 430 ºC. It is well known that the main degradation pathways of polycarbonate can be classified into two categories: chain scission of isopropylidene bonds and hydrolysis/alcoholysis of carbonate bonds, including rearrangements of some carbonate bonds like decarboxylation or cross-linking upon heating, ultimately resulting in CO_2, H_2O and char [24].

The corresponding DTG thermogram suggested that two events could be occurring at different rates due to the shoulder observed in Figure 5(a), related to a smaller quantity of material undergoing the degradation process at that temperature. The PC-f samples showed a similar one-step decomposition, where was a delay corresponding to the beginning of the process for a 1 wt% loss of about 34 ºC and of 55 ºC for a 5 wt% loss when compared to the unfoamed material for a PC-f with a relative intensity of 0.38. The DTG curve showed a T_{max} shifted 70 ºC higher than for the unfoamed PC, however the degradation process occurred faster for the PC-f compared to the unfoamed material. The delay during the beginning of the degradation process was attributed to the material's cellular structure, which acted as an improved thermal insulator, inhibiting heat transfer at the beginning of the thermal decomposition process. In general the process was delayed while decreasing the relative density due to the thermal insulator explained above and the presence of crystalline structure confirmed by WAXS and DSC.

The thermal decomposition of PC in air occurred in three stages, as can be seen in Figure 5(b). The first stage corresponded to the thermo-oxidative decomposition of PC in air. The degradation process started with the chain scission of the isopropylidene bonds, including alcoholysis and hydrolysis of the carbonate bonds, similar to that under nitrogen atmosphere. The second stage (stage II) of the degradation process presented a slighter mass loss slope than the first main stage of degradation and had the shortest period of time of the three main degradation stages. This stage was attributed to the decomposition of the remaining polymer that was kept protected from burning due to the char layer formed during stage I, as well as the degradation of part of that previous char layer. Stage III was attributed to char oxidation produced in the previous stages. No solid residues were obtained after 1000 ºC, indicating a complete thermo-oxidative decomposition process of polycarbonate.

PC-f under air presented a shift in the temperature corresponding to the first decomposition stage towards higher values when compared to the unfoamed PC; for instance, the 1 and 5 wt% loss temperatures were delayed in 25 and 30 ºC, respectively. The DTG showed how the degradation process occurred faster than for the unfoamed PC, with a T_{max} shift of 16 ºC (see Figure 5(b)). The delay observed during the beginning of the degradation process was once again attributed to the cellular structure, which acted as a thermal insulator within the material, inhibiting heat transfer at the beginning of the thermal decomposition process, and to the presence of the crystalline phase [25].

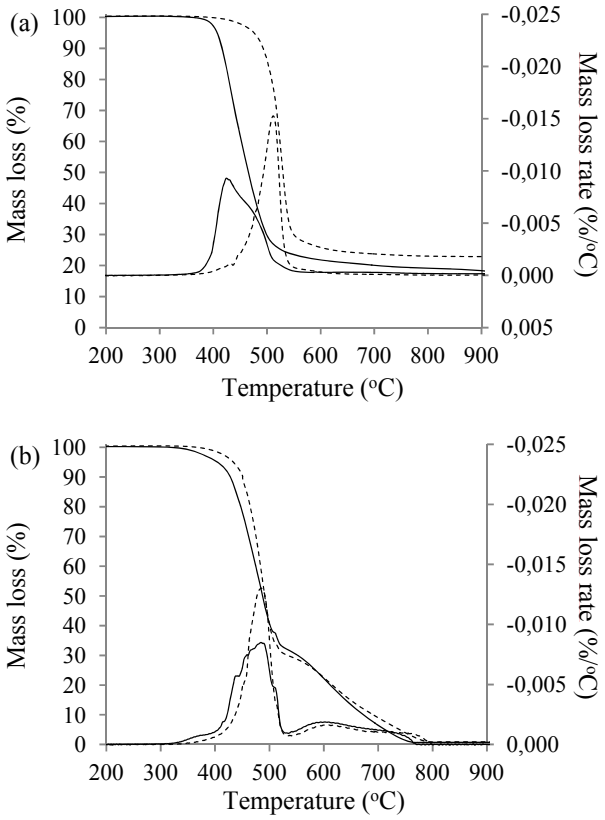

Figure 5. TGA and DTG thermograms of the unfoamed PC (continuous line) and foamed polycarbonate (PC-f, relative intensity: 0.38, dashed line), (a) under nitrogen and (b) under air atmosphere.

Conclusions

Polycarbonate foams were prepared and characterized in terms of their cellular structure characteristics. The study of the desorption kinetics of CO_2 out of PC showed similar values of the maximum CO_2 concentration dissolved into the material compared to the values found in the literature. The small difference of those values could be related to the degree of crystallinity present in the material.

The saturation/foaming temperature had a large effect on the morphology of the foams, with foams displaying smaller cell sizes with decreasing this temperature. This was attributed to a fast cooling of the polymer, which stopped foam growth once the glass transition temperature

was reached, and due to the presence of crystalline structures confirmed by WAXS and DSC measurements. In addition to the saturation temperature, other foaming parameters that resulted relevant for the degree of achieved crystallinity were the pressure and the time at saturation conditions, which promoted the formation and perfection of crystals. The simultaneous presence of the cellular structure and crystals enhanced the thermal stability of polycarbonate, which increased while decreasing the relative density of the samples.

Acknowledgements

The authors would like to acknowledge the Spanish Ministry of Economy and Competitiveness for the financial support of project MAT2011-26410.

References

1. A. Landrock, Handbook of Plastic Foams, Noyes, New Jersey (1995).
2. M.S. Yun, W.I. Lee, *Comp. Sci.Tech,* **68**, 202 (2008).
3. V. Kumar, J. Weller, *J. Eng. Industry* **116**, 413 (1994).
4. L.J. Lee, C. Zeng, X. Cao, X. Han, J. Shen, G. Xu, *Comp. Sci. Tech.* **65**, 2344 (2005).
5. A.I. Cooper, *J. Mater. Chem.* **10**, 207 (2000).
6. K. Goren, L. Chen, L.S. Schadler, R. Ozisik, *J. Superc. Fluids* **51**, 420 (2010).
7. M. Antunes, V. Realinho, J.I. Velasco, *J. Nanomater*, Article ID 306384 (2010).
8. X. Hu, A. J. Lesser, *Polymer* **45**, 2333 (2004).
9. E. Turska, H. Janeczek, *Polymer* **20**, 855 (1979).
10. J.M. Jonza, R.S. Porter, *J. Polym. Sci. Part B: Polymer Physics* **24**, 2459 (1986).
11. E. Laredo, M. Grimau, P. Barriola, A. Bello, A.J. Müller, *Polymer* **46**, 6532 (2005).
12. E. Beckman, R.S. Porter, *J. Polym. Sci. Part B: Polymer Physics* **25**, 1511 (1987).
13. T. Takahashi, K. Yonetake, K. Koyama, T. Kikuchi, *Macromol. Rapid Commun,* **24**, 763 (2003).
14. V.N. Bliznyuk, V.N. Singamaneni, R.L. Sanford, D. Chiappetta, B. Crooker, P.V. Shibaev, *Polymer* **47**, 3915 (2006).
15. G. Gedler, M. Antunes, V. Realinho, J.I. Velasco, *IOP Conference Series: Materials Science and Engineering* **31**, 012008 (2012).
16. J. Crank, The mathematics of diffusion, Oxford University Press, London (1956).
17. J. Brandrup, E.H. Immergut, Polymer Handbook, Wiley, New York, Ed. 2nd (1975).
18. G.L.A. Sims, K.C. Khunniteekool, *Cell Polym* **13**, 137 (1994).
19. L. Sorrentino, E. Di Maio, S. Iannace, *J. Applied Polym. Sci,* **116**, 27 (2010).
20. M. Tang, T.B. Du, Y.P. Chen, *J. Superc. Fluids* **28**, 207 (2004).
21. M. Tang, W.H. Huang, Y.P. Chen, *J. Chinese Institute of Chemical Engineers* **38**, 419 (2007).
22. R. Bonart, Makromol. Chem., **92**, 149 (1966).
23. Z. Fan, C. Shu, Y. Yu, V. Zaporojtchenko, F. Faupel, *Polym. Eng. Sci.* **46**, 729 (2006).
24. B.N. Jang, C.A. Wilkie, *Polym. Degrad. Stab,* **86**, 419 (2004).
25. G. Gedler, M. Antunes, V. Realinho, J.I. Velasco, *Polym. Degrad. Stab.,* **97**, 1297 (2012).

Key Words: Polycarbonate foams, Supercritical CO_2, Crystallinity microstructure.

Novel polycarbonate-graphene nanocomposite foams prepared by CO_2 dissolution

2012 IOP Conf. Ser.: Mater. Sci. Eng. 31 012008

(http://iopscience.iop.org/1757-899X/31/1/012008)

J. of Supercritical Fluids 88 (2014) 66–73

Contents lists available at ScienceDirect

The Journal of Supercritical Fluids

journal homepage: www.elsevier.com/locate/supflu

Polycarbonate foams with tailor-made cellular structures by controlling the dissolution temperature in a two-step supercritical carbon dioxide foaming process

Gabriel Gedler, Marcelo Antunes, José Ignacio Velasco*

Centre Català del Plàstic, Departament de Ciència dels Materials i Enginyeria Metal·lúrgica, Universitat Politècnica de Catalunya BarcelonaTech (UPC), C/Colom 114, E-08222 Terrassa, Spain

article info

Article history:
Received 5 November 2013
Received in revised form 21 January 2014
Accepted 22 January 2014

Keywords:
Polycarbonate foams
Supercritical carbon dioxide
Two-step foaming
Tailor-made cellular structure
Physical aging

abstract

Closed-cell polycarbonate foams were prepared using a two-step foaming process, which consisted of the initial dissolution of supercritical CO_2 ($scCO_2$) into PC foaming precursors and their later expansion by heating using a double contact restriction method. The effects of the parameters of both CO_2 dissolution and heating stages on the cellular structure characteristics as well as on the physical aging of PC in the obtained foams were investigated. A higher amount of CO_2 was dissolved in PC with increasing the dissolution temperature from 80 to 100 °C, with similar CO_2 desorption trends and diffusion coefficients being found for both conditions. PC foams displayed an isotropic-like microcellular structure at a dissolution temperature of 80 °C. It was shown that it is possible to reduce their density while keeping their microcellular structure with increasing the heating time. On contrary, when dissolving CO_2 at 100 °C and later expanding, PC foams presented a cellular morphology with bigger cells and with an increasingly higher cell elongation in the vertical growth direction with increasing the heating time. Comparatively, PC foams obtained by dissolving CO_2 at 100 °C presented a more marked physical aging after CO_2 dissolution and foaming, although this effect could be reduced and ultimately suppressed with increasing the heating time.

0896-8446/$ – see front matter © 2014 Elsevier B.V. All rights reserved.
http://dx.doi.org/10.1016/j.supflu.2014.01.013

J. of Supercritical Fluids 100 (2015) 167–174

Contents lists available at ScienceDirect

The Journal of Supercritical Fluids

journal homepage: www.elsevier.com/locate/supflu

Effects of graphene nanoplatelets on the morphology of polycarbonate–graphene composite foams prepared by supercritical carbon dioxide two-step foaming

Gabriel Gedler, Marcelo Antunes, José Ignacio Velasco*

Centre Català del Plàstic, Departament de Ciència dels Materials i Enginyeria Metal·lúrgica, Universitat Politècnica de Catalunya · BarcelonaTech (UPC), C/Colom 114, E-08222 Terrassa, Spain

article info

Article history:
Received 4 September 2014
Received in revised form 3 February 2015
Accepted 4 February 2015
Available online 21 February 2015

Keywords:
Polycarbonate foams
Graphene nanoplatelets
Supercritical carbon dioxide Two-step foaming

abstract

Low density polycarbonate foams containing different amounts of graphene nanoplatelets with variable cellular morphologies were prepared using a supercritical carbon dioxide two-step foaming process, which consisted of the dissolution of supercritical CO_2 into moulded foam precursors and their later expansion by double contact restricted foaming. The effects of the processing conditions and graphene content on the cellular morphology of the obtained foams were investigated, showing that the addition of increasingly higher amounts of graphene nanoplatelets resulted in foams with increasingly smaller cell sizes and higher cell densities, due on the one hand to their effectiveness as cell nucleating agents and on the other to their platelet-like geometry, which limited CO_2 loss during foaming due to a barrier effect mechanism. Especially significant was the addition of 5 wt.% graphene nanoplatelets, as the high concentration of graphene limited CO_2 escape and cell coalescence during expansion, enabling to obtain highly expanded microcellular foams.

http://dx.doi.org/10.1016/j.supflu.2015.02.005 0896-8446/

Chapter 4

Microstructure and thermo-mechanical properties:

Crystallinity, thermal stability and viscoelasticity

4.1 Summary.

In the previous chapter the effects of two different foaming methods (i.e., one-step and two-step foaming processes) on the cellular morphology of PC and PC-GnP foams were discussed. In this chapter the possible effects that those two foaming processes in the presence of carbon dioxide and graphene nanoplatelets can have on the final microstructure of PC, possible leading to the development of a crystalline phase in the PC foams are studied. Knowing that improvements in mechanical properties [1-2] and somewhat small enhancements of thermal stability [3-4] in polymeric materials can be associated to their microstructure; it is necessary to analyze and determine possible changes in the microstructure of our polymeric systems and correlate them with possible effects on their final properties, in this chapter, the thermal stability and viscoelasticity of foams will be the main focus. The goal is to be able to tune the processes in order to develop foams with different microstructures and a wide range of densities, making these foams to open up their range of applications in different markets.

The analyses presented in this chapter were based on different hypothesis that were established taking into consideration the plasticizing effect of carbon dioxide, the presence of GnP with flat morphology and large aspect ratio (i.e. 15 μm/7nm as reported by manufacturer) and different process conditions, which were observed to have an effect on PC microstructure in the preliminary results shown in chapter 3. The first hypothesis stated that the dissolution of CO_2 could have an effect in the microstructure of the PC depending on the foaming process and the variation of foaming parameters. Taking into consideration that foaming takes place at temperatures higher than the T_g of PC which will promote molecular mobility (especially in the presence of CO_2 as previously discussed), this could induce to the formation of ordered structures. In a similar fashion the combined presence of CO_2 and graphene nanoplatelets could potentially modify the

[1] Auras R, Harte B, Selke S. An Overview of Polylactides as Packaging Materials. Macromolecular Bioscience. 2004;4(9):835-64.
[2] Gupta B, Revagade N, Hilborn J. Poly(lactic acid) fiber: An overview. Progress in Polymer Science. 2007;32(4):455-82.
[3] Hung C-Y, Wang C-C, Chen C-Y. Enhanced the thermal stability and crystallinity of polylactic acid (PLA) by incorporated reactive PS-b-PMMA-b-PGMA and PS-b-PGMA block copolymers as chain extenders. Polymer. 2013;54(7):1860-6.
[4] Spoljaric S, Genovese A, Shanks RA. Polypropylene–microcrystalline cellulose composites with enhanced compatibility and properties. Composites Part A: Applied Science and Manufacturing. 2009;40(6–7):791-9.

microstructure (i.e order/crystallinity) of PC in a larger scale during processing when compared with processing with CO_2 but without GnP. Another hypothesis established that the presence of GnP with flat morphology and large aspect ratio could promote decrease in the diffusion of gas in composites via a mechanism known as gas tortuosity (i.e. gas barrier effect) that reduces the diffusion of gas within the polymer due to the presence of obstacles (i.e. particles), this could be beneficial for the thermal stability of the composites, delaying the thermal degradation process when compared with the neat PC. At the same time, the formation of a cellular structure would be expected to promote a decrease in the heat conduction, therefore delaying the thermal degradation of the foams. It was thought that the presence of GnP within the solid fraction of foams could promote enhancements on the viscoelastic behavior of composite foams. Enhancements in the elastic and viscous characteristics of the foams were expected throughout a range of temperature (i.e. 30 ^{o}C -180 ^{o}C). Special consideration will plan to take on the storage modulus and glass transition temperature (T_g) as the main viscoelastic characteristics.

The main objective of this study was to characterize the microstructure, the thermal stability and viscoelastic behavior of foams prepared via two different foaming processes, paying special attention to the effects of the cellular morphology, microstructure of PC and the presence of GnP contents. For this end, different specific objectives were established. Firstly, the analysis of the microstructure of PC under the influence of CO_2 foaming with and without GnP was needed. The microstructural characteristics that were looked in detail were non-crystalline ordering, crystallinity percentage and lamellar thickness [5]. Secondly, it was necessary to carry out a similar analysis but in this case, to observe the combined effect of GnP and CO_2 on the microstructure of composites during foaming [5]. In order to characterize and analyze the effects of density, cell sizes and the presence of GnP on thermal stability of foams prepared via one-step [6] and two-step foaming method [7], the thermogravimetric analysis under nitrogen and air atmospheres were set as objectives. As the last specific objective in this chapter, it was established to analyze and correlate the effect of density, cell sizes, microstructure and presence of GnP on the viscoelastic behavior of

[5] Gedler G, Antunes M, Velasco JI. Graphene-induced crystallinity of bisphenol A polycarbonate in the presence of supercritical carbon dioxide. Polymer. 2013;54(23):6389-98.
[6] Gedler G, Antunes M, Realinho V, Velasco JI. Thermal stability of polycarbonate-graphene nanocomposite foams. Polymer Degradation and Stability. 2012;97(8):1297-304.
[7] Gedler G, Antunes M, Velasco JI. Low density polycarbonate–graphene nanocomposite foams produced by supercritical carbon dioxide two-step foaming. Thermal stability. Composites Part B: Engineering. 2016;92:299-306.

the foams prepared via the two different foaming methods [8]. In order to satisfy the hypotheses and objectives established above, a detailed analysis was carried out by means of Raman spectroscopy, wide angle X rays scattering (WAXS), small angle X rays scattering (SAXS), differential scanning calorimetry (DSC), scanning electron microscopy (SEM), atomic force microscopy (AFM), thermogravimetric analysis (TGA) and dynamic mechanical-thermal analysis (DMTA).

Since it was observed that changes in the microstructure were taking place, the results were analyzed and discussed in terms of crystallization lamellar model using the Gibbs-Thomson equation [9], which allowed us to estimate the lamellar thickness of crystals by using the melting temperatures from the DSC study. From that study, the double melting behavior was detected, meaning two different melting signals were detected in the DSC analysis, this was attributed to the formation of crystals with different thermal stabilities that were nucleated at different times, therefore the use of primary and secondary nucleation model [10] was used for this analysis. Since the formation of order non-crystalline was detected by means of Raman spectroscopy and SAXS and observed by AFM, the use of the Cahn–Hilliard model (spinodal decomposition) [11] was used in the analysis of signals detected by SAXS but not by WAXS for some of the samples. Therefore the separation of phases was considered; in which one of them can be forming an ordered structure in a long range but not reaching the 3D packing ordering necessary to be detected as crystallinity. Another model that was used in order to analyze the signals from SAXS was the finite lamellar stack model [12], which allowed us to estimate the lamellar thickness of crystals and compared them to the values obtained by the Gibbs-Thomson equation which used the melting temperatures of crystals as discussed above. In the case of GnP structural changes detected by WAXS, and observed by AFM, the Bragg's law and Debye-Scherrer relationship [13,14] were used in order to estimate the thickness of these GnPs, as they are stacks of graphene monolayers, the changes in thickness was attributed to dispersion/partial exfoliation during foaming due to the interactions between the graphitic structure and the CO_2 molecules. The presence of different microstructures

[8] Gedler G, Antunes M, Velasco JI. Viscoelastic properties of polycarbonate-graphene nanoplatelets nanocomposite foams. Composites Part B: Engineering. 2016;93:143-52.
[9] Mandelkern L. Crystallization of Polymers. 2nd ed. Cambridge: Cambridge University Press; 2002.
[10] Mandelkern L. The Relation between Structure and Properties of Crystalline Polymers. Polym J. 1985;17(1):337-50.
[11] Cahn JW, Hilliard JE. Free Energy of a Nonuniform System. I. Interfacial Free Energy. The Journal of Chemical Physics. 1958;28(2):258-67.
[12] Ruland W. The evaluation of the small-angle scattering of lamellar two-phase systems by means of interface distribution functions. Colloid & Polymer Sci. 1977, 255(5):417-27.
[13] Guinebretière R. X-Ray Diffraction by Polycrystalline Materials: Wiley; 2007
[14] Chu B, Hsiao BS. Small-Angle X-ray Scattering of Polymers. Chemical Reviews. 2001;101(6):1727-62.

was analyzed taking into consideration the free volume theory [15] which was attributed in part to the high molecular mobility induced by the plasticizing effect of the CO_2 on PC under the conditions studied.

Regarding the thermal stability analyses, the degradation of polymers theories [16] was employed when characterizing the degradation mechanisms of the different foams study depending on the atmospheres in which the experiences were carried out. The delays in the degradation of different materials were attributed to reduction of heat conduction through the solid fraction due to the presence of a cellular structures with different cell sizes and densities, while in the case of composites the presence of GnP acted as obstacles to restrict the diffusion of decomposition products as well as restriction to oxygen diffusion into the material when the study was carried out under air atmosphere. Regarding the mechanical characterization of the foams prepared via the two different foaming processes, the Gibson–Ashby model [17] was used for the analysis, where the elastic and viscous contributions were correlated to the density of foams, their cell sizes, microstructure and the presence of GnP contents. The presence of crystallinity and GnP promoted enhancements to the elastic modulus when compared to the neat counterpart foams. Regarding the viscous contribution, the combined precense of PC crystalline fraction and GnP limited the mobility of PC molecules which promoted higher glass transition temperatures. In general, these theories allowed us to observe changes in the microstructure by means of crystallinity and ordered structures, changes in GnP morphology by means of changes in thickness of GnPs, enhancements on the thermal stability and viscoelastic behavior of the foams prepared.

From this chapter the following conclusions can be extracted:

1) Raman spectroscopy allowed the correlations of changes in bands associated to intrachain (733 cm^{-1}) and interchain (1235 cm^{-1}) interactions due to regular arrangements in the structure of the materials prepared via one-step process. Especially in the presence of CO_2 and GnP that promoted a synergetic effect that induced the mobility of PC molecules

[15] Godwin A. Plasticizers. In: Craver CDC, Charles E., Jr, ed. Applied Polymer Science: 21st Century. Oxford: Elsevier Science. 2000.
[16] Beyler CL, Hirschler MM. Thermal decomposition of polymers. SFPE handbook of fire protection engineering. 2002;2:110-31.
[17] Gibson LJ, Ashby MF. Cellular Solids, Structure and Properties. 2nd ed. ed. Oxford: Pergamon Press; 1999.

2) The foams prepared via one-step foaming process developed enough quantity of order structures to be detected as crystallinity by WAXS and DSC (i.e crystallinities above 1 %). While the foams prepared via the two-step foaming process did not develop enough ordering to be detected as crystallinity by these techniques. This was attributed to the low energy used during the dissolution stage, where much lower temperatures (160 ^{o}C) and pressures (60 bar) where used compared with the one-step foaming process (> 200 ^{o}C, 150 bar).

3) Enhanced GnP dispersion/partial exfoliation was correlated to the reduction/almost disappearance of the characteristic (002) diffraction plane typical of the graphitic structure in the WAXS analysis.

4) The cellular structure played a thermal insulator role in the thermal stability of the foams studied due to the insulator mechanism promoted by the presence of cells (tortuosity to heat conduction). This mechanism delayed the thermal degradation process. Specifically, larger cell sizes (> 50 μm) hindered the heatl conduction within the solid fraction of these foams, promoting a tortuous path when compared with foams with smaller cell sizes (< 30 μm) (within foams with low densities).

5) The presence of the enhanced dispersion of graphene nanoplatelets throughout the solid fraction enhanced the final thermal stability of composite foams, due to the gas tortuous effect for products of decomposition.

6) The mechanical performance of foams was mainly driven by their relative density, as the relative storage modulus values of foams varied potentially with relative density.

7) The addition of graphene nanoplatelets demonstrated the effective reinforcement effect by adding higher amount of GnP and displaying higher specific relative storage modulus. Foams prepared in two steps displayed a less dependency of GnP's concentration when compared with the one-step foams, attributed to the little changes of the exponent "*n*" from the Gibson-Ashby relationship.

8) Foams prepared by one-step foaming presented higher T_g values when compared with the foams prepared in two steps. These differences of the viscous contribution were related to the presence of a PC crystalline fraction and the presence of GnP that combined, contributed to limit the mobility of PC molecules.

4.2 Published articles.

In this chapter the results and analyses are displayed in four publications. The first publication entitled ***Graphene-induced crystallinity of bisphenol A polycarbonate in the presence of supercritical carbon dioxide*** published in **Polymer. 2013; 54(23):6389-98,** focuses on elucidating the combined effect of CO_2 and graphene nanoplatelets on the microstructure of PC.

The second publication entitled ***Thermal stability of polycarbonate-graphene nanocomposite foams*** published in **Polymer Degradation and Stability. 2012; 97(8):1297-304,** focuses on displaying the analysis of thermal stability of PC and PC/graphene foams prepared via the one-step process, discussing in detail the enhancements of thermal stability and relating them to the different densities, cell sizes, the presence of graphene nanoplatelets. The third publication entitled ***Low density polycarbonate-graphene nanocomposite foams produced by supercritical carbon dioxide two-step foaming. Thermal stability*** published in **Composites Part B: Engineering. 2016; 92:299-306**, displays a similar analysis but in this case for foams prepared via the two-step foaming process.

The fourth publication entitled ***Viscoelastic properties of polycarbonate-graphene nanoplatelets nanocomposite foams*** published in the Journal of **Composites Part B: Engineering. 2016; 93:143-52,** displays the characterization of the viscoelastic properties of foams prepared by two different foaming processes, taking into consideration the densities, cell sizes and the presence of GnP and correlating these characteristics with the elastic and viscous contributions.

Polymer 54 (2013) 6389e6398

Contents lists available at ScienceDirect

Polymer

journal homepage: www.elsevier.com/locate/polymer

Graphene-induced crystallinity of bisphenol A polycarbonate in the presence of supercritical carbon dioxide

G. Gedler, M. Antunes, J.I. Velasco*

Centre Català del Plàstic, Departament de Ciència dels Materials i Enginyeria Metal\$lúrgica, Universitat Politècnica de Catalunya, BarcelonaTech (UPC). Colom 114, E-08222 Terrassa, Spain

a r t i c l e i n f o

Article history:
Received 2 August 2013
Received in revised form
19 September 2013
Accepted 25 September 2013
Available online 2 October 2013

Keywords:
Crystallinity
Polycarbonate
Graphene

a b s t r a c t

Changes in the crystallinity of polycarbonate (PC) induced by the simultaneous presence of 0.5 wt% graphene nanoplatelets (GnP) and supercritical carbon dioxide (sc-CO_2) were examined by means of Raman spectroscopy, WAXS, SAXS and DSC. Composites were prepared by melt-mixing, compression-molding and dissolving sc-CO_2 at high pressure and temperature. It was found that dissolved CO_2 induced the formation of an ordered non-crystalline phase in PC during slow cooling under pressure. A fast depressurization and cooling did not cause such an effect in the resultant foams. GnP induced a higher crystallinity in PC, especially when combined with sc-CO_2, even during fast depressurization and cooling. Raman spectroscopy enabled to correlate changes in the PC vibration modes with the presence of ordered phases, as well as to detect interactions between GnP and PC. Additionally, evidence of GnP exfoliation in the composites could be explained by the intensity reduction of the (002) graphite diffraction peak.

0032-3861/\$ e see front matter © 2013 Elsevier Ltd. All rights reserved.
http://dx.doi.org/10.1016/j.polymer.2013.09.050

Supporting information 1 (S1).

Crystallinity calculations

Crystallinity by DSC

The glass transition temperature (T_g) of PC was determined using the inflection point heat capacity method. The melting temperature (T_m) was determined as the maximum temperature of the melting peak appearing in the melting endotherm, while the heat of fusion (ΔH_m) was obtained by direct integration of this peak. The crystallinity percentage (X_c) was calculated according to:

$$\chi_c = \frac{\Delta H_m}{\Delta H_m^0 w_f} \times 100 \quad (1)$$

where w_p is the weight fraction of PC and ΔH^0_m is the theoretical 100% crystalline PC melting enthalpy (147.79 J/g).

Crystallinity by WAXS

The crystallinity percentage (X_c) was determined by WAXS using the following equation:

$$\chi_c = \frac{A_c}{A_c + A_a} \times 100 \quad (2)$$

where A_c corresponds to the sum of the crystalline peak areas and A_a to the so-called amorphous halo area.

Supporting information 2 (S2).

Sample preparation for the measurement of the CO_2 diffusion coefficient

The samples used in the CO_2 desorption kinetics study were obtained by reducing the diameter of the foaming precursors to a typical value of 40 mm.

Measurements and testing

Dissolution/desorption experiments were carried out in order to measure the CO_2 diffusion coefficient in PC and PC-GnP. The samples used in the CO_2 desorption kinetics study were introduced in the high pressure vessel and heated to 210 ºC at a CO_2 pressure of 160 bar. After reaching the dissolution conditions, the samples were cooled to 35 ºC and the CO_2 was fully decompressed. After removing from the vessel, the samples containing CO_2 were quickly placed in a balance and the CO_2 mass loss was recorded as a function of desorption time.

The maximum concentration of CO_2 in the samples after decompression (M_0) was calculated by extrapolating to zero desorption time following the initial slope method [1]. Assuming one-dimensional diffusion in a plane sheet, the CO_2 diffusion coefficient (D_d) was determined by plotting M_t/M_0 as a function of t/l^2, where M_t is the CO_2 concentration at time t and l is the thickness of the sample, according to the following equation [2]:

$$\frac{M_t}{M_0} = 1 - \frac{8}{\pi^2} exp\left(-\frac{D_d t}{l^2}\right) \quad (1)$$

Effects of GnP on the CO_2 diffusion coefficient of polycarbonate

The maximum solubility of CO_2 in the unfilled PC and PC-GnP was found to be similar: 42.6 mg/g for the neat PC and 43.0 mg/g for PC-GnP. Nevertheless, the CO_2 desorption curves displayed in Fig. S2(a) showed abrupt differences regarding the weight loss rate of the neat PC and PC-GnP, resulting in a CO_2 diffusion coefficient of 4.45×10^{-12} m^2/s for the neat polymer and 6.69×10^{-11} m^2/s for the composite (see Fig. S2(b)). These results are comparable to those found in literature for neat PC, where D_d was found to be within 2.55×10^{-11} and 4.60×10^{-12} m^2/s [3] or between 1.55 ×

10^{-12} and 6.93×10^{-12} m^2/s [4]. As can be seen, the presence of GnP made it easier for the CO_2 to desorb from PC, which was related to the formation of preferential CO_2 diffusion paths at the interface of the polymer-graphene nanoplatelets.

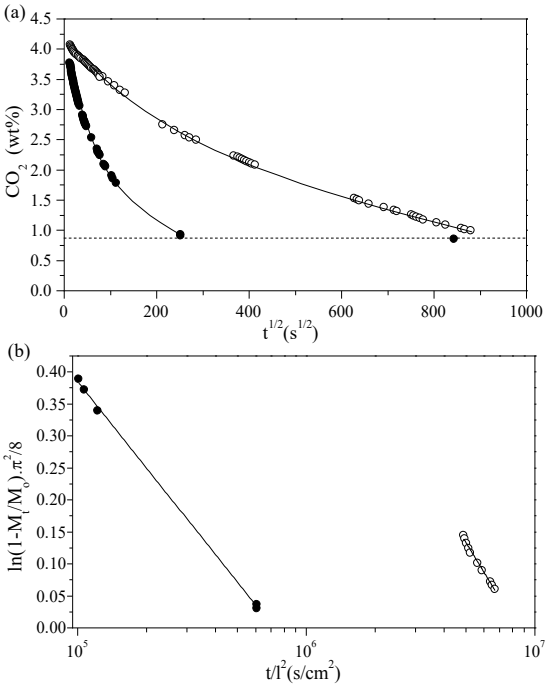

Figure S2. (a) CO_2 desorption behavior and (b) fitted data used to determine the diffusion coefficient values. Hollow symbols correspond to neat PC and filled symbols to PC-GnP composite.

References

1. Nawaby AV ZZ. Solubility and diffusivity in thermoplastic foam processing. In: ST L, editor. Thermoplastic foam processing. Principles and development. London: CRC Press, 2005.

2. Crank J. The mathematics of diffusion. London: Oxford University Press, 1956.

3. Tang M, Du T-B, and Chen Y-P. The Journal of Supercritical Fluids 2004;28(2-3):207-218.

4. Tang M, Huang W-H, and Chen Y-P. Journal of the Chinese Institute of Chemical Engineers 2007;38(5-6):419-424.

Supporting information 3 (S3).

As can be seen in Fig. S3, relevant optical changes could be observed in PC after CO_2 dissolution at 210 ºC (PC-CO_2) and subsequent slow cooling at 1.6 ºC/min until reaching room temperature.

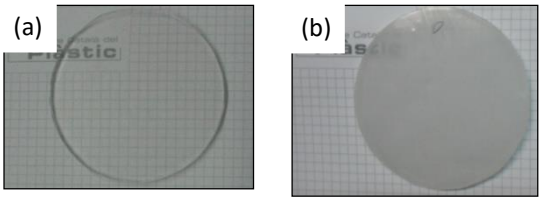

Figure S3. Polycarbonate (a) before (PC) and (b) after CO_2 dissolution (PC-CO_2).

Polymer Degradation and Stability 97 (2012) 1297e1304

Contents lists available at SciVerse ScienceDirect

Polymer Degradation and Stability

journal homepage: www.elsevier.com/locate/polydegstab

Thermal stability of polycarbonate-graphene nanocomposite foams

G. Gedler, M. Antunes, V. Realinho, J.I. Velasco*

Centre Català del Plàstic, Departament de Ciència dels Materials i Enginyeria Metal$lúrgica, Universitat Politècnica de Catalunya, BarcelonaTech. C/Colom 114, E-08222 Terrassa (Barcelona), Spain

a r t i c l e i n f o

Article history:
Received 17 May 2012
Accepted 22 May 2012
Available online 29 May 2012

Keywords:
Polycarbonate
Graphene
Foams
Thermal stability

a b s t r a c t

A thermogravimetric study in both nitrogen and air atmospheres has been carried out on unfilled and graphene-reinforced solid and foamed polycarbonate. Polycarbonate foams were prepared using a supercritical CO_2 dissolution one-step batch foaming process. Results showed that polycarbonate displayed a characteristic one-step decomposition under nitrogen, while three-step degradation was observed in air. In addition, as-received pristine graphene nanoplatelets displayed a three-step degradation in air, compared to a mild degradation under nitrogen. It was found that the thermal stability remarkably improved for the foamed composites, related to a combination of a heat transfer reduction promoted by the insulating cellular structure and the presence of the platelet-like graphene, which helped create a physical barrier effect, delaying the escape of volatile products generated during decomposition.

0141-3910/$ e see front matter © 2012 Elsevier Ltd. All rights reserved.
doi:10.1016/j.polymdegradstab.2012.05.027

Composites Part B 92 (2016) 299e306

Contents lists available at ScienceDirect

Composites Part B

journal homepage: www.elsevier.com/locate/compositesb

Low density polycarbonateegraphene nanocomposite foams produced by supercritical carbon dioxide two-step foaming. Thermal stability

G. Gedler, M. Antunes, J.I. Velasco*

Centre Català del Plàstic, Departament de Ciència dels Materials i Enginyeria Metal·lúrgica, Universitat Politècnica de Catalunya (UPC), C/Colom 114, E-08222 Terrassa, Spain

a r t i c l e i n f o

Article history:
Received 2 November 2015
Received in revised form
11 January 2016
Accepted 11 February 2016
Available online 21 February 2016

Keywords:
A. Polymer-matrix composites (PMCs)
B. Thermal properties
D. Thermal analysis
E. Autoclave
Graphene

a b s t r a c t

The thermal stability of low density polycarbonateegraphene nanocomposite foams prepared by supercritical carbon dioxide two-step foaming was investigated. Unfilled polycarbonate foams showed improved thermal stabilities when compared to the unfoamed polycarbonate, as the cellular structure of foams effectively slowed down the heat transfer process. Comparatively, polycarbonate foams with larger cells exhibited the highest delays in the early stage of thermal decomposition. Low density polycarbonate egraphene nanocomposite foams (relative densities between 0.07 and 0.28) displayed even higher thermal stabilities, with enhancements of up to 70 °C in terms of the onset of decomposition when compared to the unfilled PC, which was attributed to a combination of a heat transfer reduction promoted by the cellular structure and the presence of the dispersed graphene nanoplatelets, which acted as a physical barrier to the release of volatile decomposition products.

http://dx.doi.org/10.1016/j.compositesb.2016.02.025
1359-8368/

Composites Part B 93 (2016) 143e152

Contents lists available at ScienceDirect

Composites Part B

journal homepage: www.elsevier.com/locate/compositesb

Viscoelastic properties of polycarbonate-graphene nanoplatelets nanocomposite foams

G. Gedler, M. Antunes, J.I. Velasco*

Centre Català del Plàstic, Department of Materials Science and Metallurgy, Universitat Politècnica de Catalunya (UPC · BarcelonaTech), C/Colom 114, E-08222, Terrassa, Spain

a r t i c l e i n f o

Article history:
Received 22 February 2016
Accepted 11 March 2016
Available online 19 March 2016

Keywords:
A. Foams
A. Polymer-matrix composites (PMCs)
D. Mechanical testing
E. Autoclave
Graphene

a b s t r a c t

The viscoelastic properties of polycarbonate (PC) nanocomposite foams containing graphene nanoplatelets (GnP), prepared by one and two-step supercritical CO_2 dissolution, were characterized by dynamic-mechanical-thermal analysis. Three factors were detected to influence the mechanical performance of foams: relative density, the eventual presence of a PC crystalline phase and GnP's amount. Relative density was found to be the most important one, with the storage modulus following a power-law behavior with increasing relative density. Foams prepared in one-step presented higher storage moduli than two-step foams even having bigger cells, explained by their higher relative density. The eventual presence of PC crystals in one-step foams, induced by the combination of high CO_2 dissolution temperatures and GnP's presence during foaming, was found to be the cause of their higher storage moduli when compared to two-step foams at similar relative density. A slight effect of GnP could only be observed in two-step foams with 5% GnP, as these foams displayed storage moduli as high as one-step foams having lower relative densities. Regarding the viscous contribution, PC's glass transition temperature resulted higher in one-step foams, related to a restriction in the molecular mobility of PC induced by the presence of a PC crystalline fraction and GnP.

* Corresponding author. Tel.: þ34 937837022.
E-mail address: jose.ignacio.velasco@upc.edu (J.I. Velasco).

http://dx.doi.org/10.1016/j.compositesb.2016.03.032
1359-8368/

Chapter 5

Transport properties:

Thermal and electrical conductivity and electromagnetic shielding efficiency

5.1 Summary.

After analyzing in detail the effect of the process parameters and presence of graphene nanoplatelets on the cellular morphology, microstructure, thermal stability and viscoelasticity of the PC-GnP composite foams in the previous chapters, this chapter is focused on the analysis of functional characteristics such as electrical and thermal conductivities as well as the electromagnetic interference shielding effectiveness (EMI SE) of the composite foams, taking into consideration the effects that the cellular morphology and the presence of graphene nanoplatelets could have on these transport properties for the composite foams. Knowing that dispersion of conductive particles in polymer composites is essential to develop conductive paths along the material in order to enhance transport properties [1], the idea is to prepare composite foams with a broad range of transport characteristics, which may lead to new applications of polymeric lightweight materials with dispersed conductive particles in electrostatic dissipation (ESD), sensors and electromagnetic shielding interference (EMI) applications [2,3].

It is well known that the incorporation of graphene into insulating polymeric materials benefits the enhancement of transport properties (i.e. electrical and thermal conductivities) of the new composite material, mainly due to the excellent transport properties of graphene (electron mobility at room temperature 250,000 cm^2/Vs and exceptional thermal conductivity 3000-5000 $W.m^{-1}.K^{-1}$ [4]). It has been shown that filled composite materials exhibit a non-linear increase of the electrical conductivity as a function of the filler concentration [5]. At certain loading fraction, known as percolation threshold, the fillers are able to form a network leading to a sudden rise of the electrical and possible thermal conductivities [6]. The use of graphene particles in development of composites could be used to target applications such as thermal interface materials and heat spreaders. However, since the production of monolayer graphene is not yet at large scale

[1] Antunes M, Velasco JI. Multifunctional polymer foams with carbon nanoparticles. Progress in Polymer Science. 2014;39(3):486-509.
[2] Chung DDL. Electrical applications of carbon materials. Journal of Materials Science. 2004;39(8):2645-61.
[3] Liang J, Wang Y, Huang Y, Ma Y, Liu Z, Cai J, et al. Electromagnetic interference shielding of graphene/epoxy composites. Carbon. 2009;47(3):922-5.
[4] Young RJ, Kinloch IA, Gong L, Novoselov KS. The mechanics of graphene nanocomposites: A review. Composites Science and Technology. 2012;72(12):1459-76.
[5] Stankovich S, Dikin DA, Dommett GHB, Kohlhaas KM, Zimney EJ, Stach EA, et al. Graphene-based composite materials. Nature. 2006;442(7100):282-6.
[6] Kirkpatrick S. Percolation and Conduction. Reviews of Modern Physics. 1973;45(4):574-88.

production, there is increasing attention being paid to the use of exfoliated graphene-nanoplates (GNPs) in polymers to produce thermally conductive nanocomposites [7].

In particular, the dispersion of graphene particles in polymer foams has shown enhancement in applications such as electromagnetic interference shielding effectiveness (EMI SE) properties [8,9]. It needs to be pointed out that EMI consists of many unwanted radiated signals which can cause unacceptable system performance. These unwanted radiated signals are a consequence of the increasing complexity of electronic devices in the form of higher packing density for quick response [10]. These electromagnetic signals need to be shielded in order to protect electronic systems. Shielding effectiveness is used to measure the ratio of impinging energy to the residual energy. When an electromagnetic wave passes though a shield, absorption and reflection take place [11]. Therefore the content of well disperse graphene particles could enhance and homogenize the number of sites for prospect electromagnetic shielding. With all that in mind, the development of PC-GnP composite foams will be target to enhance the GnP dispersion and improve their final transport properties.

The analyses displayed in this chapter resulted from three main hypotheses that were taken into consideration when establishing the objectives of this chapter, as the first hypothesis was thought that foaming could enhance the dispersion of GnP and possible leading to the formation of 3D conductive networks in PC-GnP composites. With that, electrical and possible thermal conductivities could be increased. As a second hypothesis, which is closely related to the first one, we have that foaming will push the particles closer to each other within the solid fraction, promoting the reduction of particle-particle distance that could promote enhancements in electrical and/or thermal conductivities. As the third hypothesis, it was thought that since foaming was expected to enhance the dispersion of GnP and it was observed in the previous chapters that some degree of GnP exfoliation could be taking place, this will increase the homogeneous dispersed sites for shielding, then electromagnetic interference shielding effectiveness would be expected to be enhanced after foaming.

[7] Kim H, Abdala AA, Macosko CW. Graphene/Polymer Nanocomposites. Macromolecules. 2010;43(16):6515-30.
[8] Zhang H-B, Yan Q, Zheng W-G, He Z, Yu Z-Z. Tough Graphene−Polymer Microcellular Foams for Electromagnetic Interference Shielding. ACS Applied Materials & Interfaces. 2011;3(3):918-24.
[9] Yan D-X, Ren P-G, Pang H, Fu Q, Yang M-B, Li Z-M. Efficient electromagnetic interference shielding of lightweight graphene/polystyrene composite. Journal of Materials Chemistry. 2012;22(36):18772-4.
[10] J. L. Norman Violette, Donald R. J. White, Violette. MF. Electromagnetic Compatibility Handbook. New York: Van Nostrand Reinhold Company; 1987.
[11] Geetha S, Satheesh Kumar KK, Rao CRK, Vijayan M, Trivedi DC. EMI shielding: Methods and materials—A review. Journal of Applied Polymer Science. 2009;112(4):2073-86

The main objective of this chapter is to determine the effects of the cellular morphology, content of graphene nanoplatelets and its dispersion on the transport properties and EMI shielding effectiveness of PC-GnP composites prepared via 2 different foaming processes. With this in mind, different specific objectives were established. Firstly it was necessary to analyze the effects of the foam densities and cell sizes on the electrical conductivity behavior of PC-GnP composites [12]. Subsequently, the next objective was established as to investigate the effects of the content of GnP, foam densities and cell sizes on the thermal conductivity behavior of neat PC and PC-GnP composites [13]. After this, the third objective was to determine the effects of the foam density, cell sizes and content of GnP on the EMI SE behavior of PC-GnP composites prepared via the one-step [14] and the two-step [15] foaming processes. With the aim to satisfy the hypotheses and objectives established above, experiments and measurements of electrical and thermal conductivities, electromagnetic shielding effectiveness, small angle/wide angle X-ray scattering (SAXS/WAXS), atomic force microscopy, scanning electron microscopy and transmission electron microscopy were carried out.

In the previous chapters it was suggested that partial exfoliation of GnP was taking place during foaming, for this end the Debye–Scherrer relationship and Bragg's law [16] were used to show the reduction of thickness of GnP observed after WAXS analysis. This analysis showed the reduction/disappearance of the graphitic structure signal (i.e. 002) from the spectra. With that in mind, if exfoliation was taking place, electrical conductivity and EMI shielding protection will be expected to be enhanced in foamed materials, because these properties would require well dispersed GnP at low contents in order to have enough particles to form a conductive network and to work as shielding sites for electromagnetic waves. With this in mind and taking into consideration the lowest content of GnP used in this thesis (i.e. 0.5 wt.%), the analysis and discussions of electrical conductivity measurements were carried out in terms of percolation threshold and tunneling theories

[12] Gedler G, Antunes M, Velasco JI. Enhanced electrical conductivity in graphene-filled polycarbonate nanocomposites by microcellular foaming with sc-CO2. Journal of Adhesion Science and Technology. 2016;30(9):1017-29.
[13] Gedler G, Antunes M, Borca-Tasciuc T, Velasco JI, Ozisik R. Effects of graphene concentration, relative density and cellular morphology on the thermal conductivity of polycarbonate–graphene nanocomposite foams. European Polymer Journal. 2016;75:190-9.
[14] Gedler G, Antunes M, Velasco JI, Ozisik R. Enhanced electromagnetic interference shielding effectiveness of polycarbonate/graphene nanocomposites foamed via 1-step supercritical carbon dioxide process. Materials & Design. 2016;90:906-14.
[15] Gedler G, Antunes M, Velasco JI, Ozisik R. Electromagnetic shielding effectiveness of polycarbonate/graphene nanocomposite foams processed in 2-steps with supercritical carbon dioxide. Materials Letters. 2015;160:41-4.
[16] Guinebretière R. X-Ray Diffraction by Polycrystalline Materials: Wiley; 2007.

[17,18], showing that the electrical conductivity of composite foams was enhance after foaming when compare with the unfoamed neat PC and PC-GnP composite. It was observed that this enhancement was strongly related to the cell sizes and foam density, suggesting that for certain cell sizes (i.e. 80 μm -150 μm) the particles will be pushed closer to each other, until a point (i.e. cell sizes > 200 μm) where the opposite effect could take place, this would be pushing the particles away from each other during cells' growth, breaking any possible favorable network formed during foaming. The other case scenario possible would be that cell's growth would not even reach a minimum cell size to actually push the particles closer to each other enough to enhance the electrical conductivity value of the foam (i.e. cell sizes < 80 μm).

For the case of electromagnetic shielding protection, the electromagnetic waves theory (plane wave shielding effectiveness) [19,20] was implemented, based on this theory the Schelkunoff decomposition expresses the plane wave shielding effectiveness as of three decibel loss terms: absorption loss (also called penetration loss), reflection loss, and multiple reflections loss (also called the correction term for internal reflections). However, taking into consideration that the mismatch loss and dissipation loss, are closely related to the reflectance/absorptance the calculations were based on the mismatch decomposition which expresses the plane wave shielding effectiveness as the sum of only two terms, the absorption (which includes the absorption and multiple reflections correction terms) and the reflection term. This allowed us to perform the calculations by directly using the values from the measurements. With this being said, after foaming, it was shown that the effectiveness of shielding was enhanced when compared with the unfoamed composite, which reinforced the previous results regarding the enhanced GnP dispersion and exfoliation taking place during foaming. This analysis puts in evidence that the larger and well dispersed number of sites for shielding promoted the EMI SE of the composite foams. Even though, there was GnP enhanced dispersion/exfoliation, the degree of conduction network for thermal conductivity to take place is expected to be very high. With that in mind the characterization of thermal conductivity was carried on. For this end, the steady state one-dimensional heat conduction [21] and heat conduction tortuosity [22] were the theories taking into consideration for the analysis. The presence of gas phase distributed in different volumes (i.e. cells sizes) and different solid

[17] Rhodes SM. Electrically Conductive Polymer Composites: The University of Akron; 2007.
[18] Knauth P, Masquelier C, Traversa E, Wachsman ED. Solid State Ionics - 2004: Cambridge University Press; 2005.
[19] Schelkunoff SA. Electromagnetic Waves: Van Nostrand; 1943.
[20] McDowell AJ, Hubing TH. Analysis and Comparison of Plane Wave Shielding Effectiveness Decompositions. IEEE Transactions on Electromagnetic Compatibility. 2014;56(6):1711-4.
[21] Nield DA, Bejan A. Heat Transfer Through a Porous Medium. Convection in Porous Media. New York, NY: Springer New York 1999, p. 23-31.
[22] Turns S. Thermal-Fluid Sciences: An Integrated Approach: Cambridge University Press; 2006.

fractions paths associated to the densities of the foams were strongly related to the final thermal conductivity of the foams. For instance for low density foams (relative densities < 0.3) the behavior translated into less solid fraction resulted into a hard/tortuous path for phonons to travel through. However, in PC-GnP composite foams the thermal conductivity was enhanced with the presence of GnP, which increased with the addition of larger quantities (from 0.5 to 5 wt.% GnP) when compared with their counterpart neat PC foams with similar densities.

From this chapter the following conclusions can be extracted:

1) Thermal conductivity behavior and the density/morphology of the foams were strongly associated, increasing the thermal conductivity while increasing the foam density.

2) Thermal conductivity calculated for PC-GnP composite foams using a three-phase model displayed a better fit than when calculating using a two-phase model. This was attributed to the fact that this model takes into account the individual contribution of the gas phase, polymer phase and filler phase to calculate the thermal conductivity.

3) The one-step foaming process enhanced the electrical conductivity in four order of magnitude of PC-GnP composites for cell sizes larger than 140 μm when compared with values of the unfoamed composite.

4) SAXS measurements revealed anisotropic features, showing a strong correlation between processing conditions, cellular morphology developed and final possible orientation of particles. The observation of orientation of particles was carried out on TEM images.

5) Both the one-step and two-step foaming processes promoted the enhancement of electromagnetic interference shielding effectiveness. This was associated to the well dispersed GnPs and the effect of foaming, which pushed GnP closer to each other while maintaining and even distribution through the solid fraction, guaranteeing sites for shielding.

6) Changes in GnPs morphology were associated to the (002) diffraction signal intensity, with this and the enhancements shown in transport properties and EMI SE values, the enhanced dispersion and partial exfoliation during foaming was demonstrated.

5.2 Published articles.

The first section of this chapter is focused in the analysis of transport properties of PC-GnP foam systems aiming to determine their thermal and electrical conductivities. With this in mind, two publications are presented, first, ***Effects of graphene concentration, relative density and cellular morphology on the thermal conductivity of polycarbonate-graphene nanocomposite foams*** published in **European Polymer Journal. 2016; 75:190-9,** focuses on the thermal conductivity characterization of neat PC and PC-GnP composite foams; while a second publication entitled ***Enhanced electrical conductivity in graphene-filled polycarbonate nanocomposites by microcellular foaming with sc-CO_2*** published in **Journal of Adhesion Science and Technology. 2016; 30(9):1017-29,** displays the electrical conductivity characterization of the composite foams prepared via one-step foaming process.

Furthermore, since conductive particle dispersion in composites ultimately may enhance EMI SE of some systems [1-4]. The results and analysis regarding EMI shielding properties are discussed and displayed in two publications. The first publication entitled ***Enhanced electromagnetic interference shielding effectiveness of polycarbonate/graphene nanocomposites foamed via 1-step supercritical carbon dioxide process*** published in **Materials & Design. 2016; 90: 906-914,** displays the EMI SE study of foams prepared via the one-step foaming process, while a second publication entitled ***Electromagnetic shielding effectiveness of polycarbonate/graphene nanocomposite foams processed in 2-steps with supercritical carbon dioxide*** published in **Materials Letters. 2015; 160:41-44,** is focused on presenting the results and analysis of the PC-GnP composite foams prepared via the two-step foaming process.

European Polymer Journal 75 (2016) 190–199

Contents lists available at ScienceDirect

European Polymer Journal

journal homepage: www.elsevier.com/locate/europolj

Effects of graphene concentration, relative density and cellular morphology on the thermal conductivity of polycarbonate–graphene nanocomposite foams

G. Gedler[a,b], M. Antunes[a], T. Borca-Tasciuc[c], J.I. Velasco[a,⇑], R. Ozisik[b,d,⇑]

[a] Centre Català del Plàstic, Departament de Ciència dels Materials i Enginyeria Metal-lúrgica, Universitat Politècnica de Catalunya (UPC-BarcelonaTech), C/Colom 114, E-08222 Terrassa, Spain
[b] Department of Materials Science and Engineering, Rensselaer Polytechnic Institute, Troy, NY 12180, USA
[c] Department of Mechanical, Aerospace, and Nuclear Engineering, Rensselaer Polytechnic Institute, Troy, NY 12180, USA
[d] Rensselaer Nanotechnology Center, Rensselaer Polytechnic Institute, Troy, NY 12180, USA

article info

Article history:
Received 6 November 2015
Received in revised form 9 December 2015
Accepted 22 December 2015
Available online 23 December 2015

Keywords:
Thermal conductivity
Polycarbonate
Graphene
Nanocomposite foams

abstract

The thermal conductivity of polycarbonate–graphene nanocomposite foams was studied as a function of relative density, developed cellular structure and graphene concentration. Two types of supercritical CO_2 foaming processes were employed to obtain foams with a wide range of relative densities and cellular morphologies. The thermal conductivity of unfoamed nanocomposites increased in more than two times upon addition of 5 wt% graphene. Foaming led to lowered thermal conductivity values, as low as 0.03 W/(m K), with thermal conductivity being mainly controlled by relative density and in a lower extent by graphene concentration. Higher thermal conductivities were obtained with increasing relative density and cell size, as well as with increasing graphene concentration, especially in those cases where improved graphene dispersion was achieved with foaming. Thermal conductivity values displayed a better fit when using a three-phase model when compared to the two-phase model previously proposed for polymer composite foams.

⇑ Corresponding authors at: Department of Materials Science and Engineering, Rensselaer Polytechnic Institute, Troy, NY 12180, USA (R. Ozisik).
E-mail addresses: jose.ignacio.velasco@upc.edu (J.I. Velasco), ozisik@rpi.edu (R. Ozisik).

http://dx.doi.org/10.1016/j.eurpolymj.2015.12.018 0014-3057/

Journal of adhesion science and Technology, 2016
Vol. 30, no. 9, 1017–1029
http://dx.doi.org/10.1080/01694243.2015.1137700

Taylor & Francis
Taylor & Francis Group

Enhanced electrical conductivity in graphene-filled polycarbonate nanocomposites by microcellular foaming with sc-CO_2

Gabriel Gedler, Marcelo Antunes and José Ignacio Velasco

Centre Català del Plàstic, Departament de Ciència dels Materials i Enginyeria Metal·lúrgica, UPC BarcelonaTech, Universitat Politècnica de Catalunya, Terrassa, Spain

ABSTRACT

Electrically conductive polycarbonate (PC) foams containing a low concentration of graphene nanoplatelets (0.5 wt.%) were produced with variable range of expansion ratio by applying a high-pressure batch foaming process using sc-CO_2. The structure of the foams was assessed by means of SEM, AFM and WAXS, and the electrical conductivity was measured in the foam growing direction. Results showed that electrical conductivity of PC composite foams remarkably increased when compared to that of non-foamed PC composite, with both the electrical conductivity and the main cell size of the foams being directly affected by the resultant expansion ratio of the foam. This interesting result could be explained by the development of an interconnected graphene nanoparticle network composed by increasingly well-dispersed and reoriented graphene nanoplatelets, which was developed into the solid fraction of the foam upon foaming by sudden depressurising of the plasticised CO_2-saturated PC preform. Some evidences of morphological changes in the graphene nanoplatelets after foaming were obtained by analysing variations in graphene's (0 0 2) diffraction plane, whose intensity decreased with foaming. A reduction of the average number of layers in the graphene nanoplatelets was also measured, both evidences indicating that improved dispersion of graphene nanoparticles existed in the PC composite foams. As a result, foams with a proper combination of low density and enhanced electrical conductivity could be produced, enabling them to be used in applications such as electromagnetic interference shielding.

ARTICLE HISTORY
received 4 June 2015
revised 22 december 2015
accepted 29 december 2015

KEYWORDS
foams; polycarbonate; electrical conductivity; graphene; carbon dioxide

CONTACT José ignacio Velasco jose.ignacio.velasco@upc.edu

Materials and Design 90 (2016) 906–914

Contents lists available at ScienceDirect

Materials and Design

journal homepage: www.elsevier.com/locate/matdes

Enhanced electromagnetic interference shielding effectiveness of polycarbonate/graphene nanocomposites foamed via 1-step supercritical carbon dioxide process

G. Gedler [a,b], M. Antunes [a], J.I. Velasco [a,*], R. Ozisik [b,c,**]

[a] Centre Català del Plàstic, Departament de Ciència dels Materials i Enginyeria Metal lúrgica, Universitat Politècnica de Catalunya, BarcelonaTech (UPC), C/Colom 114, E-08222 Terrassa, Barcelona, Spain

[b] Department of Materials Science and Engineering, Rensselaer Polytechnic Institute, Troy, NY 12180, USA

[c] Rensselaer Nanotechnology Center, Rensselaer Polytechnic Institute, Troy, NY 12180, USA

article info

Article history:
Received 31 July 2015
Received in revised form 28 October 2015
Accepted 5 November 2015
Available online 10 November 2015

Keywords:
Composite foams
Graphene
Polycarbonate
Electromagnetic interference shielding
Small angle X-ray scattering
1-Step foaming

abstract

The dielectric and electromagnetic interference (EMI) shielding properties of polycarbonate/graphene nanocomposites foamed using supercritical carbon dioxide were studied as a function of their cellular and composite morphology. Foamed polycarbonate filled with 0.5% (by weight) graphene exhibited enhanced EMI shielding effectiveness, which was found to depend on cellular and composite morphology in a complex manner. Foamed composites presented a maximum specific EMI shielding effectiveness of ~39 dB cm^3/g, which is approximately 35 times greater than that of unfoamed composite (1.1 dB cm^3/g). In addition, the relative permittivity was found to increase up to 3.25 times. The results suggest that graphene filled polymer foams can enhance the performance of electronic devices, opening up the possibility of using these materials in electronic applications.

* Corresponding author.
** Correspondence to: R. Ozisik, Department of Materials Science and Engineering, Rensselaer Polytechnic Institute, Troy, NY 12180, USA.
E-mail addresses: jose.ignacio.velasco@upc.edu (J.I. Velasco), ozisik@rpi.edu (R. Ozisik).

http://dx.doi.org/10.1016/j.matdes.2015.11.021
0264-1275/

Materials Letters 160 (2015) 41–44

Contents lists available at ScienceDirect

Materials Letters

journal homepage: www.elsevier.com/locate/matlet

Electromagnetic shielding effectiveness of polycarbonate/graphene nanocomposite foams processed in 2-steps with supercritical carbon dioxide

G. Gedler [a,b], M. Antunes [a], J.I. Velasco [a,n], R. Ozisik [b,c,nn]

[a] Centre Català del Plàstic, Departament de Ciència dels Materials i Enginyeria Metal·lúrgica, Universitat Politècnica de Catalunya BarcelonaTech (UPC), C/ Colom 114, E-08222 Terrassa, Barcelona, Spain
[b] Department of Materials Science and Engineering Rensselaer Polytechnic Institute, Troy, NY 12180, USA
[c] Rensselaer Nanotechnology Center, Rensselaer Polytechnic Institute, Troy, NY 12180, USA

a r t i c l e i n f o

Article history:
Received 11 July 2015
Accepted 15 July 2015
Available online 17 July 2015

Keywords:
Porous materials
Polymeric composites
Graphene
X-ray techniques
Electron microscopy

a b s t r a c t

The electromagnetic interference (EMI) shielding properties of polycarbonate/graphene composites foamed with supercritical carbon dioxide were investigated as a function of cellular morphology and graphene particle dispersion. The 2-step foaming method used was found to improve graphene dispersion and led to a different cellular structure compared to traditional 1-step foaming. Reflection was found to be the dominant EMI shielding mechanism and EMI shielding effectiveness was improved with large cell morphology that promoted isotropic/random orientation of graphene particles. A maximum EMI specific shielding effectiveness of """78 dB cm^3/g was achieved in foams, which was more than 70 times higher than that of the unfoamed polymer (1.1 dB cm^3/g). The study shows that by controlling foaming process conditions and nanoparticle characteristics, it is possible to improve multiple properties while achieving lightweight materials suitable for various applications.

[n] Corresponding author. Centre Català del Plàstic, Departament de Ciència dels Materials i Enginyeria Metallúrgica, Universitat Politècnica de Catalunya BarcelonaTech (UPC), C/Colom 114, E-08222 Terrassa, Barcelona, Spain.
[nn] Corresponding author at: Department of Materials Science and Engineering Rensselaer Polytechnic Institute, Troy, NY 12180, USA.
E-mail addresses: jose.ignacio.velasco@upc.edu (J.I. Velasco), ozisik@rpi.edu (R. Ozisik).

http://dx.doi.org/10.1016/j.matlet.2015.07.070
0167-577X/

Chapter 6

General discussion and conclusions

6.1 General discussion.

This thesis addressed the preparation of polycarbonate and polycarbonate-graphene nanoplatelets foams via two different foaming processes. The main goal originally set was to establish a correlation between processing parameters with the final morphology, microstructure and properties of the foams prepared. The study focused on the understanding of these relationships while aiming to develop foams with a broad range of densities. With the addition of GnP, one of the specific targets was to provide the foams with multifunctional characteristics. Since multifunctionality refers to the ability of a single material to possess multiple engineering functions such as enhanced mechanical, thermal, transport properties, the correlation of the presence of GnP with the final characteristics of the foams was analyzed in detail.

In Chapter 3 the characterization of the cellular structure of the foams was displayed and analyzed by means of SEM imaging analysis, aiming to correlate the cellular structure with the processing parameters. Firstly, the analysis focused on the final morphology of the foams prepared via the one-step foaming process. It was shown that the cellular structures developed were closed-cell. This was attributed to the considerable good response of PC during expansion due to its melt strength under the particular foaming conditions. It was possible to use the one-step foaming process with changes in temperature (i.e. 200 ºC – 220 ºC) and time of dissolution (i.e. 40 min- 160 min) to prepare PC rigid foams of medium relative densities (i.e. ~0.33-0.46). The addition of GnP made possible to prepare composite foams of mid-high relative densities ranging between ~0.34 and 0.79. In addition on the higher end, PC-GnP foams prepared with 5 wt.% GnP were in the high relative density range (i.e. ~0.50-0.80).

Particularly, the temperature had a large effect on the final morphology of the foams, increasing cell sizes from 70 μm to 150 μm when increasing the temperature from 200 ºC to 213 ºC . While the addition of 5 wt. % GnP showed that under the process conditions studied, the particles had a nucleation effect, reducing cell sizes from 160 μm to 30 μm and increasing cell densities (i.e. from 4.64 x 10^5 cell/cm^3 to 1.18 x 10^7 cell/cm^3) when compared with neat PC foams. This was attributed to the nucleation effect of GnP and the increment of the melt flow of the composite during foaming. It was also discussed that the residual pressure (i.e. remaining pressure after expansion and kept during cooling) played a key role when promoting isotropic cell morphology.

Displaying aspect ratios very close to 1 when using a residual pressure of 10 bar. This pressure helped to provide stability to the structure at the considerable high temperatures after expansion, specially taking into account that the T_g in the presence of CO_2 was expected to be lower when compared to the T_g of PC (i.e. ~150 ^oC).

The second section of Chapter 3 was dedicated to the analysis of the cellular morphology of the foams prepared via the two-step process. This foaming process promoted the formation of closed-cell morphology with low relative densities (i.e. down to 0.07) and a much broader range of cell sizes (i.e. 7-700 μm) when compared to the foams prepared in one-step (i.e. 30-200 μm). This was attributed to the long CO_2 dissolution time (> 200 min) and the smaller pressure drop (~60 bar) at the moment of expansion when compared with the one-step process (>150 bar). It was discussed how tuning this foaming process enabled the preparation of PC foams of low relative densities (i.e. ~0.07-0.15) and PC-GnP foams with 0.5 wt.%GnP of mid-low relative densities (i.e. ~0.08-0.30). In addition on the higher end PC-GnP foams with 5 wt.% GnP were in the mid relative densities range (i.e. ~0.40-0.50). This was attributed to the quantity of CO_2 dissolved in the samples when using different dissolution temperatures (varying from 3 to 7 wt.% CO_2). This variations in the process enabled the development of isotropic (i.e. dissolution temperatures of 80 ^oC) and anisotropic (i.e. dissolution temperatures of 100 ^oC) cellular morphologies with expansion ratios of up to 14. The use of the two-step foaming process also promoted the nucleation effect for larger contents of GnP, for instance, the most remarkable nucleation effect was observed for the dissolution temperature of 100 ^oC, where cell sizes for the neat PC reached the hundreds of microns (i.e. 700 μm) and for composite foams with 5 wt% GnP the cell size was reduced to a few microns (i.e. 7 μm). Preliminary results in this chapter showed that the use of this foaming process allowed the preparation of foams that remained amorphous. This was analyzed by WAXS and DSC measurements, which was discussed in more detail in Chapter 4.

After understanding the effect of the foaming processes on the foam's cellular morphology, Chapter 4 focused on the study of the effects of process parameters and foams' morphology on the microstructure, thermal stability and viscoelasticity of the final foams developed. Here, it was discussed that the use of long times of CO_2 dissolution (i.e. 60 min) combined with high temperatures (> 200 ^oC) and high pressure of CO_2 (i.e. 150 bar) was triggering crystallinity, which was confirmed by DSC, XRD and Raman spectroscopy for foams prepared via the one-step process.

This was attributed to the plasticizing effect of CO_2, which under those particular conditions resulted beneficial for the formation of just a small amount of crystallinity for the neat PC foams.

In addition, the effect of GnP on the PC microstructure had a remarkable effect on the final microstructure of the foams. The synergetic effect of the graphene nanoplatelets and CO_2 under foaming conditions via one-step process promoted a enhancement of PC crystallinity (i.e. 8 %) as compared to the PC foams (i.e. 1%). The double melting behavior observed in the DSC analysis for the composite foams was discussed; this was attributed to the presence of crystals with different thermal stabilities that had different nucleation speeds. On the other hand, the 2-step foaming process guaranteed the development of PC and composite foams with amorphous characteristics, regardless the long times used to dissolve CO_2 in the samples. This was attributed to the considerable lower dissolution temperature used (i.e. 80 ^oC and 100 ^oC) when compared with the temperature used in the 1-step process (i.e. > 200 ^oC), which did not enhance the molecular mobility of PC when compared with the conditions used in the one-step foaming process.

Particularly, in this chapter the advantage of using Raman spectroscopy was discussed, as a powerful tool capable to detect and quantify the amount of crystallinity in the foams. The use of an empirical correlation was used to estimate values of crystallinity and compared with values calculated by WAXS and DSC. The correlation used the subtraction of the areas of bands from the composite foam (i.e. 733 cm^{-1} or 1235 cm^{-1}) and the area from the "control" peak (i.e. 733 cm^{-1} or 1235 cm^{-1} from neat PC), and then divide it by the area of the "control" band. These values were fairly close to the values calculated from DSC and WAXS in some cases but in others they showed large differences. Those differences were attributed to the detection of ordered structures and not exclusively crystalline structures, the phase that did not crystallize but had some degree of order in its structure was also been detected. This led us to correlate those differences to non-crystalline phases as well. Interactions shown by particular bands (i.e. 480 cm^{-1}, 733 cm^{-1}, 1235 cm^{-1} and 2440 cm^{-1}) were then associated to these type if non-crystalline phases.

Another section in Chapter 4 was dedicated to the discussion of the thermal stability of the foams. It was shown that the presence of cellular structures enhanced thermal stability of foams attributed to the delay of the early degradation process consequence of the inhibition of heat transfer through the material. The materials were acting as insulators, attributed to the presence of well distributed gaseous phase (i.e. homogeneous cellular structure). With the addition of GnP, the

stability was increase even more. The well dispersed graphene nanoplatelets, delayed the escape of volatile degradation products during decomposition. This promoted the contribution on thermal stability of foams composites associated to the restriction of gases to diffuse within the PC, known as gas tortuous path effect.

Later in this chapter, the viscoelastic properties of the PC and PC-GnP foams were discussed. The materials exhibited cellular structure dependence, increasing the specific relative storage modulus from 0.1 to 0.6 when decreasing the cell sizes from 70 μm to 7μm in the case of foams prepared via the two-step foaming process. Different behaviors were observed for the foams prepared by one-step process and the foams prepared using the two-step foaming process. In the case of the foams prepared via the one-step process exhibited higher storage moduli (i.e. up to ~1000 MPa) as compared to those prepared in two steps (i.e. < 100 MPa), it was suggested that the presence of a crystalline phase enhanced the mechanical behavior of the composites foams. In addition, the foams prepared in two steps exhibited a more drastic reduction of stiffness while reducing density.

The addition of graphene nanoplatelets in conjunction with the presence of a crystalline phase counteracted the reduction of the glass transition temperature (contributing to limit the mobility of PC molecules) for foams prepared by a one-step process. However, for foams prepared via the two-step process with amorphous nature promoted the reduction of the maximum in the *tan δ* signal, this was attributed to the reduction of damping effect, causing the mechanical behavior of these foams less dependent on the graphene content.

Chapter 5 was dedicated to characterize the multifunctional properties of the developed foams, with the main objective of supporting the initial hypothesis and preliminary results that showed the dispersion of GnP was taking place. For this, the thermal conductivity of composite foams was characterized. With the main goal of elucidating if the degree of GnP dispersion reached during foaming was enough to significantly enhance the thermal conductivity on the foams; knowing that remarkably high fillers' dispersion will be required in order to improve high values of thermal conductivities. Results showed that thermal conductivity increased from 0.1 $W.m^{-1}.K^{-1}$ to 0.3 $W.m^{-1}.K^{-1}$ when reducing cell sizes from 160 μm to 30 μm in the case of foams prepared via one-step process, this was attributed to the heat conduction through the solid fraction which resulted in the shorting of the length of conduction paths. Remarkably reduction of density (~90 %) of pure

PC by using a two-step foaming process promoted a reduction of ~80 % of thermal conductivity as compared to the neat unfoamed PC. This was attributed to the larger cells and thinner walls (less solid fraction) that made the conduction path through the solid fraction slower.

The effects of the addition of graphene nanoplatelets on the thermal conductivity of composites foams were also discussed. Particularly, the addition of 0.5 wt.% GnP promoted a 95 % enhancement of the thermal conductivity as compared to neat PC foams with similar relative densities, these foams prepared using the one-step foaming process showed to induce an isotropic particle dispersion at high foaming temperatures. The well dispersed graphene nanoplatelets within the cell walls favored the thermal conductivity through the solid fraction of the composite foams. However, the values of thermal conductivity (i.e. ~ 0.18 $W.m^{-1}.K^{-1}$) were very similar when compared with the unfoamed PC (i.e. ~ 0.18 $W.m^{-1}.K^{-1}$). With that in mind, higher graphene nanoplatelets contents (5 wt. %) were used. This larger amount of GnP in the composite foams promoted higher thermal conductivity ~ 0.3 $W.m^{-1}.K^{-1}$ higher than the unfoamed PC and close to the unfoamed composite (5 wt. %) value of ~ 0.35 $W.m^{-1}.K^{-1}$, while reducing the density a 20 %. This was related to the high relative density of the foam (i.e. ~0.85) and the reduced inter-particle distance after foaming, mainly due to the larger amount of GnP used during the preparation of the composite material. Comparisons with theoretical predictions were carried out, showing that a 3-phase model can make a closer prediction to the real thermal conductivity behavior of the foam when compared with a 2-phase model. This was attributed to the fact that the 3-phase model takes into consideration individual theoretical contributions of each of the phases in the nanocomposites (i.e. gas, polymer matrix and filler).

In closing, transverse DC electrical conductivity behavior of composite foams prepared via one-step foaming process was characterized. This showed an increment up to four orders of magnitude of the electrical conductivity values in foams compared with the unfoamed composite. This was related to the increment of cell sizes (i.e. stretching of solid fraction) and the interaction between CO_2 molecules and the initial graphitic-like structures. This suggested the space reduction between graphene nanoplatelets during foaming, ultimately resulting in the formation of a more effective electrically-conductive pseudo-network throughout the material. Even though the values of electrical conductivity increased up to four orders of magnitude, the conductive network was not enough to reach values of conductor materials. For transporting larger quantity of electrons needed for higher electrical conductivity values, a higher interconnected network will be needed. Similar

results were observed for AC conductivity measurements. However, this increment in conductivity suggested that foaming improved the graphene nanoplatelets dispersion and possible exfoliation of the graphene stacks suggested by the (002) diffraction peak intensity signal reduction observed for the composite foams.

TEM imaging analysis was used to observe the dispersion of graphene nanoplatelets in composite foams, which was suggested due to the enhancements observed in the composite foams properties previously discussed. Indeed, this dispersion was enough to promote the enhancement of electromagnetic interference shielding effectiveness of the materials, from ~1 dB before foaming to ~15 dB after foaming in some cases at certain frequencies. Another hypothesis that was discussed was the possible orientation of GnP during foaming, since the stretching of the material during foaming might induce certain degree of orientation. With this in mind, SAXS measurements were used to reveal anisotropic features by means of azimuthal distribution analysis. It was discussed that depending on the cellular morphology developed slight orientation of particles degree was observed, finding that higher heating times during the two-step foaming process (i.e. 100 s) and low foaming temperatures in the one-step foaming process (i.e. 200 ^{o}C) induced preferential orientation of particles. It was concluded that the EMI SE was enhanced after foaming, regardless the foaming process used.

The discussions presented in this thesis focused on the effects of the processing variables and the use of GnP on the cellular morphology, microstructure and its correlation with the final properties of the materials. This led to the understanding of how the two foaming processes used in this work can be tuned in order to develop foams with a wide range of densities and multifunctionalities, improving the chances of polycarbonate to be considered as one of the engendering thermoplastics to be used in the preparation of multifunctional lightweight materials in industries such as aerospace, automotive, electronics and construction.

With this thesis it has been possible to prepare and characterize PC foams and PC/graphene foams with enhanced multifunctional properties. It was shown that multifunctional lightweight materials can be tuned in order to exhibit different properties. With the experiences carried out throughout this thesis, many experiments hasve been proposed and interesting questions are unanswered at the moment. Therefore some ideas that were discussed and some of them attempted to be carried out are proposed as future research. For instance, the variation of the

dissolution/foaming variables in the one- and two-step foaming process could be finely tuned in order to try to develop foams with smaller cell sizes (e.g. nanorange). Variables such as pressure and temperature that were shown to reduce the glass transition temperature under the presence of carbon dioxide in the foams, could be quantified for different polymers and composites. For this end a DSC high pressure chamber will be required. It would be very interesting to carry out a systematic preparation and characterization of composite foams by means of multiple expansions, in which monitoring the microstructure after each expansion will be of paramount importance, because the presence of crystallinity could restrict the diffusion of CO_2 and as a consequence the formation of a homogeneous cellular structure and a more efficient filler dispersion. Since it was shown that foaming promoted the dispersion of fillers within a composite, but still the formation of a very efficient conductive path was not form, it is suggested the addition of combined CNT and graphene into polymeric materials, which could be use with the aim to enhance the formation of conductive path and enhance the electrical and possible the thermal conductivity along with EMI SE of composite foams. In that study it would be suggested the use of different contents of GnP and CNT (independently and combined) in order to determine the percolation thresholds for electrical conductivity of the composite foams.

6.2 Conclusions.

After all the discussions presented in the different chapters, and taking into consideration the starting objectives of this thesis, the main conclusions are listed as following:

1. The preparation of polymeric foams with a broad range of densities (~0.08-0.95) was successfully achieved by the use of two different foaming methods.

2. The cellular morphology was remarkably dependant on processing parameters, especially on temperatures. High foaming and CO_2 dissolution temperatures (> 213 ^oC) induced larger cell sizes (> 150 μm), attributed to the increased molecule mobility in the presence of CO_2 under the foaming conditions.

3. The increment of CO_2 dissolution times and pressures combined with large temperatures of dissolution promoted larger amounts of CO_2 dissolved in the sample (> 5 wt.%), which induced

larger cell sizes , in some cases promoted by cell coalescence (i.e. PC foams prepared via two-step process).

4. The presence of GnP promoted the reduction of cell sizes, especially for high contents (i.e. 5wt.%). This was attributed to the cell nucleation effect and the restriction of cell growth during foaming.

5. GnP promoted the gas barrier effect in composites (especially for 5 wt%.), slowing down CO_2 diffusion from the sample while increasing GnP concentration.

6. The presence of CO_2 and GnP promoted a synergetic effect, increasing the mobility of PC molecules favoring the 3D order of lamellae structures detected as crystalline phase. The presence of GnP also promoted the heterogeneous nucleation of crystals developing two populations of crystals with different thermal stabilities.

7. Raman spectroscopy was shown to be capable to detect intrachain and interchain interactions which were correlated to regular arrangements in the structure (crystalline and non-crystalline phases)

8. Enhanced GnP dispersion was correlated to the reduction/almost disappearance of the characteristic (002) diffraction plane typical of the graphitic structure, attributed to the interactions of CO_2 molecules and graphitic structures during CO_2 dissolution and expansion. This was supported by the increment of electrical conductivity and EMI SE increments after foaming.

9. The two-steps foaming process of PC-GnP composites did not promote relevant changes in microstructure, remaining amorphous under the process conditions used. This was related to the low temperature during CO_2 dissolution (80 ^oC and 100 ^oC).

10. An insulator mechanism promoted by the presence of cellular structures was demonstrated, which was one of the main factors to enhance the thermal stability of the materials. At the same time, linear relationships for the mass loss temperatures and the relative density were established.

11. The presence of the enhanced dispersion of graphene nanoplatelets throughout the solid fraction enhanced the final thermal stability of composite foams.

12. The mechanical performance of foams was mainly driven by their relative density, as the relative storage modulus values of foams varied potentially with relative density.

13. The presence of nanosized GnP promoted foams with enhanced specific elastic moduli, showing the efficiency of these fillers as reinforced elements.

14. The foams prepared in two steps displayed a less dependency of GnP's concentration when compared with the one-step foams. Attributed to the small changes of the exponent "*n*" from the Gibson-Ashby relationship.

15. Foams prepared by one-step foaming presented higher T_g values when compared with the foams prepared in two steps. These differences of the viscous contribution were related to the presence of a PC crystalline fraction and the presence of GnP that combined, contributed to limit the mobility of PC molecules.

16. Remarkably large density reduction of pure PC foams are achieved by two-step foaming process (i.e., ~94 %), considerable reducing the thermal conductivity as compared to the pure unfoamed PC. This improves the insulator behavior at the same time that the density is reduced.

17. The thermal conductivity behavior and the density/morphology of the foams were strongly associated. However, the presence of GnP promoted enhanced conduction throughout the solid fraction of the samples, attributed to partial-path of particles in multiple sections of the sample, improving the transfer of heat through the solid fraction of the samples.

18. The three-phase model displayed a better fit than the two-phase model for PC-GnP composite foams. This indicates that treating these materials as a three-phase system (gas phase, polymer phase and filler phase) is more appropriate along a broad range of densities.

19. The cellular structure was attributed as one of the main factor for the enhancement of the final electrical conductivity of the materials, not only enhancing the dispersion of GnP but also pushing them closer together partially improving the conductive networks within the solid fraction.

20. EMI SE was enhanced based on both absorption and reflection shielding mechanisms. This was attributed to the well dispersed GnPs and the presence of the cellular structure, regardless the not very high electrical conductivity values of the composite foams.